Design, Characterization and Application of Amphipathic Peptides for siRNA Delivery

by

Mousa Jafari

A thesis
presented to the University of Waterloo
in fulfillment of the
thesis requirement for the degree of
Doctor of Philosophy
in
Chemical Engineering

Waterloo, Ontario, Canada, 2013

AUTHOR'S DECLARATION

I hereby declare that I am the sole author of this thesis. This is a true copy of the thesis, including any required final revisions, as accepted by my examiners.

I understand that my thesis may be made electronically available to the public.

Abstract

Short interfering RNAs (siRNAs) are 21-23 nucleotide-long double-stranded RNA molecules that can trigger the RNA interference (RNAi). RNAi is a post-transcriptional gene silencing process whereby siRNAs induce the sequence-specific degradation of complementary messenger RNA (mRNA). Despite their promising therapeutic capabilities, siRNA-based strategies suffer from enzymatic degradation and poor cellular uptake. Several carrier-based approaches have been employed to enhance the stability and efficiency of siRNA delivery. Considering their safety, efficiency, and targeting capabilities, peptide-based delivery systems have shown great promise for overcoming the main obstacles in siRNA therapeutic delivery. Peptides are versatile and easily designed to incorporate a number of specific attributes required for efficient siRNA delivery.

This thesis focuses on the design, characterization and utilization of a new class of amphipathic peptides for siRNA delivery. The study includes: (i) designing amphipathic, amino acid pairing peptide sequences for siRNA delivery, (ii) siRNA delivery experiments *in vitro* to evaluate transfection efficacy of the designed peptides, (iii) physicochemical characterization of the interaction between promising peptides and siRNA, and (iv) identifying internalization pathway and kinetics of a promising peptide, C6M1.

The peptide C6, an 18-mer amphipathic, amino acid pairing peptide, was designed as an siRNA delivery carrier by incorporating three types of amino acids, i.e., arginine, leucine, and tryptophan. This peptide adopted a helical structure upon co-assembling with siRNA. The C6-siRNA co-assembly showed a size distribution between 50 and 250 nm, confirmed by dynamic light scattering and atomic force microscopy. The C6-siRNA interaction enthalpy and stoichiometry were 8.8 $kJ.mol^{-1}$ and 6.5, respectively, obtained by isothermal titration calorimetry. A minimum C6:siRNA molar ratio of 10:1 was required to form stable co-assemblies/complexes, indicated by agarose gel shift assay and fluorescence

spectroscopy. C6 showed lower toxicity and higher efficiency in cellular uptake of siRNA, compared with Lipofectamine 2000, a lipid-based positive control. Fluorescence microscopy images confirmed the localization of C6-siRNA complexes in the cytoplasm.

In order to enhance the solubility and delivery efficiency further, a modified peptide, C6M1, was designed by replacing three leucine with tryptophan residues in the C6 sequence. The fluorescence assay confirmed that the sequence mutation significantly increased the solubility of C6M1. C6M1 adapted a stable helical structure in saline or upon interaction with siRNA. The toxicity assay showed lower toxicity of C6M1 with an IC50 (the concentration of peptide at 50% cell viability) of 22 μM, compared with C6 with that of 12 μM. Naked siRNA was completely degraded after 4 h incubation in 50% serum, while the siRNA in complex with C6M1 was preserved even after 24 h. Western blotting showed a significant decrease in GAPDH protein contents (75%) in CHO-K1 Chinese hamster ovary cells, 48 h after treatment with C6M1-GAPDH siRNA complexes.

The interaction of C6M1-siRNA complexes with cell surface and the mechanisms involved in the internalization of the complex in different size ranges were studied. Heparin and chlorate treatments revealed that the electrostatic interaction of the C6M1-siRNA complex with heparan sulphate proteoglycans at the cell surface is required to trigger the uptake process. Using endocytic inhibitors, it was found that small C6M1-siRNA complexes (mean ~155 nm) mainly enter CHO-K1 cells through an energy-independent mechanism, most likely involving direct translocation. In contrast, large complexes (mean ~460 nm) internalize the cells mainly through a lipid raft-dependant macropinocytosis. The integrity of the cytoskeletal components also showed significant impact on the efficient internalization of the C6M1-siRNA complex. The kinetics experiments confirmed the fast internalization of small complexes (with uptake half-time of 25 min) in comparison to large complexes (70 min). This work provides essential information for peptide design and characterization in the development of amphipathic peptide-based siRNA delivery.

Acknowledgements

I would like to express my deep gratitude and appreciation to my supervisor, Professor Pu Chen, for his valuable advisory and unlimited support during my PhD program. His scientific advice and professional attitude helped me through difficulties I encountered in the research. I also thank him for providing me an invaluable research environment to work in this innovative research area.

I would also like to thank Professor Elizabeth Gillies, Professor Raymond Legge, Professor John Honek, Professor Michael Tam, and Professor Neil McManus for serving as my committee members and for providing me with constructive comments for this thesis.

I also appreciate all financial supports, scholarships, and awards I received during my PhD program: Alexander Graham Bell Canada Graduate Scholarship (NSERC CGS-D), Ontario Graduate Scholarship (OGS), Ontario Graduate Scholarship in Science and Technology (OGSST), Waterloo Institute of Nanotechnology Fellowship (WIN), President's Graduate Scholarship of University of Waterloo, and Murray Moo-Young Biotechnology Scholarship.

I also would like to thank the following individuals who have contributed to the experiments or provided suggestions during my research. Wen Xu and Ran Pan for gel electrophoresis and AFM experiments, Catherine Taylor and Kevin Zheng from professor John Thompson's lab for western blot experiment, Mishi Savulescu from biology department for flow cytometry analysis, professor Thorsten Dieckmann's lab for early ITC experiments, professor David Spafford's lab for fluorescence microscopy, professor Kamahl Haghbeen for his advice on fluorescence spectroscopy and ITC experiments, and Dale Weber for his trainings for confocal microscopy and TEM.

I also want to extend my special thanks to our research group members and visiting scholars:

Sheva Naahidi, Dr. Madjid Soltani, Parisa Sadatmousavi, Kaveh Sarikhani, Dr. Hamid Firouz, Bahram Zargar, Baoling Chen, Tatiana Sheinin, and Professor Nedra Karunaratne for their assistance in performing experiments and contributions to my publications. I am also thankful to undergraduate research assistants who helped me in performing physicochemical experiments: Chad Sweeting, Juno Song, Huara Nadir, Qin Chen, and Arash Farhadi.

I would like to pass my special thanks to all my friends for their supports during my PhD study and their suggestions in thesis preparation: Dr. Keyvan Nowruzi, Dr. Amin Rajabzadeh, Dr. Nima Rezaei, Dr. Navid Omidbakhsh, Dr. Ali Shafiei, Dr. Saeid Mehdiabadi, Dr. Sohrab Zendehboudi and Dr. Ali Mohsenipour and other friends.

Last, but not least, I would like to express my heartfelt appreciation and love to my family for their love and constant encouragement throughout my life. This thesis is dedicated to all of them, especially to my lovely wife, Farzaneh Zaker.

Table of Contents

List of Figures

List of Tables

Nomenclature

Acronym	Full name
AAP	Amino Acid Pairing
ADSA-P	Axisymmetric Drop Shape Analysis-Profile
AFM	Atomic Force Microscopy
ANS	1-Anilinonaphthalene-8-Sulfonic Acid
CAC	Critical Aggregation Concentration
Cav-ME	Caveolae-Mediated Endocytosis
CCK-8	Cell Counting Kit
CD	Circular Dichroism
CDE	Clathrin-Dependent Endocytosis
CHO	Chinese Hamester Ovary
CIE	Clathrin-Independent Endocytosis
CMC	Critical Micelle Concentration
CPP	Cell Penetrating Peptide
Cpz	Chlorpromazine
CTP	Cell Targeting Peptide
CytoD	Cytochalasin D
DLS	Dynamic Light Scattering
DMEM	Dulbecco's Modified Eagle Medium
DMSO	Dimethyl Sulfoxide
DNA	Deoxyribonucleic Acid
DOPC	Dioleoyl Phosphatidyl-Choline
EDTA	Ethylenediaminetetraacetic Acid

eGFP	Enhanced Green Protein Fluorescence
EIPA	5-(N-Ethyl-N-Isopropyl) Amiloride
EPR	Enhanced Permeability Retention
FACS	Fluorescence-Activated Cell Sorting
FBS	Fetal Bovine Serum
GAG	Glycosaminoglycan
GAPDH	Glyceraldehyde 3-Phosphate Dehydrogenase
H.I	Hydropathy Index
HBS	Hepes Buffered Saline
HEPES	4-(2-Hydroxyethyl)-1-Piperazineethanesulfonic Acid
HIV	Human Immunodeficiency Virus
HPLC	High Performance Liquid Chromatography
HSPG	Heparan Sulphate Proteoglycans
ITC	Isothermal Titration Calorimetry
LacCer	Lactosylceramide
MBCD	Methyl-B-Cyclo- Dextrin
MPC	Macropinocytosis
MR	Molar Ratio
mRNA	Messenger RNA
MTT	3-(4,5-Dimethylthiazol-2-Yl)-2,5-Diphenyltetrazolium Bromide
Mw	Molecular Weight
NA	Nucleic Acid
NC	Negative Control
NLS	Nuclear Localization Signal
PAGE	Polyacrylamide Gel Electrophoresis

PAMAM	Polyamidoamine
PBS	Phosphate Buffer Saline
PCI	PhotoChemical Internalization
PEG	Polyethylene Glycol
PEI	Polyethyleneimine
PFA	Paraformaldehyde
PLA	Polylactic Acid
PLGA	Poly(D,L-Lactide-Co-Glycolide)
PMT	Particle-Mediated Transfection
PTGS	Post Transcriptional Gene Silencing
RES	Reticuloendothelial System
RISC	RNA Induced Silencing Complex
RNA	RiboNucleic Acid
RNAi	RNA Interference
SDS	Sodium Dodecyl Sulfate
SEM	Scanning Electron Microscopy
siRNA	short interfering RNA
T/H	Trypsin/Heparin
TAT	Trans-Activation of Transcription
TEM	Transmission Electron Microscopy
THF	Tetrahydrofuran
Tris	Tris(Hydroxymethyl)Methylamine
Trp	Tryptophan
US	Ultra Sound
UV	Ultraviolet

Chapter 1
Introduction

1.1 Overview

Thanks to the genome projects, new classes of pharmaceuticals (peptides, proteins and nucleic acid (NA) based therapeutics) are emerging. These novel drugs have shown promising therapeutic potential in the lab; however, they have experienced only limited success in clinical studies. Poor stability and transport through biological barriers, such as the cell membrane, prevent these drugs from reaching their target(s). These new drugs typically cannot be effectively delivered by conventional means. For instance, conventional liposomes, as drug delivery carriers, have been suffering from major limitations in rapid removal from bloodstream, low drug loading capacity, and physical or chemical instability. Furthermore, the efficacy of many conventional pharmaceutical agents may be improved and the side effects reduced if the drug is continuously released in a controlled manner rather than through conventional burst release techniques [1].

Over the past two decades, we have witnessed tremendous progress in our understanding of the role of RNA molecules in the regulation of gene expression. The main contribution to this progress was offered by the discovery of RNA interference (RNAi) process. First identified in C. elegans by Fire and Mello [2], RNAi is an evolutionarily conserved mechanism that brings about a sequence specific, post transcriptional gene silencing (PTGS) through the use of short RNAs. The basic idea behind RNAi is that a double stranded RNA, termed short interfering RNA or siRNA, complementary to a segment of the mRNA, can be exogenously synthesized and introduced into the cell. This triggers a process which finally degrades the homologous mRNA and inhibits the production of the corresponding protein.

siRNA is a double stranded RNA molecule with 19-23 base-pair core duplex followed by two nucleotides at the 3' end overhang on both the sense and anti-sense strands (Figure 1.1). It can be either produced synthetically or can be a product of the enzymatic cleavage of long dsRNA by RNase III-like enzyme called Dicer [3]. Upon its introduction to the cytoplasm, siRNA assembles into endoribonuclease-containing complex known as RNA-induced silencing complex (RISC). RISC then mediates the unwinding of siRNA duplex. The anti-sense strand of siRNA then directs the RISC to complementary RNA molecule to cleave it. Cleavage of cognate RNA takes place near the middle of the region bound by the siRNA strand [4,5]. Since the cleaved RNA fragments lack either the cap structure m7G or the polyA tail, which are essential to RNA stability, this leads to further degradation of the mRNA molecule (Figure 1.1).

Like other newly-emerging NA-based therapeutics, the major limitations for the use of siRNA are the instability of naked siRNA in physiological conditions and the bloodstream, and the inability to cross the cellular membrane to gain access to the intracellular environment. Due to their small size and hydrophilicity, a significant portion of these NA-based drugs are removed from bloodstream through the reticuloendothelial system (RES). It was also reported that highly charged particles can be recognized by the RES more rapidly than neutral or slightly charged particles [6,7]. Furthermore, the enzymatic degradation of NA based drugs during circulation and within the cell declines their potency, and in some cases an increase of drug dosage is required to compensate these effects. Chemical modifications of siRNA may be applied to improve these characteristics without interfering with its silencing efficiency. Chemical modifications in the sugars, nucleobases, and the phosphate ester backbone of siRNA can significantly increase its nuclease resistance [8-10]. In order to improve cellular uptake, conjugation with hydrophobic functional groups has also been reported [11].

The carrier-mediated delivery system has been recently applied as the main solution to overcome the delivery obstacles and improve the cellular uptake of siRNA therapeutics. The carriers, self-associated or covalently conjugated with siRNA, are designed to enhance cell targeting, prolong

drug circulation time, and improve membrane permeation. Different types of carriers including lipids, peptides, polysaccharides, synthetic and natural polymers, and virus capsids have been applied to improve the delivery of nucleic acids [12].

In this research, a special class of short amphipathic peptides was designed and used to explore their capabilities in encapsulating siRNA and delivering it *in vitro*. The interaction of peptide with siRNA was characterized using several biophysical, thermodynamic, spectroscopic and microscopic approaches. The penetration mechanism of the designed peptide was also identified.

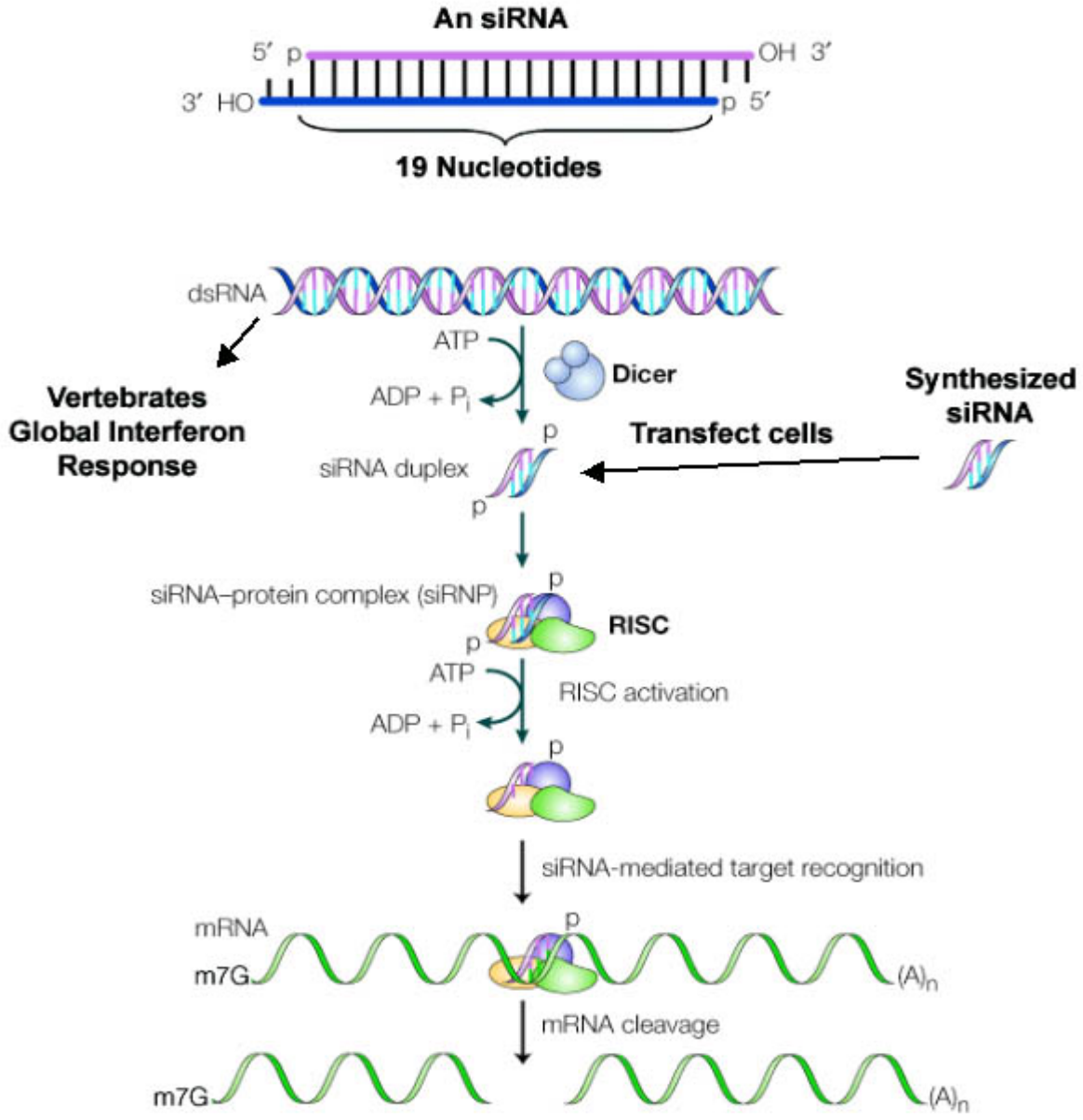

Figure 1.1 The RNA interference process and the biochemical machinery involved. Double-stranded RNA is cut into short pieces (siRNA) by the endonucleases Dicer. The antisense strand is loaded into the RISC complex and links the complex to the mRNA strand by base-pairing. The RISC complex cuts the mRNA strand, and the mRNA is subsequently degraded. (Adapted from [5])

1.2 Research objectives

The main objective of this study was to design and apply a novel class of peptides for siRNA delivery into mammalian cells. To achieve this goal, a comprehensive study of the interaction of peptide with siRNA and cell membrane and also the cellular internalization pathway of the peptide was required.

The specific objectives of this thesis are listed in the following:

1. Design a class of amphipathic peptides considering several parameters such as size, surface charge, self/co-assembly, and siRNA interaction, loading capacity, and penetration ability.
2. Screen the library to evaluate the efficacy of peptides as carriers for siRNA delivery *in vitro*.
3. Conduct experiments for physicochemical characterization of promising peptides and their complexes with siRNA assemblies using several spectroscopic, microscopic, thermodynamic, and biophysical approaches.
4. Perform experiments to identify the major pathway(s) of peptide's cellular uptake.

1.3 Outline of the thesis

This thesis consists of seven chapters. The scope of each chapter is listed as follows:

Chapter 1 gives a brief introduction to siRNA structure, RNAi process, gene delivery systems, and peptides and their applications in gene delivery. The research objectives and the thesis organization are also given.

Chapter 2 provides a review of current gene delivery approaches including physical methods and viral and non-viral carrier-based delivery systems. Different classes of peptides applied in gene delivery are also reviewed.

Chapter 3 introduces peptide C6, a designed amphipathic peptide for siRNA delivery. The design

principles and physicochemical properties of C6 and its complex with siRNA are discussed. Cellular toxicity and uptake of C6 in Chinese hamster ovary (CHO-K1) cells are also reported in this chapter.

Chapter 4 reports the modification of the sequence of peptide C6 to design peptide C6M1. The effect of this modification on peptide solubility, secondary structure, cytotoxicity and cellular internalization are also explained.

Chapter 5 investigates the effect of ionic strength of solution on size, charge, and secondary structure of C6M1. The stability of C6M1-siRNA complexes against serum RNase degradation and the knockdown efficiency of C6M1-GAPDH siRNA complexes in CHO-K1 cells are also studied.

Chapter 6 deals with size-dependent cellular internalization mechanism of C6M1 and its complex with siRNA. The cytotoxicity and specificity of several chemical endocytosis inhibitors and internalization kinetics of C6M1-siRNA complex are also reported.

Chapter 7 summarizes principle outcomes and original contributions of this research and recommendations for future work.

Chapter 2*

Literature review

2.1 Current advances in gene delivery

Gene therapy is based on the substitution or replacement of a defective gene with a functional copy or manipulation of a gene function or expression using short nucleic acids (NAs). Therapeutic NAs comprise DNA (oligonucleotides, plasmid, viruses, artificial chromosomes, and bacteria) and RNA (oligonucleotides, ribozymes, siRNA, mRNA, and viruses). The polyanionic nature and high molecular weight of free nucleic acids prevent them from efficiently crossing the negatively-charged plasma membrane. Inside the cell, further hurdles, such as escape from the endosome and transport to the nucleus, need to be overcome [13]. All these obstacles emphasize the importance and necessity of a safe and effective delivery system.

The two essential components in carrier-mediated gene delivery are the features of the delivery system, carrying the therapeutic to the target site, and the effectiveness of the gene expression at the target site. Several viral and non-viral carriers have been developed to overcome problems associated with naked NA delivery. Viral vectors show high transfection efficiency, but have some serious safety problems such as inflammatory responses and mutagenesis. Non-viral methods are preferred due to their low pathogenicity. However, they tend to have lower efficiency compared with viral vectors in gene transfer in clinical applications. Incorporation of targeting ligands to the non-viral carriers can manipulate and direct the biodistribution of the

---

* This Chapter is adapted from published papers:
M. Jafari, M. Soltani, S. Naahidi, N. Karunaratne, P. Chen, Nonviral approach for targeted nucleic acid delivery, *Current Medicinal Chemistry*, **2012**, 19: 197-208.
M. Jafari, P. Chen, Peptide Mediated siRNA Delivery, *Current Topics in Medicinal Chemistry*, **2009**, 9: 1088-1097

systemically administrated gene to the target cells or tissue, resulting in higher gene expression at the target site [14].

Besides carrier-mediated gene delivery, targeting the therapeutic to the treatment site may be achieved by 'physical targeting' which relies on physical methods. Several methods, such as hydrodynamic delivery, ultrasound (US), electroporation, magnetofection, gene gun or photodynamic therapy where a physical force (mechanical impact, magnetic or electrical field), heat or light is used to target a specific localization have been reported. Local delivery is advantageous over systemic delivery since it avoids first pass hepatic clearance and is likely to reach the target site at higher concentration. Therefore lower doses can be utilized, which may result in fewer side effects and more site specific delivery [15].

In this chapter, the methods utilized for physical targeting of NAs and carrier optimization techniques that have been developed to ensure efficient delivery of NAs have been reviewed.

2.1.1 Physical targeting of nucleic acids

Physical forces such as electric or magnetic field, light, hydrodynamic pressure or mechanical forces are used in some strategies for NA delivery. Some of these approaches have shown high efficiency. These physical methods are further explained here.

2.1.1.1 Naked DNA injection

The main advantage of this method is its simplicity, involving direct plasmid injection, but results in low levels of gene transfer. Several reports on direct injection to various tissue sites have been documented with one example of this method being the intratumoral delivery of a cytosinedeaminase suicide gene [16].

2.1.1.2 Hydrodynamic delivery of NAs

Hydrodynamic delivery employs the force generated by a relatively rapid injection of a large

volume of solution into the bloodstream to overcome the physical barriers of endothelium and cell membranes. This approach introduces naked plasmid DNA into cells in highly perfused internal organs such as liver with a remarkable efficiency [17,18]. Gene delivery efficiency in this method is a function of factors which include the anatomic structure of the organ, the injection volume, and the speed of injection [19]. A large variety of substances with different molecular weights and chemical structures such as small dye molecules, proteins, oligonucleotides, siRNA, and linear or circular DNA fragments can be transferred by this method [20,21]. Naturally this method is nonspecific; therefore, it can be applied to intracellular delivery of any water-soluble compounds, small colloidal particles, or viral particles directly into cytoplasm without endocytosis [19]. However, successful liver transfection has been achieved using balloon catheter–based procedures indicating that with modification, this method can be clinically relevant [22-24].

2.1.1.3 Electroporation

In this method, short-duration electric field pulses are applied to various tissues such as muscle, skin, liver, lung, and tumor after local administration of NAs to overcome the barrier of the cell membrane [25,26]. Although, this method was introduced to handle gene transfer problems, it is now applicable in delivering of a large variety of molecules and materials such as ions, drugs, dyes, tracers, antibodies, oligonucleotides, RNA and DNA, both *in vivo* and *in vitro*. Injection of DNA followed by local electroporation in tumors enhances gene transfer into cells [26-28]. Another example is applying local electroporation in targeting brain region in RNAi induced gene knockdown [29]. New advancements in this method have minimized the cell damaging effects. This approach has been effectively applied in humans in order to increase gene transfer and is now showing promise for application to some diseases such as brain carcinomas, Alzheimer, Parkinson, and depression [25].

2.1.1.4 Ultrasound (US)

This approach facilitates the intratumoral injected DNA delivery into tumor tissues and gene transfer at cellular and tissue levels [30-32]. In a transient process, called sonoporation, US waves cause microbubbles to cavitate, making the cell membrane temporarily more permeable to the therapeutical macromolecules. Several factors such as the frequency, the output strength of the US applied, the duration of US treatment, and the amount of plasmid DNA used are important to transfection efficiency of this method [33]. Recently, vehicles such as gas-filled poly(D,L-lactide-co-glycolide) (PLGA) microparticles were systemically used to encapsulate plasmid DNA and US was applied to destruct the gas core and release the plasmid at the target site [34]. Applying this method, a 10- to 20-fold enhancement of reporter gene expression can be achieved with respect to naked DNA [19]. This method appears to be ideal for noninvasive gene transfer into cells of the internal organs as it is able to target deep tissues with minimum damage [19,26].

2.1.1.5 Gene gun

Particle-mediated transfection (PMT) or gene gun is a useful approach of non-viral gene transfer in cancer therapy. Recent studies show that this approach is an efficient non-viral transfection method for a system in which high-level of gene expression is not required [35]. In this approach, a helium gas gun shoots DNA, coated on the surface of microscopic biocompatible heavy metal (gold or tungsten) beads, into the tissue in which target cells are in the upper cell layers of tissue. The main applications of this method are DNA vaccination and cytokine gene therapy [36].

2.1.1.6 Photochemical internalization (PCI)

Photodynamic therapy is an emerging technique which can be applied efficiently for NA delivery to a specific light-exposed site. For instance, in order to improve endosomal escape of NAs, Høgset *et al.* [37] developed a new technique, photochemical internalization (PCI), in

which photosensitizing compounds localized in endocytic vesicles can be excited by the light in a specific wavelength and initiate photochemical reactions. The result of this procedure is the destruction of endocytic membrane structures with the release of co-endocytosed NAs into the cell cytosol. Applying this method, recent studies show promising results in improving the efficiency of NA/polycation polyplexes, including EGF receptor-targeted polyplexes [38].

2.1.2 Carrier-mediated nucleic acid delivery

2.1.2.1 Viral vectors

The gene delivery vectors can be generally categorized into viral and nonviral vectors. Typically, viral systems are the most effective carriers for gene delivery. A virion is made up of genetic materials protected by a protein coating, which is referred to as capsid. Virus capsids or virus-like particles are made up of multiple copies of one or a few proteins. Drug particles can be loaded within the capsid or grafted on the exterior. Also, various types of molecules such as fluorophores, antibodies, and peptides can be conjugated to specific locations on the capsid surface for cell targeting, to act as probes, or to improve solution properties of carrier-drug complexes [12].They can selectively target cells and usually possess a high transfection efficiency [12]. However, their isolation from biological sources and their processing can be very costly. Furthermore, the safety risks due to their oncogenic potential and their inflammatory and immunogenic effects have limited the clinical application of the strategies based on viral vector delivery [39,40]. New generation of adenoviral vectors, where all viral coding genes are removed, have shown high transfection efficiency with significantly reduced cytotoxicity [39,40].

2.1.2.2 Non-viral vectors

Although viral vectors possess many of the desired characteristics for efficient NA delivery, nonviral vectors offer several advantages. Due to their lack of immunogenicity, synthetic vector systems are usually safer than viral vectors. In addition, they can be easily modified and

produced in large scale. A wide spectrum of materials has been engineered and developed to obtain desired capabilities to act as carriers for drug/gene delivery. They may include lipids [41,42], polymers [43,44], peptides [45,46], gold particles [47], and ceramics [48]. Among them, lipids and polymers have been widely applied in gene delivery.

2.1.2.2.1 Lipids

siRNA molecules are associated with liposomes mainly via electrostatic interaction with the charged head group. Among the non-viral drug carrier systems, liposomes represent a mature technology for both drug and gene delivery [42,49]. However, some issues have led to limited clinical usage of the liposomal systems. The immune system, which tracks foreign materials for destruction, can be a major obstacle to liposomes. Furthermore, the lipid toxicity and lack of long term expression and targeting are problems associated with their use *in vivo* [50,51]. Recent studies based on neutral liposomes have shown promising results. Delivery of siRNA for cancer treatment using neutral liposomes based on Dioleoyl phosphatidyl-Choline (DOPC) carriers will be going into Phase 1 clinical trials since safety studies have been completed or are underway in mice and in nonhuman primates [52]. These researchers have found that neutral nanoliposomal siRNA is a safe and effective delivery system for intratumoral administration. An indepth analysis on the use, design and stability of lipid-based carriers for therapeutic siRNA delivery is reviewed by Schroeder *et al.* [53].

2.1.2.2.2 Polymers

Synthetic and natural polymers, made up of repeated units of covalently bonded monomers, are other classes of non-viral macromolecules which have been widely used as carriers for various drug molecules over the past three decades. In particular, such synthetic polymers as polylactic acid (PLA) and polylactic-co-glycolic acid (PLGA) are very attractive, as compared to biopolymers, since they can be produced in high quantity for relatively low costs. Among the cationic polymers, polyethyleneimine (PEI) has been widely examined for siRNA delivery

[54,55]. Chitosan [56], polyamidoamine (PAMAM) [57], and poly ß-amino esters [58] are other examples of cationic polymers, employed in gene delivery.

Over the past few years, there have been several drug delivery systems developed that rely on organic polymer technology. Such delivery systems are based on drug entrapment within micelles [59,60], nanoparticles or the hydrophobic corona formed by block copolymers [44,61], and they are used to improve solubility and protection of drugs. In particular, polyethylene glycol (PEG) is one of the most frequently used polymers for drug delivery with high water solubility, biocompatibility and chain flexibility [62,63]. In some cases, it was employed to help protect the siRNA due to its minimum interaction with serum proteins. It was also found that covalent attachment of the PEG to the siRNA or its delivery system enhanced stability and efficient delivery to targeted sites [64,65].

2.2 Different classes of peptides in gene delivery

Peptides are short sequences of amino acids, usually 30 or less amino acids, covalently linked through an amide or peptide bond. Considering the safety concerns and efficacy issues, peptide-based drug/gene delivery constructs are emerging as alternatives for safe and efficient delivery means since the 1990s. Due to their relatively high polarity, it was generally believed that peptides would be unable to translocate through cell membrane. However, the complex nature of the cell membrane was neglected. The rationale for peptide mediated NA delivery initially evolved from the biochemical knowledge that the active sites of enzymes, receptor ligands and antibodies involve about 5 to 20 amino acids. Thus, it should be possible to design small synthetic peptides to mimic the active sites of proteins, especially the sites which are responsible for cell penetration, and formulate synthetic peptide based drug/gene delivery systems that may be as efficient as viruses without their limitations. Peptide-based delivery systems have the potential to deliver therapeutic proteins, bioactive peptides, small molecules, and any size nucleic acids [66-68].

Several peptides investigated as NA carriers are of biological origin which makes them biodegradable and likely to be biocompatible. For example, cell penetrating peptides (CPPs) [66], fusogenic peptides [69], and receptor-based targeting peptides [70] are derived from existing cellular or viral proteins. The main attraction of the peptide carriers is their versatility, through the use of the 20 naturally occurring amino acids, each with different hydrophobicity, size, and other solution properties. Because of their diversity and versatility in design, through the use of amino acids with different physicochemical properties, peptides might be the only biomaterials which can actually play all the roles to safely and efficiently deliver genes to the target sites. Cationic peptides rich in basic amino acids can electrostatically interact with small NAs or condense DNA into small stable particles. CPPs can facilitate the translocation of the complex through the cell membrane. Histidine-rich pH-sensitive or fusogenic peptides can enhance the endosomal escape and cytoplasmic release of the gene complex. Involvement of CTPs in gene delivery systems mediates cell and/or tissue-specific targeting. Finally, attachment of a nuclear localization signal NLS peptide improves nuclear localization of the gene complex [66].

The secondary structure of peptides seems to play an important role in the cell membrane translocation. Depending on the sequence and the solvent, a peptide can attain such secondary structures as an α-helix or β-pleated sheet. The importance of α-helical [71] and β-sheet [72] structures to membrane translocation has been discussed previously. However, some peptides, such as oligoarginine, can also deliver drugs across the cell membrane in the random coil conformation, indicating that the secondary structure is not the only factor that determines cellular uptake of drug molecules [73].

In the next sections, different classes of peptides employed in gene delivery including protein-derived CPPs, cationic peptides, and model amphipathic peptides, cell targeting peptides (CTP) [70], and peptides containing a nuclear localization signal [74] will be discussed.

2.2.1 Protein-derived cell penetrating peptides

A cell penetrating peptide, by definition, is a relatively short peptide, 5-40 amino acids, with the ability to gain access to the cell interior by means of different mechanisms and with the capacity to promote the intracellular delivery of covalently or noncovalently conjugated bioactive cargoes. The mechanism(s) by which peptides enter the cell and mediate the entry of cargo molecules inside the cell are still not understood in any detail. In the early 1990s, the discovery of CPPs led to proposals of direct entry mechanism [66]. In general, cellular uptake can either be energy dependent or independent. The energy dependent pathways for cells generally include macropinocytosis, clathrin-mediated endocytosis, and caveolin-mediated endocytosis [75]. Endocytotic mechanisms were almost ruled out in the present cases because the translocation could be observed at low temperature. The most discussed energy independent cellular uptake mechanism is inverted micelle based [76]. In this model, the peptide first associates with the bilayer surface through electrostatic interaction. The lipid bilayer reorganizes the peptide-cargo complex, and minimizes the exposure of the complex to the solvent, which eventually leads to the formation of an inverted micelle in the bilayer and is later released to the cytosol.

Table 2.1 shows a number of CPPs derived from some viral proteins. These peptides are the shortest peptide sequences responsible for cell penetration in the corresponding viruses. Among these peptides, penetratin and Tat are the most studied peptides. Penetratin is the third α-helix of Antennapedia, a membrane transduction protein [77]. It is internalized by energy-independent mechanism at both 4 and 37 °C, and has access to the cytoplasm and nucleus. The presence of three lysine residues confers to the peptide an isoelectric point above 12. It has α- helical structure in a hydrophobic environment but is poorly structured in aqueous solution. Experiments have shown that the basic amino acids and the tryptophan residue at position 6 of the peptide (48 of Antp) are essential to cellular uptake of penetratin [78]. Moreover, the α-helical structure is not essential to membrane translocation since disturbing the secondary structure of the peptide by point mutation with proline did not prevent its internalization [79].

Table 2.1 Sequences of some protein-derived CPPs

Peptide	Origin	Sequence	Reference
Penetratin (43-58)	Antennapedia	RQIKIWFQNRRMKWKK	[80]
Tat (48-60)	HIV-1	GRKKKRRQRRRPPQ	[81]
Transportan	Galanin-wasp venom	GWTLNSAGYLLGKINLKALAALAKKIL	[82]
pVEC		LLIILRRRIRKQAHAHSK	[83]
peptide mu	Adeno virus	MRRAHHRRRRASHRRMRGG	[84]
E5	Influenza virus	GLFEAIAEFIEGGWEGLIEG	[85]
E5CA	Influenza virus	GLFEAIAEFIEGGWEGLIEGCA	[86]
E5WYG	Influenza virus	GLFEAIAEFIEGGWEGLIEGWYG	[87]
gp41 fusion	Influenza virus	GALFLGWLGAAGSTMGA	[88]
H5WYG	Influenza virus	GLFHAIAAHFIHGGWHGLIHGWYG	[89]
HA	Influenza virus	GLFEAIAGFIENGWEGMIDG	[90]
HBV		PLSSIFSRIGDP	[91]
hCT		LGTYTQDFNKFHTFPQTAIGVGAP	[92]
Integrin		VTVLALGALAGVGVG	[93]
INF-1	Influenza virus	GLFEAIAGFIENGWEGMIDGGGC	[94]
INF-7	Influenza virus	GLFEAIEGFIENGWEGMIDGWYG	[95]
K5	Influenza virus	GLFKAIAKFIKGGWKGLIKG	[96]
Melittin	venom of Apis	GIGAVLKVLTTGLPALISWIKRKRQQ	[97]
MPM	K-FGF	AAVALLPAVLLALLAP	[98]
PDX-1		RHIKIWFQNRRMKWKK	[99]
SynB1	Protegrins	RGGRLSYSRRRFSTSTGR	[100]

Discovered in 1988 by two independent groups, trans-activating transcriptional activator (Tat)

from Human Immunodeficiency Virus 1 (HIV-1) can be efficiently taken up from the surrounding media by numerous cell types in culture [46,101]. The Tat protein has 86 amino acids but only the cluster of basic amino acids, RKKRRQRRR, residues 49 to 57, is responsible for the cell penetrating property of the Tat peptide. Due to charge repulsion resulting from six arginine and two lysine residues, the Tat peptide undergoes a random coil configuration in solution. The Tat peptide has been successfully used to deliver oligonucleotides [102], proteins [103], and fluorophores [104] in both *in vitro* and *in vivo* models.

2.2.2 Cationic peptides

Basic amino acids, such as lysine (K) and arginine (R), are positively charged in physiological pH; thus, they can interact with negatively charged drug molecules, such as siRNAs, and cell membranes through columbic interactions. Fuchs *et al.* reported that the oligomers of the four cationic amino acids, arginine, lysine, histidine, and ornithine can cross the cell membrane and be localized in the cytosol and the nucleus [105]. Due to the removal of highly charged oligolysine by the RES, the transfection efficiency of therapeutic materials delivered by oligolysine is generally low [6,7]. Various methods have been employed to increase its efficiency. It was found that incorporation of cysteine in a lysine-rich peptide allows the formation of disulfide bond between peptide molecules, resulting in smaller complexes and lower opsonisation rate compared with uncross-linked complexes [106]. Also, the disulfide bond reduction in the cytosol triggers the release of NAs, resulting in higher *in vitro* transfection efficiency [107]. Bhadra *et al.* have also reported that Conjugation of oligolysine with PEG can increase transfection efficiency and protect it from serum attacks [63].

2.2.3 Designed Amphiphilic Cell Penetrating Peptides

Since the lipid bilayer of a cell membrane is amphiphilic, it seems reasonable to employ an amphiphilic peptide to carry a drug across the cell membrane. In this delivery model, the hydrophilic section of the peptide first interacts with the membrane surface with subsequent

translocation to the cytosol assisted by the hydrophobic section of the peptide. There are two major types of amphiphilic cell penetrating peptides, namely primary and secondary amphiphilic peptides (Figure 2.1). Primary amphiphilic peptides have specific hydrophobic and hydrophilic domains joined by a linker in the primary sequence. The hydrophobic region can interact with hydrophobic drugs and anchor itself in the cell membrane. The hydrophilic region, on the other hand, interacts with hydrophilic drugs and the cell membrane surface through electrostatic interactions. In general, the primary amphiphilic peptides adopt a random coil structure at neutral pH but a defined secondary structure upon a change in pH or interaction with the cell membrane [72,108]. The high efficiency of primary amphiphilic peptides may be attributed to the change in secondary structure at low pH, which can induce leakage of the endosomal membrane and facilitate endosomal escape of carrier-drug complexes.

In secondary amphiphilic peptides, the amphiphilic nature of the molecule is originated from its secondary structure, i.e., α-helix or β-sheet structures. Many peptide delivery carriers are designed based on α-helix amphiphilicity [71,109] while investigations based on amphiphilic β-sheet peptides are relatively limited [72,110]. Secondary amphiphilic peptides can be embedded in the cell membrane so that the hydrophobic side is anchored in the hydrophobic core of the bilayer and the hydrophilic side interacts with the hydrophilic heads of the lipid bilayer. Alternatively, the peptides can first form micelles or aggregates to minimize the exposure of hydrophobic residues to the solvent, and then associate with the cell membrane. One example of this class of peptides is model amphiphilic peptide (MAP) with a sequence of KLALKLALKALKAALKLA [101]. Table 2.2 shows some sequences of amphiphilic cell penetrating peptides and their types of amphiphilicity.

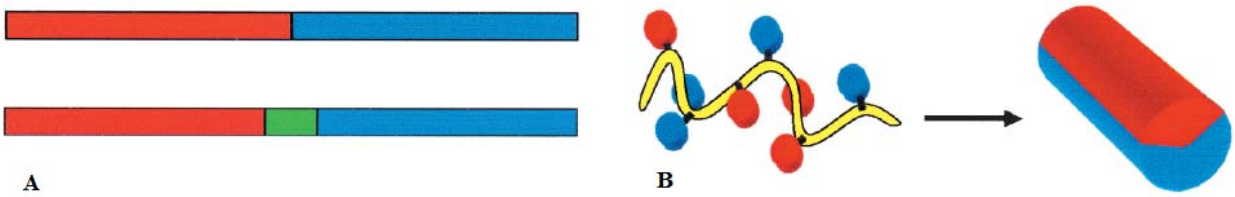

Figure 2.1 Schematic representation of amphiphilic peptides. (A) In a primary amphiphilic peptide, hydrophobic and hydrophilic segments at the opposite ends of the peptide can be separated by a linker, usually polyglycine (green), (B) A secondary amphiphilic peptide requires adapting a secondary structure (helical conformation) to attain amphiphilicity. In this arrangement, the hydrophobic and hydrophilic residues face opposite sides of helical structure [111].

MPG was the first peptide used to introduce siRNA into cells. It consists of a hydrophobic domain derived from a HIV gp41 fusion sequence GALFLGFLGAAGSTMGA and a nuclear localization sequence (NLS) KSKRKV, joined through a linker WSQP [72]. The linker domain contains a proline residue, which improves the integrity of both hydrophobic and hydrophilic domains. The sequence of MPG has been modified by a single mutation of a lysine residue in NLS to a serine residue in order to limit its nuclear translocation and rapid release of the cargo in the cytoplasm. The resulting peptide, $MPG^{\Delta NLS}$, MPG with mutated NLS sequence, has shown high efficiency in siRNA delivery as the target site of the siRNA is the cytoplasm. MPG family mediated delivery of siRNA has shown significant gene knock-down both *in vitro* [112-117] and *in vivo* [66]. The Divita group has also recently reported high siRNA delivery efficiency of CADY peptide in different cell lines [118].

Table 2.2 Amphiphilic cell penetrating peptides

Names	Sequence	Amphiphilicity	Reference
CADY	GLWRALWRLLRSLWRLLWRA	Secondary	[118]
MPG	GALFLGFLGAAGSTMGAWSQPKKKRKV	Primary	[72]
MPG-NLS	GALFLGFLGAAGSTMGAWSQPKSKRKV	Primary	[72,119]
Pep-1	KETWWETWWTEWSQPKKKRKV	Primary	[120]
Pep-2	KETWFETWFTEWSQPKKKRKV	Primary	[120]
GALA	WEAALAEALAEALAEHLAEALAEAEALEALAA	Secondary	[121]
KALA	WEAKLAKALAKALAKHLAKALAKALKACEA	Secondary	[122]
MAP	KLALKLALKALKAALKLA	Secondary	[123]
SP	MGLGLHLLVLAAALQGAWSQPKKKRKV	Primary	[124,125]
SP-NLS	MGLGLHLLLAAALQGAKKKRKV	Primary	[124,126]
SPM	MGLGLWLLVLAAALQGAKKKRKV	Primary	[127]
Transportan	GWTLNSAGYLLGKINLKALAALAKKIL	Primary	[82]
Hel 9-9	KLLKKLLKLWKKLLKKLK	Secondary	[109]
Hel 11-7	KLLKLLLKLWKKLLKLLK	Secondary	[109]
Hel 13-5	KLLKLLLKLWLKLLKLLL	Secondary	[109]}
[Pa]	GALFLAFLAAALSLMGLWSQPKKKRKV	Primary	[72]
[Pb]	GALFLGFLGAAGSTMGAWSQPKKKRKV	Primary	[72]
gp41 fusion	GALFLGWLGAAGSTMGA	Primary	[128]

2.2.4 Cell targeting and NLS containing peptides

Because of their small size and biocompatibility, short cell targeting peptides (CTPs) are emerging as alternatives to monoclonal antibodies for targeting purposes. These peptides can directly bind to cell surface receptors or the endothelial cell surface of tumor vasculatures. This ability to specifically target a specific cell/tissue could significantly reduce the required drug dose and potential side effects. Among all CTPs, RGD is the most used and investigated peptide. This short segment of fibronectin protein has shown high affinity to most integrins, the cell surface glycoproteins over-expressed in neovasculature of tumor sites [129]. Several attempts have been made to improve the affinity and specificity of RGD peptide to the integrins by modification of the RGD sequence, *e.g.* cyclization of RGD [130]. This simple modification showed 200-fold more affinity for binding $\alpha_V\beta_3$ integrins than linear RGD [131].

2.2.5 Peptide-siRNA conjugates/complexes

In order to enhance the cellular uptake and gene silencing efficiency, siRNA should properly bind or co-assemble with its carrier molecules. Two different strategies are mainly applied to form peptide-siRNA conjugates: either peptides are covalently attached to siRNAs, or they interact through electrostatic interactions to form non-covalent complexes.

2.2.5.1 Covalent peptide-siRNA conjugates

Covalent attachment of peptides to siRNA molecules offers a potential strategy for peptide-mediated siRNA delivery. It can be of several advantages for *in vivo* applications, including reproducibility of the procedure, and control of the stoichiometry of peptide/siRNA ratios. Also, less peptide is required in this method as compared to non-covalent strategies. This is especially important if the peptide shows toxicity in high concentrations. Several options are available for covalent conjugation of peptides to NAs, including the use of cross-linking agents, triplehelix-forming oligonucleotides, and chemical attachment to the end of linear NAs [66,132]. The main method applied for the peptide-siRNA conjugation is disulfide linkage, which is cleaved in the cytosol due to its reducing environment. There are limited literature (Table 2.3), reporting significant gene silencing through covalent attachment of peptides and siRNAs as it is suspected to alter the biological activity of siRNA molecules [133].

2.2.5.2 Non-covalent peptide-siRNA complexes

As an alternative to covalent strategies, non-covalent interactions of carrier peptides and cargos have recently been developed. Positively charged peptides can interact with the negatively charged backbone of siRNA through non-specific electrostatic interactions, providing cell permeability for siRNA molecules by covering the siRNA surface with positive charges of the peptides. This is a very simple and effective strategy for carrier mediated siRNA delivery without any need to chemical modification of siRNA. However, if high peptide/siRNA molar ratios are applied, the high concentration of positively charged peptides may induce some side-

effects through interactions with anionic molecules in the cell. The molar excess of the peptide as compared to siRNA can also yield complexes of varying sizes. This could be considered as a disadvantage of this strategy as a certain size of complexes is required in most therapeutic applications. One example of peptides employing this strategy is MPG as we discussed before. Table 2.3 lists some reports of using non-covalent peptide-siRNA complexes for RNAi.

Table 2.3 siRNA delivery by covalent and non-covalent peptide-siRNA conjugates/complexes

Peptide	Cell line	Target gene	Reference
Covalent conjugates			
Tat	NIH-3T3 MDR	MDR1	[134]
Tat	Hela	P38	[135]
Penetratin	Neuron	SOD1	[136]
Penetratin	CHO	Luciferase	[137]
Transportan	CHO	Luciferase	[137]
Non-covalent complexes			
CADY	U_2OS	GAPDH	[118]
MPG, MPG-NLS	HS-68	GAPDH	[117]
MPG, MPG-NLS	Hela	Luciferase	[117,138]
MPGα	ECV304	Luciferase	[139]
H2A-Penetratin	Hela	Luciferase	[140]
Bprp	Hela	Luciferase	[140]
Tat	CHO	EGFP	[141]

Chapter 3*

A New Amphipathic, Amino Acid Pairing (AAP) Peptide as siRNA Delivery Carrier: Physicochemical Characterization and *in vitro* Uptake

RNA interference has emerged as a powerful tool in biological and pharmaceutical research. However, the enzymatic degradation and polyanionic nature of short interfering RNAs (siRNAs) lead to their poor cellular uptake and eventually biological effects. Among non-viral delivery systems, cell-penetrating peptides (CPPs) have been recently employed to improve the siRNA delivery efficiency. Here, we introduce an 18-mer amphipathic, amino acid pairing peptide, C6, as an siRNA delivery carrier. Peptide C6 adopted a helical structure upon co-assembling with siRNA. The C6-siRNA co-assembly showed a size distribution between 50 and 250nm, confirmed by dynamic light scattering and atomic force microscopy. The C6-siRNA interaction enthalpy and stoichiometry were 8.8 $kJ.mol^{-1}$ and 6.5, respectively, obtained by isothermal titration calorimetry. A minimum C6:siRNA molar ratio of 10:1 was required to form stable co-assemblies/complexes, indicated by agarose gel shift assay and fluorescence spectroscopy. Peptide C6 showed lower toxicity and higher efficiency in cellular uptake of siRNA, compared with Lipofectamine 2000. Fluorescence microscopy images also confirmed the localization of C6-siRNA complexes in the cytoplasm using Cy3-labeled siRNAs. These results indicate high capabilities of C6 in forming safe and stable complexes with siRNA and enhancing its cellular uptake.

---

* This chapter is adapted from a paper "M. Jafari, W. Xu, S. Naahidi, B. Chen, and P. Chen, A New Amphipathic, Amino Acid Pairing (AAP) Peptide as siRNA Delivery Carrier: Physicochemical Characterization and *in vitro* Uptake. *J. Phys. Chem. B*, **2012**, 116: 13183–13191".

3.1 Introduction

The field of gene therapy has witnessed significant expansion over the past decades. The discovery of RNA interference (RNAi) offered the main contribution to this growth. RNAi is a highly regulated process, in which double-stranded, short interfering RNA, siRNA, cleaves the complementary messenger RNA (mRNA), causing post-transcriptional gene silencing (PTGS) [2]. This sequence-specific gene knockdown eventually hinders the production of the target protein in a highly specific manner. This exceptional feature of RNAi makes it a valuable tool in studying gene function and signaling pathways, as well as developing siRNA-based pharmaceutical agents.

However, despite abundant promise, the translation of RNAi to a realistic therapeutics has faced serious obstacles. The large size and polyanionic nature of free siRNAs prevent them from translocating across the negatively-charged cell membrane. Moreover, without protection, siRNAs are subject to enzymatic degradation in physiological conditions. These highlight the importance of developing an efficient siRNA delivery system, which can (i) interact with siRNA and condense it into small nanoparticles, (ii) protect siRNA against degradation, (iii) cross the cell membrane, and (iv) release siRNA to the target site, i.e., cytosol. Several non-viral siRNA delivery systems, including polymers [142-144], lipids [41,42,49], and peptides [45,118,133,145,146], have been developed for this purpose.

Cell penetrating peptides (CPP), net positively charged peptides with less than 30 amino acids, have been widely applied to deliver cargos into cells. Despite numerous reports on CPP's high efficiency, their cellular uptake mechanism is still under debate. Several pathways including energy-dependent endocytosis [147,148] and direct translocation [149,150] have been proposed as the major uptake mechanism of CPPs. The interaction of CPP with the cargo can occur through either chemical linkage or non-covalent forces. Considering the negatively-charged backbone of siRNA, the non-covalent electrostatic interaction is usually preferred to obtain stable peptide-siRNA complexes without any need for chemical linkage or modification of

siRNA.

Considering the amphiphilic nature of the cell membrane, most CPPs possess both hydrophilic and hydrophobic moieties. The hydrophilic side interacts with the hydrophilic heads of the lipid bilayer, and hydrophilic drugs/genes through electrostatic interaction, while the hydrophobic side is anchored in the hydrophobic core of the bilayer, triggering the endocytosis pathways or assisting the direct translocation of peptide-cargo to the cytosol. The amphiphilicity of the peptides may evolve from their primary structure, *e.g.*, MPG [72], or secondary structure, *e.g.*, penetratin [80], and CADY [118]. In the latter case, the peptide needs to adapt a helical structure in order to organize hydrophilic and hydrophobic moieties at different sides of the peptide [80,118].

Over the past several years, we have been studying the concept of amino acid pairing (AAP) and have established principles to design peptides to form a variety of stable nanostructures, such as fibers, rods, tubes, and globules [146,151-154]. Different mechanisms including electrostatic, hydrogen bonding, hydrophobic, and π-π stacking are incorporated in peptide assembly. Applying this strategy, we designed the 18 amino acid peptide, C6, as siRNA delivery carrier.

Three types of amino acids were incorporated in the design of C6 peptide (Ac-RLLRLLLRLWRRLLRLLR-NH_2). i) Seven arginine residues to interact with siRNA and cell membrane. Positively charged arginine residues can interact with the negatively charged phosphate groups on the siRNA backbone via ionic interactions. These basic residues also interact with negatively charged cell surface proteoglycans to initiate their cellular uptake [155]. CPPs with six to nine arginine residues have been reported to have the highest translocation efficiency [156]. ii) Ten leucine residues to induce the amphiphilicity and helicity to the peptide structure. These hydrophobic residues are found abundantly in the helical regions of proteins [157]. They also interact with hydrophobic tails of lipid bilayer and facilitate the translocation of peptide [66]. iii) An aromatic tryptophan residue incorporated in the middle of the sequence for

use as an intrinsic fluorescence probe to study the structural change of the peptide upon changing the environment or interaction with siRNA.

As each turn of a peptide helix includes 3.6 residues, arginine residues were distributed along the peptide sequence in three or four residue intervals, so when the helical structure is formed, they all face the same side of the helix (Figure 3.2A). This induces amphiphilicity to the peptide structure as polar (R) and non-polar (L, W) residues face opposite sides, when the peptide adopts a helical structure. This arrangement of amino acids facilitates the self-assembly of the peptide, mainly through hydrophobic interaction of leucine faces of the helices. Furthermore, the presence of all arginine residues on the hydrophilic face of the helix facilitates ionic interaction of positively charged residues with the siRNA backbone, maximizing the loading capacity of the peptide.

This chapter will focus on physicochemical characterization of C6 and its co-assembly/complex with siRNA, as well as C6-mediated cellular uptake of siRNA, using several biophysical, spectroscopy and microscopy approaches.

3.2 Experimental Methods

3.2.1 Peptide and siRNA

The C6 peptide (Ac-RLLRLLLRLWRRLLRLLR-NH_2, MW=2470.2 g/mol) was purchased from CanPeptide, Inc. (Quebec, Canada). High performance liquid chromatography (HPLC) analysis indicated that the synthetic peptide was at least 98% pure. The unlabelled (AM4624) and 5' cy3 dye labeled glyceraldehyde 3-phosphate dehydrogenase (GAPDH) siRNA (AM4649) were purchased from Ambion (Austin, USA). The siRNA used in agarose gel electrophoresis and fluorescence spectroscopy is eGFP siRNA, which was purchased from Dharmacon with an

extinction coefficient of 362408 L/mol cm. The sense sequence is GACGUAAACGG CCACAAG UUC and antisense sequence is ACUUGUGGCCGU UUACGUCGC.

3.2.2 Cell culture

The CHO-K1 (Chinese hamster ovary) cells were purchased from American Type Culture Collection (ATCC CCL-61). Cells were cultured in F-12K (Thermo Scientific, Ottawa, Canada) supplemented with 10% FBS (Sigma-Aldrich, Oakville, Canada). Cells were incubated at 37 °C in a humidified atmosphere containing 5% CO_2.

3.2.3 Preparation of peptide-siRNA co-assembly/complex

The C6 peptide was prepared by dissolving peptide powder in RNase free water. A stock solution of 1mM was made and diluted at desirable concentrations for various experiments. The solution was vortexed for 10 seconds and sonicated for 10 minutes in a tabletop ultrasonic cleaner (Branson, model 2510, USA). siRNA was diluted in RNase free water to a concentration of 50μM. Peptide-siRNA complexes were formed by adding peptide solution into siRNA in proportion according to the designed experiment. The complexes were incubated for 20 minutes at room temperature before each experiment.

3.2.4 Dynamic Light Scattering (DLS) and Zeta potential

The hydrodynamic diameter of the peptide C6 self-assemblies/aggregates (4 μM) and the C6-siRNA co-assemblies/complexes were measured on a Zetasizer Nano ZS (Malvern Instruments, U.K.) equipped with a 4 mW He-Ne laser operating at 633 nm. Samples at molar ratios of 10:1, 20:1 and 40:1 with final siRNA concentration of 100nM were prepared as mentioned above. A quartz microcell (45 μL) with a 3 mm light path was used and the scattered light intensities were collected at an angle of 173°. Clear disposable zeta cells were used for Zeta potential measurements. The intensity-based size distribution and zeta potential values were acquired using the multimodal algorithm CONTIN, Dispersion Technology Software 5.0. Three

independent measurements were performed for each sample 20 min after sample preparation at 25°C.

3.2.5 Atomic Force Microscopy (AFM)

The nanostructures of peptide C6 (40μM) and C6-siRNA (molar ratio of 40:1) complex were characterized by AFM. The sample solution (10 μl) was placed on a freshly cleaved mica surface, fixed on a glass slide, and incubated for 30 min at room temperature to allow the sample to adhere onto the mica surface. The mica was then rinsed five times with Milli-Q water to remove any unattached particles, followed by air-drying overnight. The mica surface was analyzed by a PicoScan^{TM} AFM (Molecular Imaging, Phoenix, AZ) at room temperature using the tapping mode with silicon single-crystal tips (NCL type, Molecular Imaging, Phoenix, AZ), with a typical tip radius of 10 nm and resonance frequency of <170 kHz. A scanner with the maximum scan size of 5 μm × 5 μm was used. All AFM images were obtained at a resolution of 512 × 512 pixels on a scale of 2 μm × 2 μm.

3.2.6 Circular Dichroism (CD) spectroscopy

Spectra from 250 to 190 nm with spectral resolution and pitch of 1 nm and scan speed of 200 nm/min were recorded with a J-810 spectropolarimeter (Jasco, USA). Increasing amounts of siRNA were added to a fixed peptide concentration of 20 μM to obtain different molar ratios. Samples were transferred into 1 mm long quartz cells and maintained at 25°C. Spectra shown are the average of three replicates.

3.2.7 Isothermal Titration Calorimetry (ITC)

Isothermal titration calorimetry experiments were conducted on a Nano-ITC calorimeter (TA Instruments) with a cell volume of 174 μl. The peptide C6 (250 μM) and siRNA (6 μM) were prepared in RNase-free water. All samples were degassed in a degassing station (TA Instruments) prior to experiments. Milli-Q water was used in the ITC reference cell. For each

titration, 2 µl of the peptide in a pipette stirring at 300 rpm was automatically added to siRNA solution in the sample cell of the calorimeter, equilibrated at 25°C, with an interval of 300s between injections. The heat of dilution was measured by titrating C6 solution into RNase free water and subtracted from the measured sample heat. A single site independent model was used to determine the binding constant (K), stoichiometry (n), and the binding enthalpy (ΔH), using NanoAnalyze software v.2.3.0. The change in free energy (ΔG) and entropy (ΔS) were calculated using the equations $\Delta G = -RT\ln K$ and $\Delta G = \Delta H - T\Delta S$, respectively, where R is the gas constant, T is absolute temperature, and K is the equilibrium constant.

3.2.8 Agarose gel-shift assay

The ability of C6 to co-assemble with siRNA was investigated by agarose gel (1.2% wt/vol) shift assay. siRNA was incubated for 30 minutes at 37°C in RNase free water with different concentrations of C6 to obtain peptide:siRNA molar ratios ranging from 1:1 to 80:1. The samples (10 µl containing 0.3 µg of siRNA per well) and loading dye were loaded to each well and electrophoresis was carried out at a constant voltage of 55V for 1.5 h in TBE buffer (4.45 mM Tris–base, 1 mM sodium EDTA, 4.45 mM boric acid, pH 8.3) containing 0.5 µg/ml ethidium bromide.

In the case of heparin competition, different amounts of heparin corresponding to final concentrations from 0.5 to 10 µg heparin per 10 µl of complex were added to C6/siRNA complexes at molar ratios of 15:1, 40:1, 60:1, and 80:1. Ten microliters of each sample, corresponding to 50 pmol of siRNA, was then analyzed by electrophoresis on agarose gel (1.2% wt/vol) stained with ethidium bromide.

3.2.9 Fluorescence spectroscopy

Since the peptide C6 has a tryptophan (Trp) residue, which is an important intrinsic fluorescent probe, fluorescence spectroscopy was applied as a powerful technique to characterize the

interaction between siRNA and peptide. The peptide fluorescence was acquired on a Photon Technology International spectrafluorometer (Type LS-100, London, Canada) with a pulsed xenon lamp as the light source. Samples (80 µl) were transferred to a quartz cell (1cm×1cm) and excited at 280 nm and spectra were collected in the range of 300nm-500nm. The standard fluorescence intensity I_s was obtained by taking the average of the fluorescence of C6 only sample from 480 to 500 nm. Different volumes of siRNA stock solution were added to the fixed peptide concentration of 160 nM to obtain peptide:siRNA molar ratio from 80:1 to 1:1.

Cy-3 labeled siRNA was also used as an extrinsic fluorescent probe, and the change in fluorescence spectra was studied at a fixed concentration of siRNA (2 µM) and increasing concentration of peptide to achieve different molar ratios. The samples were excited at 540nm and spectra were collected in the range of 550-800 nm. The spectra were normalized by taking I_s as the average of the fluorescence of Cy-3 siRNA only sample from 780 to 800nm.

3.2.10 Cytotoxicity

CHO-K1 cells were used for *in vitro* cellular toxicity studies of C6 and C6-siRNA complexes. Cells were detached from the flasks by adding trypsin-EDTA and incubating for 5 min, centrifuged at 500 rpm for 5 min, and resuspended in fresh cell culture media at a concentration of 6×10^4 cells per mL. 100 µL of cell suspension was added into each well of a flat bottom, 96-well plate and incubated for 24 h. The media was then replaced with fresh media with different final concentrations of C6 or C6-siRNA complex or control (Lipofectamine 2000). 48 hr post-treatment, the cell counting kit-8 (CCK-8) (Dojindo, Japan) was used to perform cytotoxicity assays. 10µl of CCK-8 substrate was added to each well and incubated for an additional 2 h at 37°C in the dark. Absorbance was measured at a wavelength of 450nm with a reference wavelength of 620nm using a microplate reader (FLUOstar OPTIMA, BMG, NC).

3.2.11 Fluorescence-activated cell sorting (FACS)

The amount of Cy-3 labeled siRNA uptaken by the cells was studied by Flow Cytometry (type

BD Biosciences, BD FACSVantage SE Cell Sorter, USA). Approximately 50,000 CHO-K1 cells were seeded in a 24-well cell culture plate 24 hours before treatment. Cy3 labeled GAPDH siRNA was complexed with C6 peptide at molar ratios of 15:1, 25:1, and 40:1 and incubated at room temperature for 20 minutes. Lipofectamine 2000 (Invitrogen) was complexed with labeled siRNA according to manufacturer's protocol and used as a positive control. The complexes were added to cells with a final siRNA concentration of 50nM per well and incubated at 37°C for 3 hours in Opti-MEM (Invitrogen). The medium was removed by aspiration and the wells were washed with heparin (10 U/ml, three times totally for one hour at 37°C). After washing, the cells were detached from the plate by adding trypsin-EDTA and re-suspended in fresh 4% paraformaldehyde (PFA) in phosphate bufferred saline (PBS) and collected in FACS tubes for analysis.

3.2.12 Fluorescence microscopy

To investigate the distribution of the C6-siRNA complexes in CHO-K1 cells, Cy-3 labeled siRNA was used. CHO-K1 cells were treated with C6-Cy3siRNA complexes at molar ratios of 15:1 and 40:1 or Lipofectamine 2000 at 37 °C for 3 hours in Opti-MEM as described above. The medium was discarded and the wells were washed with PBS and heparin and fixed with 500 µl/well of fresh 4% PFA solution for 30 minutes. The fixation agent was aspirated, and the cells were washed twice with PBS and covered with Fluoroshield with DAPI solution (Sigma-Aldrich, Oakville, Canada) to stain the cell nuclei. The samples were visualized using an inverted fluorescence microscope (Zeiss AxioObserver Z1, Canada). Images were analyzed using AxioVision software package.

3.3 Results and Discussion

3.3.1 Morphology, size, and zeta potential of C6-siRNA co-assemblies

Considering net positively-charged C6 and net negatively-charged siRNA, the non-covalent electrostatic interaction was used to prepare peptide-siRNA co-assemblies.

Considering 7 arginine residues in C6 sequence and 42 phosphate groups in siRNA backbone, 6 molecules of C6 were theoretically required to form C6-siRNA core (Figure 3.1A). This ratio was confirmed by ITC experiment (Figure 3.4). However, further experiments showed that the formed peptide-siRNA core was not stable and extra layers of peptide were required to enhance the stability and efficiency of the siRNA. Taking advantages of amino acid pairing properties of C6, more layers of peptide was formed to protect the C6-siRNA core. The C6 molecules self-assembly also facilitated the presence of arginine residue on the surface of the complex, improving its solubility and enhancing its cellular uptake via interaction with negatively charged cell membrane.

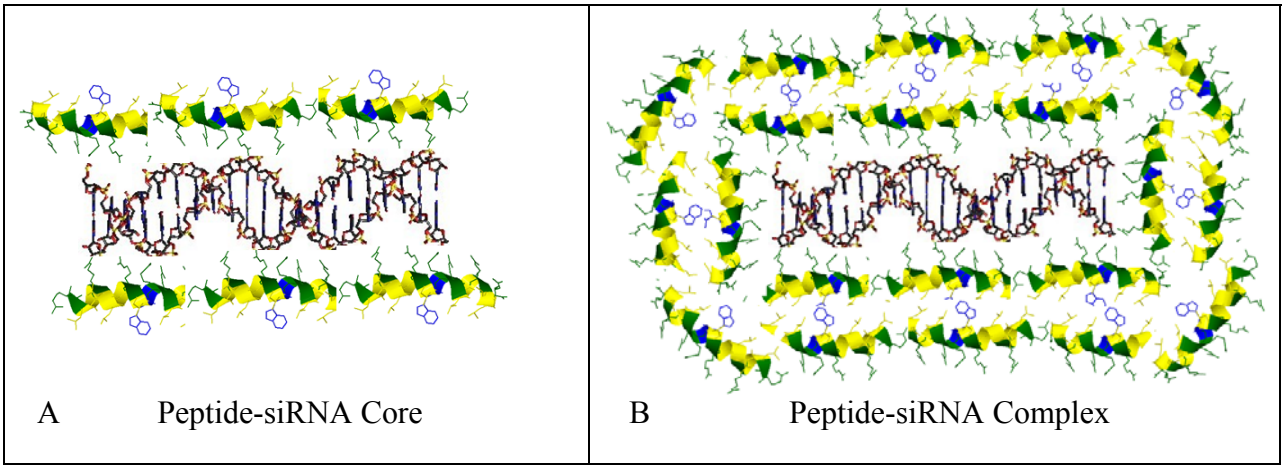

Figure 3.1 A) One siRNA molecule co-assembles with six C6 molecules through electrostatic interaction to form C6-siRNA core. B) More C6 molecules interact with the first layer, taking advantages of amino acid pairing properties of the peptide, to form C6-siRNA complex (at molar ratio of 20:1 at this case). Arginine, Leucine and Tryptophan residues are shown in green, yellow and blue, respectively

The particle size and charge significantly affect its circulation in the blood stream, biodistribution and uptake by the cells. The particle size ranging from 100 to 500 nm would be ideal for passive targeting to solid tumors through the enhanced permeability and retention (EPR) effect [158-160]. The size can also dictate the pathway of cellular uptake [161]. It was also reported that highly charged particles can be recognized by the reticuloendothelial system (RES) more rapidly than neutral or slightly charged particles [6,7]. Thus, engineering the nanoparticle to obtain appropriate physical properties could significantly enhance its therapeutic effect.

Figure 3.2 shows the average intensity and number based size and zeta potential of C6-siRNA co-assemblies at different molar ratios. The intensity-based data is highly influenced by the presence of large particles even though they are a few in the solution. Number-based data represents the size distribution of particles based on their population. For monodisperse particles, these two values should be almost identical. However, the intensity-based average size is always higher than that of number-based in polydisperse particles.

As shown in Figure 1B, the majority of C6-siRNA co-assemblies at molar ratios of 10:1 to 20:1 had the average size of ~50 nm. However some larger particles (~200 nm) were also observed. The average size of complexes was increased by adding more peptides, as the extra peptides added layers to the initially formed peptide-RNA cores. This finding was in agreement with AFM images (Figure 3.3 A), which shows the high population of small nanoparticles (~50 nm) as well as the presence of larger complexes (~100-200 nm). At the molar ratio of 40:1, the complexes became more uniform as the intensity and number based DLS results showed the average size between 150 and 250 nm.

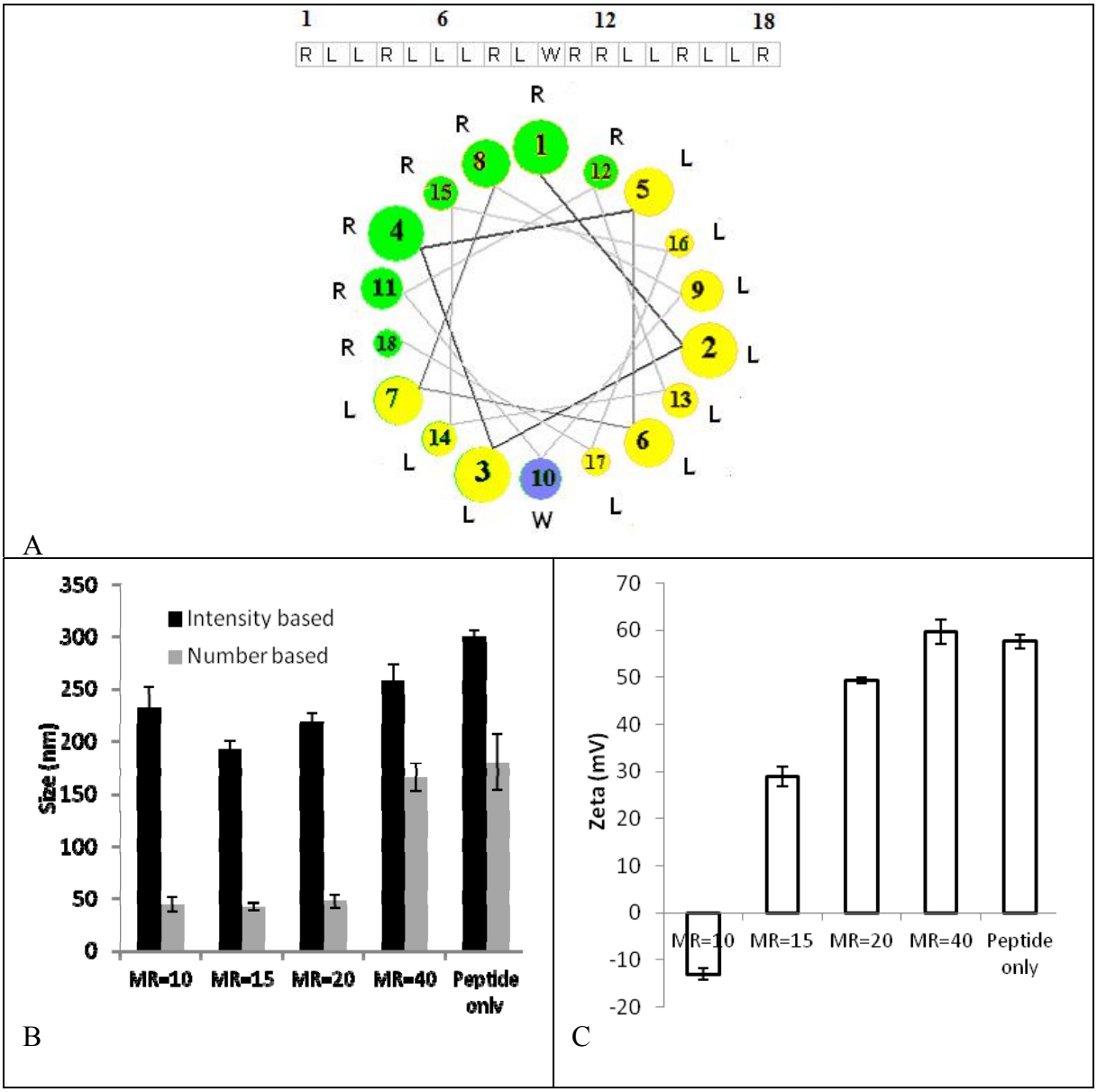

Figure 3.2 (A) Helical wheel projection of peptide C6. A downward cross-sectional view of the alpha helix axis, orthogonal to the paper plane, is shown. The bigger the circle is, the upper turn the residue is located at, when viewing from the top. R (green), L (yellow), and W (blue) represent Arginine, Leucine and Tryptophan residues, respectively. Size (B) and zeta potential (C) of C6-siRNA complexes at different molar ratios. The siRNA concentration was 100 nM and the peptide concentration in "peptide only" sample was 4 μM. Three independent measurements were performed for each sample 20 min after sample preparation at 25 °C. Error bars represent standard deviation of three replicates. (MR= peptide:siRNA molar ratio)

The peptide only sample formed aggregates of 200-300 nm in solution. However on the mica surface (Figure 3.3 B), the peptide sample formed globular structures with an average diameter of ~45nm, eventually organized to form a network of strings of nanospheres. The formation of these globular structures was derived by hydrophobic attraction between leucine residues, distributed along the peptide sequence. As there was not such a template for nanoparticles in solution in DLS experiment to form the network, they aggregated, instead, as larger particles to minimize the interaction of hydrophobic residues and water molecules. This self-assembly/aggregation process is thermodynamically favored by minimizing Gibbs free energy through limiting the exposure of hydrophobic residues to the aqueous environment and having mostly charged arginine residues on the surface of globules. We have already reported similar morphology for another AAP peptide [162].

The surface charge of C6-siRNA complex at molar ratio of 10:1 was slightly negative which implies that siRNA molecules was not fully saturated by peptides (Figure 3.2 C). Considering 7 positively charged arginine groups of the peptide C6 and 21 pairs of negatively charged nucleotides in a siRNA molecule, it was theoretically expected to neutralize negative charge of siRNA at molar ratio of 6:1. However at a higher molar ratio, *i.e.*, 15:1, the zeta potential of the complex jumped to +30mV, indicating that peptides fully covered the surface of the complex. With the increasing concentration of peptide at the same siRNA concentration, the positive value of the surface charge of the complexes increased from +30mV (MR=15:1) to +60mV (MR=40:1) due to the increase in the number of positively-charged arginine residues. The net positive charge of the particles is crucial as it inhibits particle aggregation and enhances electrostatic interaction with the negatively charged phospholipids of the cell membrane upon siRNA delivery.

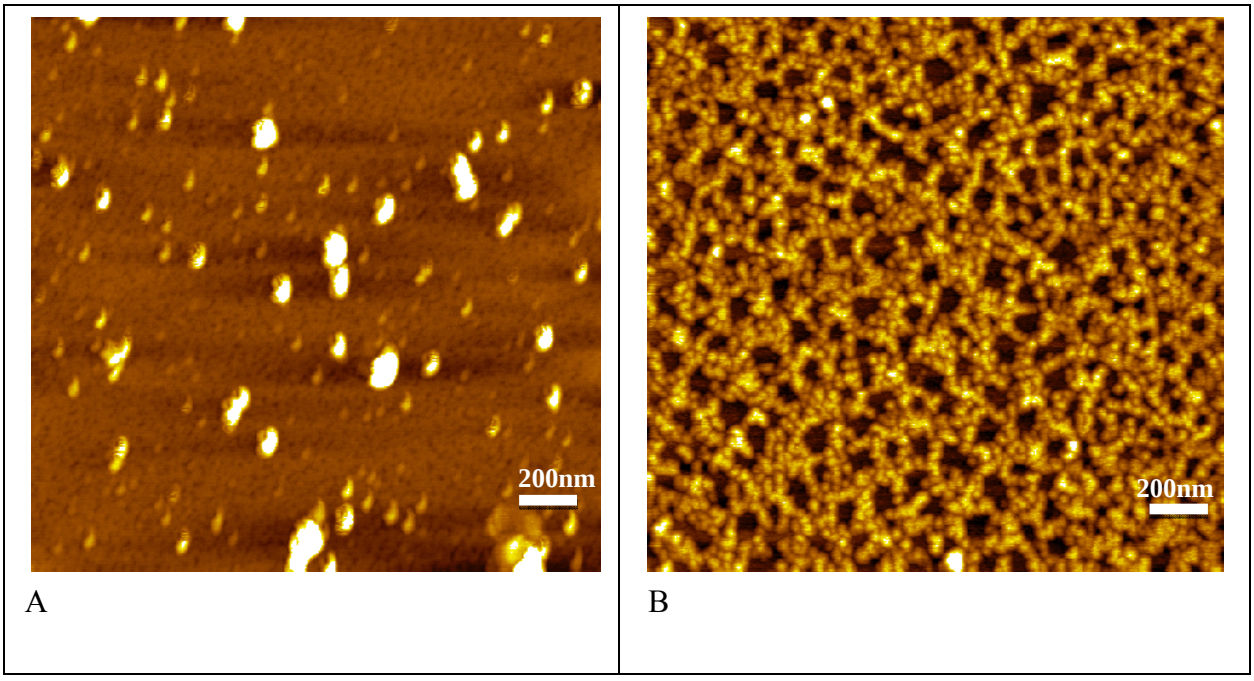

Figure 3.3 AFM images of (A) C6-siRNA complex (MR=40:1) and (B) C6 peptide aggregates/assemblies (40μM). The sample solution (10 μl) was placed on the mica surface, and incubated for 30 min at room temperature. The mica was then rinsed five times with Milli-Q water, followed by air-drying overnight. The scan size of the images is 2 × 2 μm^2.

3.3.2 Peptide-siRNA co-assembly detected by ITC

In order to study the thermodynamic aspects of C6-siRNA interaction, ITC was used to detect the heat exchanged during the titration of siRNA with C6 solution.

As shown in Figure 3.4, the interaction between C6 and siRNA created small exothermic peaks, followed by a gradual decrease in the exchanged heat after the first several injections. The heat measured for the last injections was almost the same as the dilution heat (control experiment), implying there was no significant interaction after saturation ratio. The thermodynamic parameters of the interaction were obtained by fitting the raw ITC data to a single site model using NanoAnalyze software v.2.3.0 (Table 3.1).

Table 3.1 Thermodynamic parameters of the interaction between peptide and siRNA

stoichiometry	K (10^6 M^{-1})	ΔH (kJ/mol)	TΔS (kJ/mol)	ΔG (kJ/mol)
6.49 ± 0.33	9.23 ± 0.63	-8.86 ± 0.55	30.95 ± 1.14	-39.81 ± 1.69

A single site independent model was used for fitting the data points in Figure 3 (solid curve in lower panel) to determine the binding constant (K), stoichiometry (n), the binding enthalpy (ΔH), the change in free energy (ΔG), and entropy (ΔS).

Interestingly, the obtained molar stoichiometry of ~6.5 was very close to the theoretical one, i.e., 6. With a low enthalpy of 8.8 $kJ.mol^{-1}$, the binding was mostly entropy driven, with a ΔS of 103 $J.mol^{-1}.K^{-1}$, which contributes to 78% of the binding free energy. This combination of thermodynamic parameters, i.e., low enthalpy and high positive entropy values, is consistent with a typical charge neutralization or ionic interaction process, *e.g.*, the interaction of basic amino acids with RNA [163] or DNA [164].

It should be noted that the thermodynamic parameters of the interaction are strong functions of experimental conditions, *e.g.*, temperature, pH and ionic strength. The values reported here were the results of experiments conducted in water (pH=6) at 25 °C.

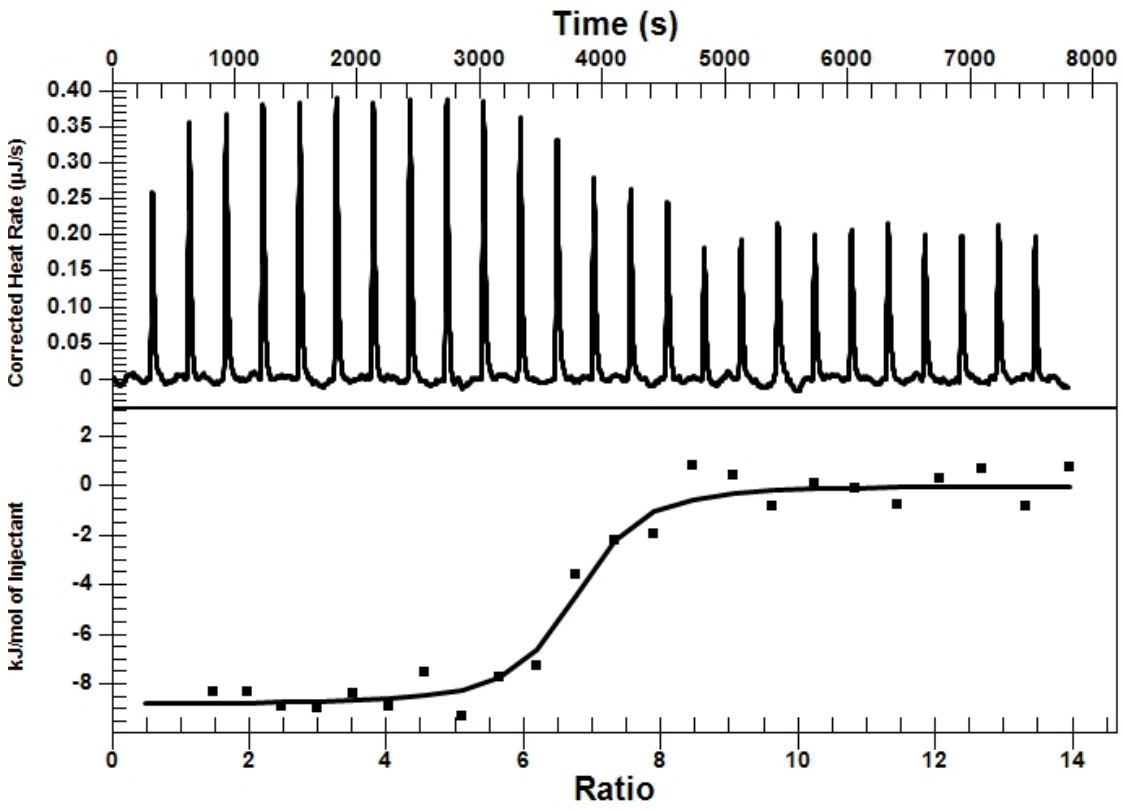

Figure 3.4 Titration of 250 µM peptide C6 into the solution of 6µM siRNA. The upper panel shows baseline-corrected thermogram of released heat at each injection and the lower graph shows the integrated areas of the net heat of each titration after subtracting the heat of the dilution of peptide to water as a function of the molar ratio of peptide to siRNA. A single site independent model was used for fitting the data points (solid curve in lower panel).

3.3.3 Agarose gel shift assay

Agarose gel shift assay was used to detect the interaction between siRNA and peptide molecules and the stability of the formed complex in the presence of heparin. Peptide can interact with siRNA through non-covalent interactions such as coulombic forces and hydrogen bonding. In particular, basic amino acids such as lysine, arginine or histidine can interact with the negatively charged phosphate groups on the siRNA sugar rings through electrostatic interactions. Free

siRNA molecules could move toward the positive electrode when the voltage is applied; while, the inability of peptide-siRNA complexes to enter the agarose gel suggests the formation of stable complex with no free siRNAs to be shown in siRNA bands.

As shown in Figure 3.5 B, the effective formation of the peptide-siRNA complex started at molar ratio of as low as 5:1, since the band was less bright than that of siRNA only. At the molar ratio of 10:1, siRNA molecules were almost completely associated with peptide C6, as very small amount of free siRNA was observed on siRNA band. This band completely disappeared at the molar ratio of 15:1. This finding suggests that excess peptide molecules are needed to obtain stable peptide/RNA complexes as six molecules of peptides are theoretically required to electrostatically neutralize one molecule of siRNA. Further experiments showed that the excess peptide molecules can provide a shield to protect siRNA molecules against degradation, and also interact with cell membrane to initiate the peptide-siRNA cellular uptake.

The stability of C6-siRNA complexes at different molar ratios in the presence of heparin was also analyzed by gel electrophoresis. As shown in Figure 3.5 A, C6-siRNA complexes were stable in the absence of heparin (second well from left) and no free siRNA was shown in siRNA bands at all MRs. The complex at MR of 15:1 was stable at very low concentration of heparin, i.e., 0.5 μg per 10 μl of sample, but dissociated at higher heparin concentration. The minimum concentration of heparin required for dissociation of the complex increased by increasing the MR up to 60:1. However, the complex at the molar ratio of 80:1 was completely stable even at high heparin concentration (10 μg in 10 μl of loaded sample).

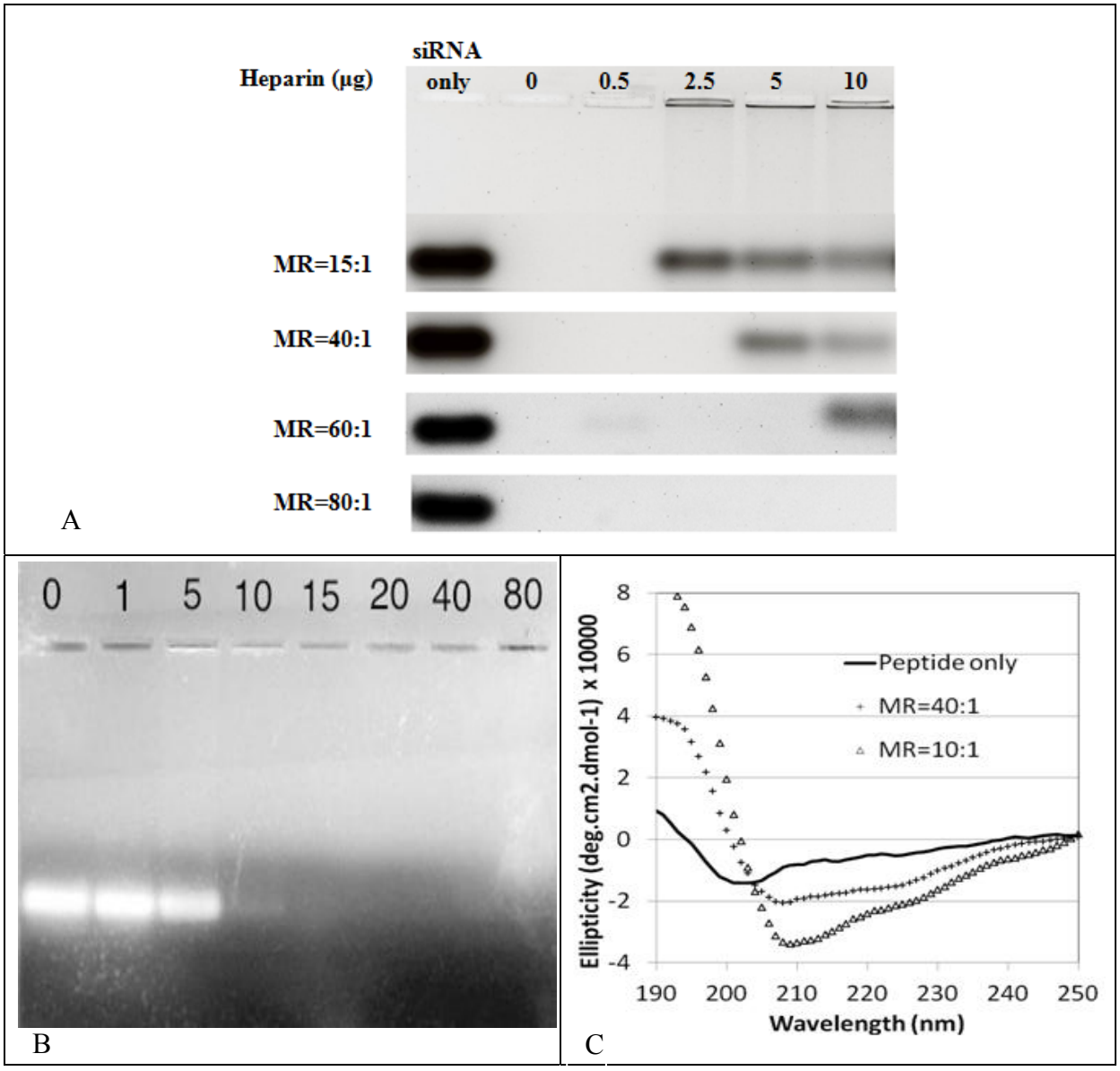

Figure 3.5 (A) Stability of C6-siRNA complex indicated by heparin competition assay. Different amounts of heparin were added to C6-siRNA complexes at different molar ratios (MRs). Stability of complexes was analyzed by electrophoresis on agarose gel (1.2% wt/vol.). For better comparison, the siRNA bands of four independent gels were put in the same image. (B) The formation of C6-siRNA complexes at different MRs. siRNA was incubated with different concentrations of C6 corresponding to a MR ranging from 1:1 to 80:1. Lane 1 refers to siRNA control in the absence of C6, and lanes 2–8 to different MRs. (C) Secondary structure of peptide C6 (20 μM) alone and with siRNA at MRs of 40:1 and 10:1, obtained by CD spectroscopy.

3.3.4 Conformational Changes of C6 upon co-assembling with siRNA

The impact of siRNA on the secondary structure of C6 was evaluated by CD spectroscopy. As reported in Figure 3.5 B, C6 in water showed a small content of a random coil conformation with a minimum at 203nm. By adding a small amount of siRNA (MR of 40:1) a clear shift in the spectrum minimum from 203 to 208 along with a maximum around 190 nm were observed, which represents a typical helical conformation. The absolute values of the minima at 208 and 222 nm, and the maximum at 190 nm were increased by adding more siRNAs to MR of 10:1, which indicates the increase in helical content in secondary structure of the peptide at a higher concentration of siRNA. Adding further siRNA beyond the MR of 10:1 did not significantly change the secondary structure of the peptide (not shown), indicating a saturation point, as also observed in the gel electrophoresis and ITC tests. Considering the nature of C6 and siRNA interaction, *i.e.*, ionic interaction, the charge neutralization of seven arginine residues in the peptide sequence may decrease the repulsion between them, which eventually facilitated the peptide adoption to a helical conformation.

3.3.5 Fluorescence spectroscopy

The formation of siRNA/C6 complexes was also evaluated by intrinsic fluorescence spectroscopy, using the Trp residue in C6 as the fluorescent probe to monitor the interaction with siRNA. As shown in Figure 3.6 A, the peptide only sample had an emission peak at 354 nm. The binding of C6 to siRNA from molar ratio of 80:1 to 1:1 induced quenching of Trp fluorescence as well as a blue shift in the maximum. As shown in Figure 3.6 A, at the molar ratio of 10:1, 55% quenching of fluorescence, accompanied by a 20nm blue shift from 354 nm to 334 nm (Figure 3.6 A, inset) was observed. No significant change in fluorescence intensity and peak wavelength was observed by adding more siRNAs (*e.g.*, at MR=1:1), which indicates a saturation in peptide-siRNA interaction at MR=10:1.

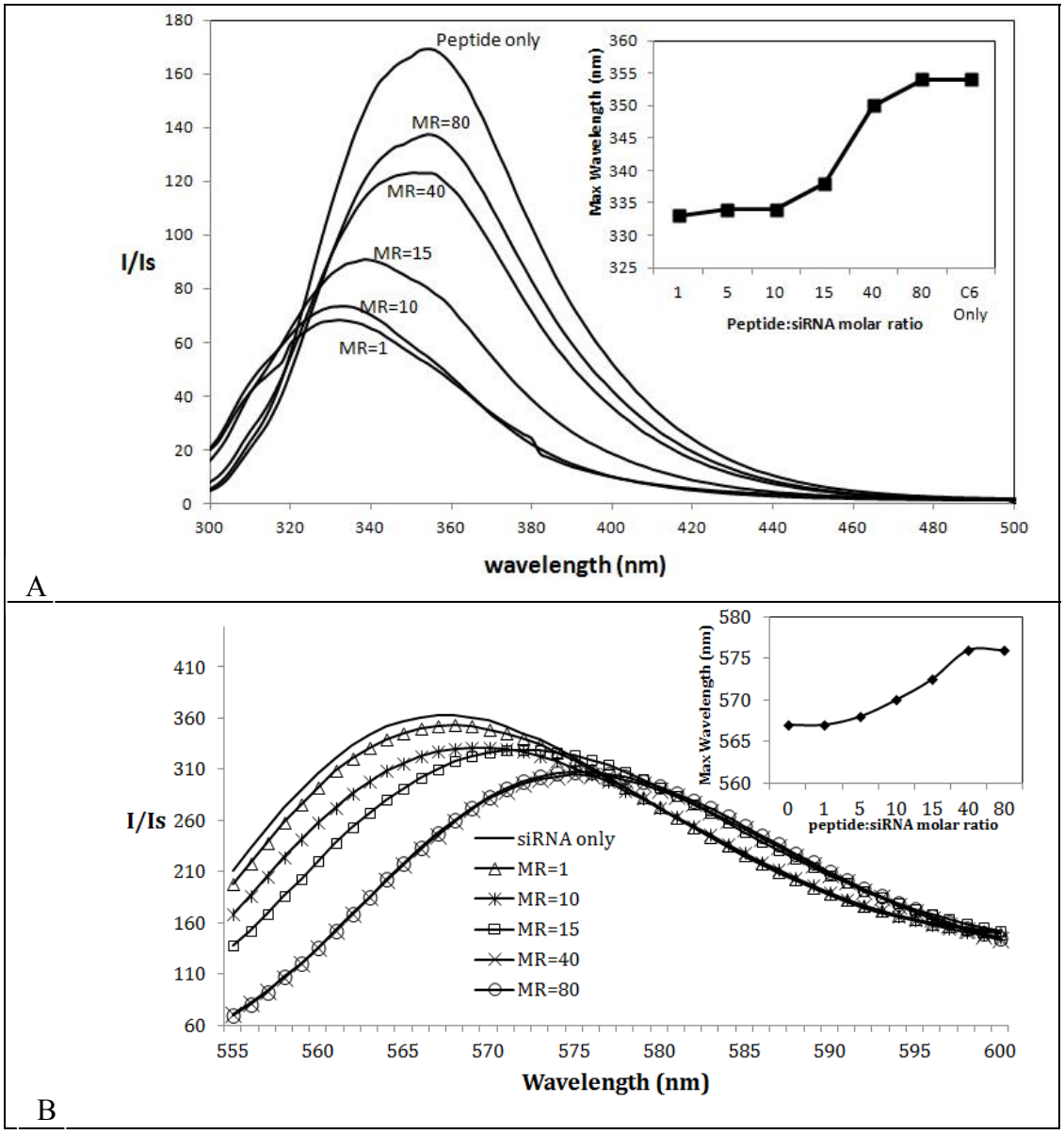

Figure 3.6 C6-siRNA interaction monitored by fluorescence spectroscopy. (A) The intrinsic Trp fluorescence of C6 was excited at 280 nm and the emission spectra were recorded from 300 to 500 nm. A fixed concentration of 160 nM of peptide was titrated by increasing siRNA concentration from molar ratio 80/1 to 1/1. (B) Cy-3 labeled siRNA was used as extrinsic fluorescent probe and the change in fluorescence spectra was studied at a fixed concentration of siRNA (2 μM) and increasing concentration of peptide to achieve different molar ratios. The samples were excited at 540 nm and spectra were collected in the range of 550-800 nm.

This finding is in agreement with what was reported for agarose gel assay. The blue shift signifies a change in the environment of Trp residue from polar to non-polar, indicating conformational change of C6 upon interaction with siRNA as also confirmed by CD [165]. Similarly, the interaction of C6 with labeled siRNA induced a red shift along with quenching in maximum spectra of extrinsic Cy-3 label of siRNA, starting from molar ratio of 10:1 (Figure 3.6 B). The red shift and quenching reached their maximum of 10nm and 15%, respectively, at molar ratio of 40:1, as adding more peptide did not change the spectra (MR=80:1). This may suggest that the extra peptides did not interact with the pre-formed C6-siRNA complexes. Considering the results of all the performed characterization experiments, a C6:RNA molar ratio between 15:1 and 40:1 was suggested to perform transfection experiments.

3.3.6 Cyto-toxicity of peptide-siRNA complex

Cell viability studies were performed, using the CCK-8 assay, on CHO-K1 cells. As shown in Figure 3.7 A, no significant difference was observed in the viability of cells treated with C6-siRNA complexes or C6 only samples at the same concentration. None of the peptide-siRNA samples showed considerable toxicity on CHO cells, as the viability of the cells was not reduced below 85% even at molar ratio of 40:1. However, the cells treated with Lipofectamine showed significant toxicity. These results clearly show that peptide C6 can be used as a safe siRNA delivery carrier with lower cytotoxicity, compared with commonly used lipid-based reagents.

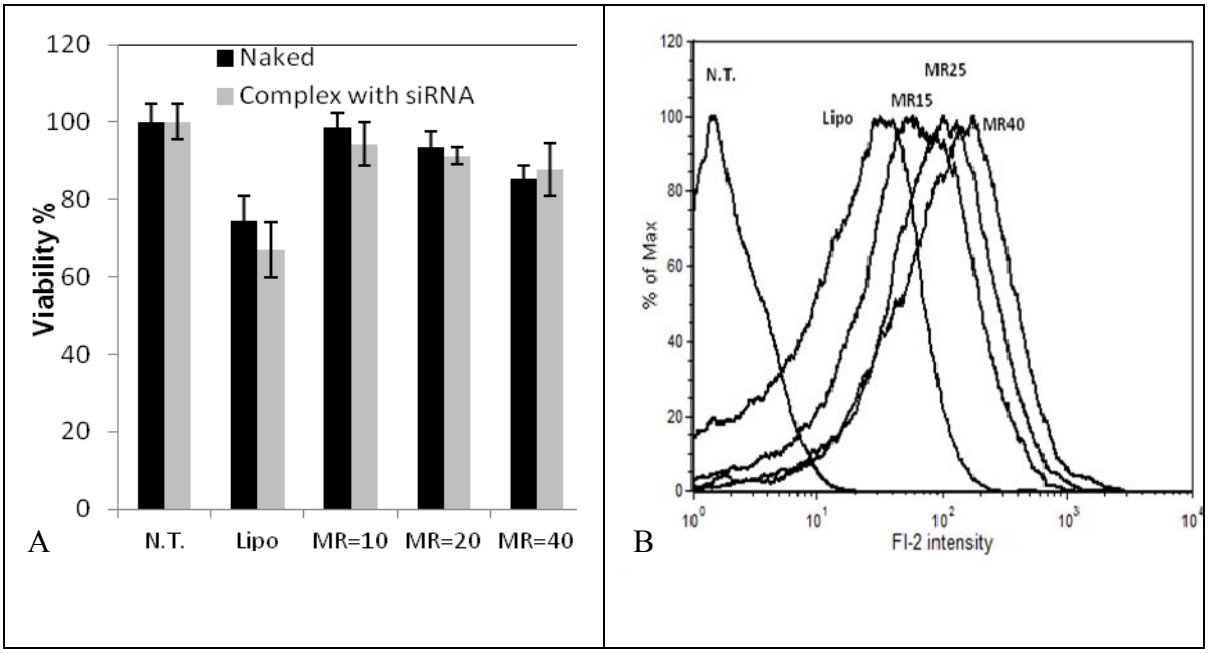

Figure 3.7 (A) Cyto-toxicity of peptide C6 in complex with siRNA (50 nM) at different molar ratios or peptide alone at the same concentrations. (N.T.=Non-treated, MR=peptide:siRNA molar ratio), (B) Flow cytometry results for Cy3- labelled siRNA delivered by Lipofectamin 2000 and C6 at different molar ratios (MRs).

3.3.7 Cellular uptake of peptide-siRNA complex

The efficiency of C6 to deliver siRNA into CHO cells was evaluated using fluorescence-activated cell sorting (FACS). As shown in Figure 3.7 B, cellular uptake efficiency of siRNA was correlated to the molar ratio of C6-siRNA. Even though a 15:1 molar ratio was sufficient to deliver even higher amount of siRNA into cells compared with lipofectamine 2000, the intracellular fluorescence intensity increased with increasing molar ratio (MR25 and MR40).

To study the cellular uptake, distribution, and localization of siRNA complexed with C6, CHO cells were transfected with Cy3-labeled siRNA alone or in complex with C6 or lipofectamine 2000. CHO cells were incubated with or without complexes for 3 hours and observed under a fluorescence microscope (Figure 3.8).

As expected, Cy-3 siRNA alone was not able to enter the cells by itself, due to the negative charge and lack of an appropriate delivery vector (Figure 3.8 B). siRNA internalization happened within three hours of incubation at the present of transfection reagent, lipofectamine 2000, as shown as small red dots in the cytosol of most of the cells (Figure 3.8 D). In the cells treated with C6-siRNA complexes (Figure 3.8 E, and F), siRNA was localized to regions in close proximity to the nuclear membrane. siRNAs delivered by C6 showed a punctual non-homogeneous distribution pattern around the periphery of the nucleus inside the cell, which indicated the possibility of endocytosis pathways [166]. Further research to study the uptake mechanism of this family of peptides is currently in progress.

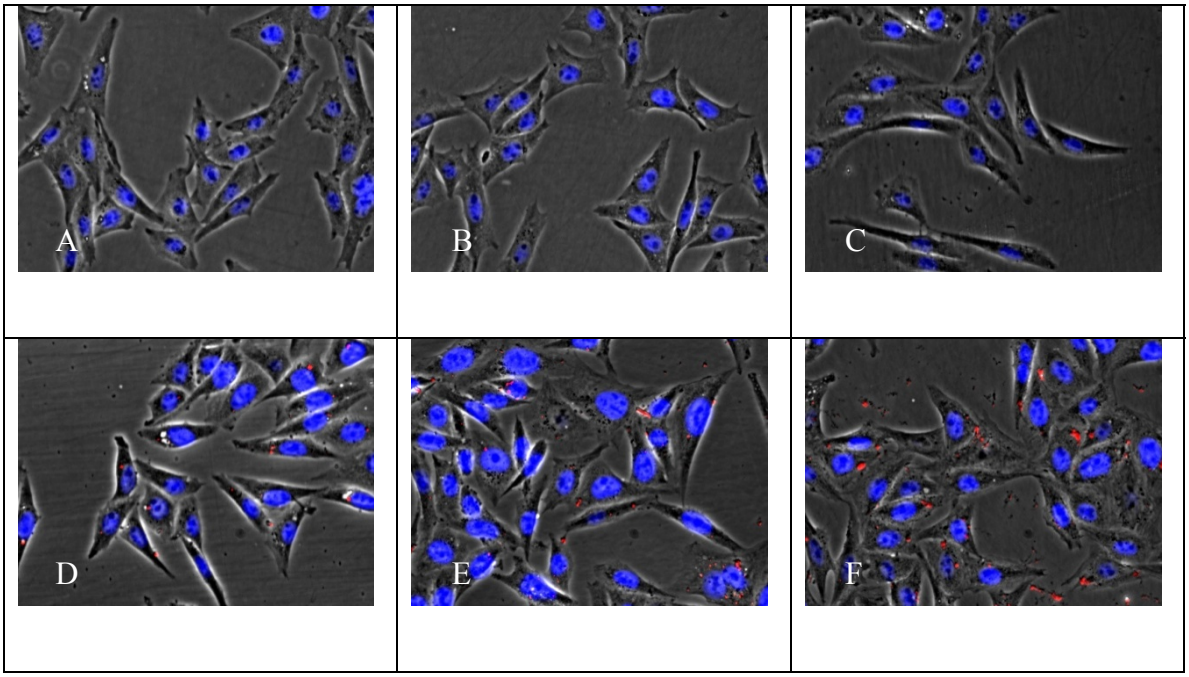

Figure 3.8 Subcellular distribution pattern of Cy3-labeled siRNA 3 hours post-treatment. Cy3-labeled GAPDH siRNA (red) was transfected to CHO cells with positive control reagent and different molar ratio of C6 at a concentration of 50nM. Cells were analyzed by fluorescence microscopy 3 hours after transfection (magnification, 40X). Nuclei were stained with DAPI (blue). (A) nontreated cells, (B) cells treated with 50nM siRNA only, (C) with C6 peptide only, (D) with Lipofectamine 2000 as positive control, (E) with siRNA complexed with C6 at molar ratio of 15:1, and (F) molar ratio of 40:1.

C6-siRNA complexes at high molar ratios (MR=40:1) may form high molecular weight complexes or aggregate, as previously documented for other CPPs. These large complexes may be internalized through the macropinocytosis pathway, which can include all pinosomes larger than 200 nm [147]. However the uptake of large aggregates by fluid phase endocytosis may not result in the effective release of siRNA into the cytoplasm and eventually significant gene knockdown. Thus, precautions should be taken into account while increasing the molar ratio, as the large aggregates might have problems dissociating and releasing siRNA in the cells, eventually decreasing the knockdown efficiency of the complex.

3.4 Conclusions

C6, an amphipathic, amino acid pairing (AAP) peptide, was introduced as a safe and efficient carrier for siRNA delivery *in vitro*. The non-covalent interaction/co-assembly between C6 and siRNA and the physicochemical properties of the resulting co-assemblies were studied. C6 alone showed a random coil secondary structure in water but adopted a helical conformation upon binding to siRNA. The ITC results showed an entropy-driven interaction between C6 and siRNA with stoichiometry of 6.5, which was close to the theoretical value of 6, required for charge neutralization. The gel electrophoresis, fluorescence spectroscopy, DLS, and AFM results confirmed stable C6-siRNA complex formation in the molar ratios from 10:1 to 40:1. The flow cytometry data and fluorescence microscopy images also indicated the high cellular uptake and cytoplasmic localization of siRNA delivered by C6. Considering these results and the fact that C6 is non-toxic at the concentrations used, this peptide demonstrated potential as an efficient carrier for siRNA delivery.

Chapter 4*

Modification of peptide C6 to improve its solubility and efficiency

The development of safe and efficient nonviral gene delivery carriers has received a great deal of attention in the last decade. A class of amphipathic peptides has shown to be able to cross cell membrane and deliver cargos to intracellular environment. Here, we introduce an 18-mer amphipathic peptide, C6M1, as a modified version of peptide C6 for short interfering RNA (siRNA) delivery. The importance of tryptophan residues and the effect of peptide sequence modification on its solubility, secondary structure, cytotoxicity, and uptake efficiency were investigated. The solubility of C6M1 in aqueous solutions was greatly enhanced compared with that of C6, confirmed by ANS fluorescence assay. C6M1 had a random/helical structure in water with ability to attain a helical conformation in the presence of anionic components or membrane-mimicking environments. The modification significantly reduced the cytotoxity of the peptide, making it a safer carrier for siRNA delivery. C6M1 was also found ~90% more efficient than C6 in delivering Cy3 labeled siRNA in CHO-K1 cells.

---

* This chapter is adapted from a paper draft "M. Jafari, N. Karunaratne, C. M. Sweeting, and P. Chen, Modification of a designed amphipathic cell penetrating peptide and its effect on solubility, secondary structure and efficiency, submitted to *J. Biochemistry*"

4.1 Introduction

With the ability of siRNA to function as a therapeutic in gene therapy, efficient delivery and transfection of siRNA are of critically importance. The traditional non-viral carriers for gene therapy, such as liposomes, and cationic polymers, are known to have more versatility than viral vectors. However, with the discovery that cell penetrating peptides (CPPs) are able to cross biological membranes and deliver cargo into the intracellular matrix, an interest in peptides as carriers of nucleic acids has emerged. Peptide-based delivery systems have also shown the potential to deliver bioactive peptides, therapeutic proteins, and nucleic acids [66-68]. Their role is to deliver polypeptides and proteins into cells through either of two strategies: covalent or complexed in a non-covalent fashion.

Primary amphipathic peptides with hydrophilic and hydrophobic parts in the two opposite ends (a highly hydrophilic N-terminus and a mainly hydrophobic C-terminus) were reported to have cellular uptake ability [72]. Most CPPs have such an arrangement of the amino acids. On the other hand, secondary amphipathic peptides with the polar residues placed on one face of the helix while the hydrophobic side chains pointing to the opposite face have been reported to have better interaction with the cell membrane [109].

Positively charged amphipathic peptides are well suited for interactions with negatively charged biomolecules, such as siRNA. They are short chain peptides usually containing 20 – 30 amino acids, and are rich in lysine and arginine residues. The interactions between these carriers and their cargo have been reported to involve a combination of hydrophobic and electrostatic contacts through aromatic and charged groups. For example, CADY [167], and PEP family peptides [168] are amphipathic peptides, which have been shown to deliver nucleic acids, peptides, and proteins into a wide variety of cells through formation of non-covalent complexes. Both the PEP and CADY peptides are rich in tryptophan residues, which appear to play a major role in stabilization of the carrier/cargo complex and insertion into the membrane owing to their hydrophobic nature. The helical conformation of these peptides, associated with their

amphipathic character, has been reported to be essential for their interaction with the cell membrane and their overall function as a CPP [169].

In biological systems, many types of supramolecular assemblies of proteins play pivotal roles. Many proteins assemble by interactions between secondary structures, such as α-helices and ß-sheets, to form large aggregates or assemblies. For example, interactions between α-helices result in capsule-like protein assemblies, such as ferritin [170] and clathrins [171]. The internal skeleton of tomato bushy stunt virus is built by the formation of intermolecular ß-sheets among C3 symmetric protein units [172]. Alzheimer patients have amyloid fibrils of extended ß-sheets deposited in their brains [173].

The design of peptides as carriers for delivery of nucleic acids must take into account the stability of the complex, its ability to penetrate and most crucially the release of the cargo inside the cell. Both lysine and arginine based peptides have been used for efficient packaging of DNA into nanoparticles to prevent cellular degradation and improve DNA availability. However, it was reported that lysine containing peptides show differential release of DNA *in vitro* compared to arginine containing peptides [174]. On the other hand, the guanidine moiety in arginine was reported to play a crucial role in interaction of the peptide with cell membrane and its internalization, as replacing arginine with lysine residues that have the same net charge significantly reduced the peptide uptake [175].

In the previous chapter, we introduced and characterized C6 peptide as an siRNA delivery carrier [176]. The current work introduces C6M1 peptide, a modified version of C6. As shown in Figure 4.1, three leucine residues in C6, i.e., leu3, leu7, and leu14, were replaced by tryptophan residues (C6M1). As mentioned, tryptophan seems to play an important role in the interaction of peptide with cell membrane components, facilitating the direct internalization or endocytosis. The effect of this modification on the peptide solubility, secondary structure, and internalization efficiency will be discussed.

4.2 Materials and methods:

4.2.1 Peptides, siRNA and Chemicals

C6 (MW=2470.2 g/mol, purity>98%) and C6M1 (MW=2689.4 g/mol, purity>98%) were purchased from CanPeptide, Inc. (Quebec, Canada). Unlabeled and Cy3-labeled Glyceraldehyde 3-phosphate dehydrogenase (GAPDH) siRNA were purchased from Ambion (Austin, USA). Trifluoro ethanol (TFE), anilinonaphthalene sulfonate (ANS) and all other chemicals for buffer preparations were obtained from Sigma-Aldrich (Oakville, ON, Canada) and used as received.

4.2.2 Formulation of peptide-siRNA complexes

The peptide solution was prepared by dissolving peptide powder in RNase free water. A stock solution of 1 mM was made and diluted at desirable concentrations for various experiments. The solution was then vortexed for 10 seconds and sonicated for 10 minutes in a tabletop ultrasonic cleaner (Branson, model 2510, USA). siRNA was diluted in RNase free water to a concentration of 50 μM. Peptide-siRNA complexes were formed by adding peptide solution into siRNA in proportion according to the designed experiment. The complexes were incubated for 20 minutes at room temperature before each experiment.

4.2.3 Fluorescence spectroscopy

To evaluate the hydrophobicity of C6 and C6M1 peptides, the well-established ANS fluorescence assay was applied. Fresh peptide solutions at different concentrations were mixed with the same volume of the ANS solution (20 μM) on a vortex mixer for 20 s. As a control sample, the ANS solution was also mixed with the same volume of pure water. The ANS fluorescence was acquired on a Photon Technology International spectrofluorometer (Type LS-100, London, Canada) with a pulsed xenon lamp as the light source. Samples (80 μl) were transferred to a quartz cell (1 cm×1 cm) and excited at 360 nm and the emission spectra were collected at wavelengths from 420 to 670 nm. The spectra were normalized with the average intensity of control sample (I_s) from 650 to 670 nm.

4.2.4 Surface tension measurement

The dynamic surface tension of fresh C6 and C6M1 solutions (100 μM) and C6M1-siRNA solutions was measured over a period of 1.5 h using the Axisymmetric Drop Shape Analysis-Profile (ADSA-P) technique [177]. A pendant drop of the sample solution was formed at the tip of a vertical Teflon needle (0.92 mm inner diameter) connected to a motor-driven microsyringe. The sample was placed in a temperature-controlled chamber, saturated with water vapor to maintain consistent humidity. The entire system was placed on a vibration-free table. The images of the pendant drop were magnified by an optical microscope and then captured by a CCD camera at 30 s intervals before being transferred to a computer. Images were analysed by image processing software to generate a profile of the pendant drop. A theoretical curve governed by the Laplace equation of capillarity was then fitted to the profile, generating the surface tension value as a fitting parameter.

4.2.5 Circular Dichroism (CD) spectroscopy

C6 and C6M1 solutions (80 μM) were prepared in water, 50% TFE, or NaCl solutions. Spectra from 250 to 190 nm with spectral resolution and pitch of 1 nm and scan speed of 200 nm/min were recorded with a J-810 spectropolarimeter (Jasco, USA). Samples were transferred into 1 mm long quartz cells and maintained at 25 °C. Spectra shown are the average of three replicates. The raw CD ellipticity (in millidegrees) was converted to residue molar ellipticity ($deg.cm^2.dmol^{-1}.residue^{-1}$): $\theta=\theta_{raw}/ (10\times C\times N\times l)$, where θ_{raw} is the ellipticity in millidegrees, C is the peptide concentration (mol/L), l is the optical path length of the cell (cm) and N is the number of residues. The secondary structure composition of the peptide was estimated from CD spectra using K2D3 program [178].

4.2.6 Fourier transform infrared (FTIR) spectroscopy

A Vertex 70 (Bruker Optics Inc., MA, USA) FTIR spectrometer, equipped with a liquid nitrogen cooled MCT detector, was used to determine the secondary structure of C6M1 (40 μM) in water

and 200 mM NaCl solution. The FTIR spectrum of the sample was recorded at a wavenumber resolution of 4 cm^{-1} between 4000 and 400 cm^{-1} using the OPUS 5.5 software (Bruker Optics Inc., MA, USA). After subtracting the baseline, the absorption spectrum was analyzed in the range of 1575–1725 cm^{-1}, where the amide I band is located.

4.2.7 Cytotoxicity

Chinese hamster ovary (CHO-K1) cells were used for *in vitro* cellular toxicity studies of C6 and C6M1 peptides. Cells were detached from the flasks by adding trypsin-EDTA and incubating for 5 min, centrifuged at 500 rpm for 5 min, and resuspended in fresh cell culture media, F-12K containing 10% FBS, at a concentration of 1×10^5 cells per mL. 100 µL of cell suspension was added into each well of a flat bottom, 96-well plate and incubated for 24 h. The media was then replaced with fresh medium with different final concentrations of C6 and C6M1 or controls. The cell counting kit-8 (CCK-8) (Dojindo, Japan) was used to perform cytotoxicity assays, 24 hr post-treatment. 10µl of CCK-8 substrate was added to each well without discarding the old media and incubated for an additional 1 h at 37 °C in the dark. Absorbance was measured at a wavelength of 450 nm with a reference wavelength of 620 nm using a microplate reader (FLUOstar OPTIMA, BMG, NC). The 50% inhibitory concentration (IC50) of peptides on cells was calculated using CCK-8 data.

4.2.8 Flow cytometry

The amount of intracellular Cy-3 labeled siRNA was quantified by Flow Cytometry (type BD Biosciences, BD FACSVantage SE Cell Sorter, USA). Approximately 50,000 CHO-K1 cells were seeded in a 24-well cell culture plate, 24 hours before treatment. Cy3 labeled GAPDH siRNA was complexed with C6 and C6M1 peptide at peptide:siRNA molar ratios of 15:1, 30:1 and incubated at room temperature for 20 minutes. The complexes or naked siRNA samples were added to cells at a final siRNA concentration of 50 nM and incubated at 37 °C for 3 hours in Opti-MEM (Invitrogen). The medium was then removed by aspiration and the wells were

washed with trypsin (0.5 mg/ml in PBS for 5 min), and heparin (0.5 mg/ml in PBS for 3×10 min) to remove surface-bound complexes. After washing, the cells were detached from the plate by adding trypsin-EDTA and re-suspended in fresh 4% paraformaldehyde (PFA) in phosphate bufferred saline (PBS) and collected in FACS tubes for analysis.

4.3 Results

4.3.1 Design of C6M1 by sequence modification of C6

The C6 peptide was previously reported as a designed amphipathic peptide for siRNA delivery [176]. Despite its ability in cellular delivery of siRNA, C6 suffered from relatively poor solubility and aggregation due to its hydrophobic nature. The solubility of a peptide in the medium is an important factor in the assembly of the peptide-siRNA complex. Moreover, the size of the complex determines the membrane penetration mechanism and efficiency [179].

Figure 4.1 shows the sequence and helical wheel projection of C6 and C6M1. In the helical wheel presentation, the side chains of residues forming the alpha-helix are projected onto a circle in a plane perpendicular to the axis of the helix. Assuming the periodicity of an ideal alpha-helix, there is a 100° angle between consecutive amino acid residues in the wheel diagram. As shown in Figure 4.1, both peptides were designed to show amphiphilicity by clustering of hydrophilic residues (i.e., arginine) on one side and hydrophobic residues (i.e., leucine and tryptophan) on the opposite side of the circle. C6M1 was originally designed from C6 by replacing leucine residues with tryptophan in 3, 7, and 14 positions. Tryptophan content and distribution were reported to alter the cellular uptake of the cell penetrating peptides [180] This modification was also meant to improve the helicity and solubility of peptide in a polar environment.

The modified 18-mer peptide, C6M1, consists of three types of amino acids, i.e., 7 arginine, 7

leucine and 4 tryptophan residues. Arginine residues interact with negatively-charged cell membrane phospholipids or proteoglycans mainly through guanidine moieties to trigger direct translocation or endocytosis [155]. They also form non-covalent complexes with negatively-charged cargos, *e.g.*, siRNA, through electrostatic interaction. Leucine residues interact with hydrophobic tails of lipid bilayer, facilitating the translocation of peptide [66]. They are also required for self-assembly of the peptide which can create external layers to protect the peptide-siRNA core from degradation. The aromatic tryptophan residues have been reported to greatly enhance the cellular uptake of arginine-rich peptides [169]. The design of C6M1 allows the arrangement of all tryptophan residues at the same face of the helix. This arrangement is also expected to stabilize the helical structure through π- π interaction between tryptophan rings.

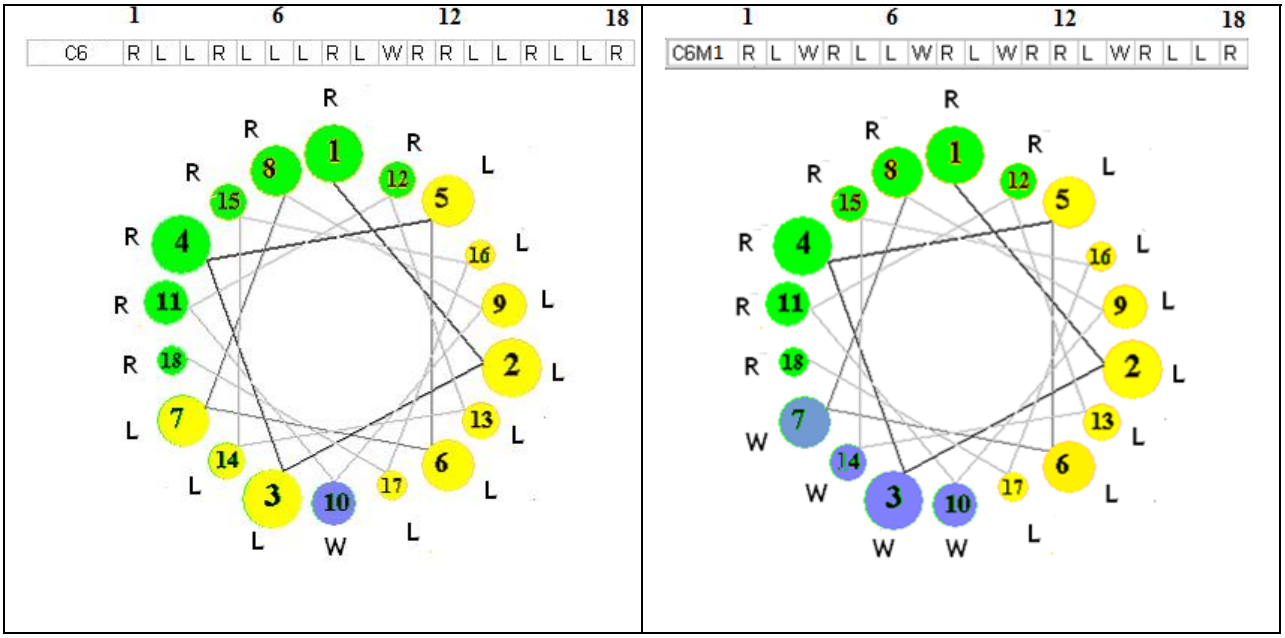

Figure 4.1 Peptides C6 and C6M1 sequences and helical wheels representation. A downward cross-sectional view of the helix axis is shown for C6 and C6M1. The axis of the alpha helix is orthogonal to the paper plane. Considering 3.6 residues per turn, each amino acid corresponds to 100° turn in the helix. R, L, and W represent Arginine, Leucine and Tryptophan residues, respectively.

4.3.2 Effect of sequence modification on the hydrophobicity of the peptide

ANS is a hydrophobic dye molecule, which binds to hydrophobic areas of folded proteins. Because of the high sensitivity of ANS to the polarity of the environment, it has been widely used as a probe to study the hydrophobicity of the molecules, protein aggregation, and cell membrane composition [181,182]. The fluorescence intensity and peak position of ANS change depending on its environment. In a low polar environment, the fluorescence intensity of ANS increases along with a blue shift in fluorescence spectrum peak toward lower wavelengths.

As shown in Figure 4.2, the peak positions for ANS fluorescence were different at different solutions; it located at ~520 nm for water (inset), but shifted to ~490 and ~460 nm for C6M1 (500 μM) and C6 (500 μM) solutions, respectively. The normalized ANS fluorescence intensity was also much higher for C6, compared with that of C6M1 at the same concentration. This indicates that the sequence modification in C6M1 has greatly decreased its hydrophobicity and improved its solubility in aqueous solutions. The calculation of hydropathy indexes (H.I.) of both peptides by averaging those of all amino acids also confirms the ANS results. The replacement of three leucine resides (H.I. of +3.8) with three tryptophan residues (-0.9) led to the H.I. of -0.47 for C6M1, compared with that of C6 (+0.31). The number of arginine residues (H.I. of -4.5) remained the same in both peptides. Further experiments with C6 showed that the intensity of the fluorescence was concentration-dependant. At higher C6 concentrations, ANS molecules had access to more hydrophobic regions at the surface of C6 aggregates, leading to more pronounced shift in peak position along with higher fluorescence intensity, until it reached saturation at concentrations above 400 μM.

The hydrophobicity of the drug/gene carrier is an important factor as it can affect the drug-carrier complex formation, biodistribution, and bioavailability and limit the solubility of the complex in aqueous solutions.

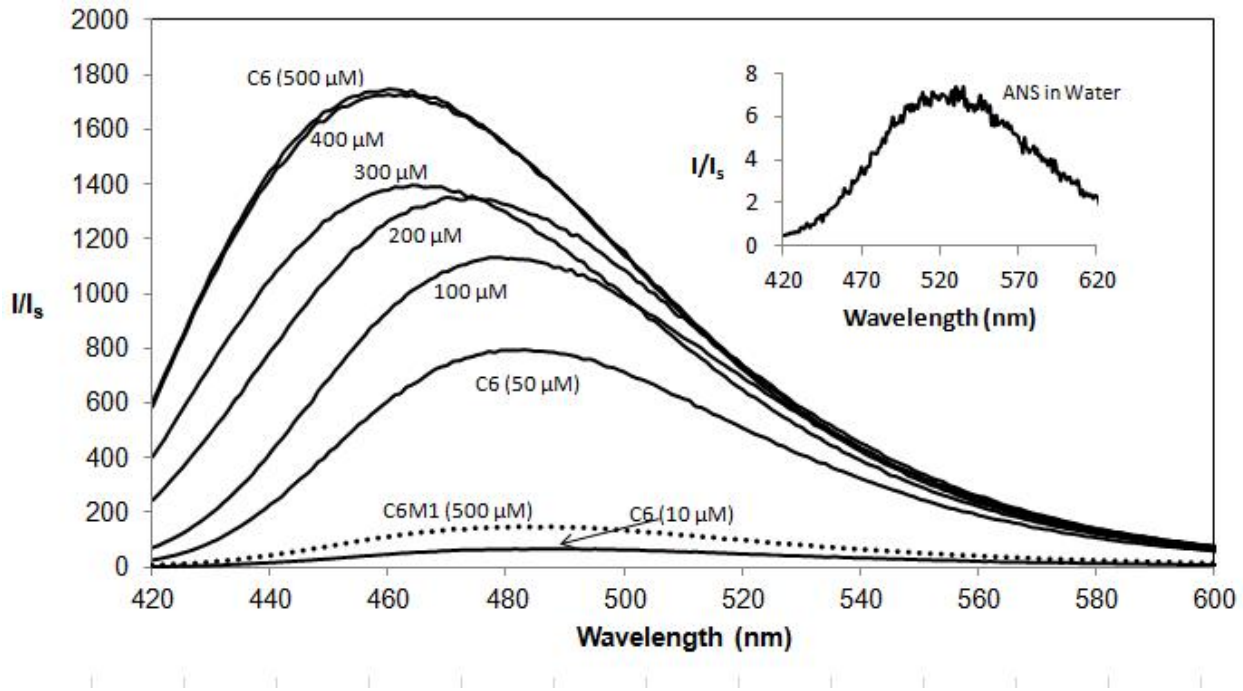

Figure 4.2 ANS fluorescence of C6 (10-500 μM) and C6M1 (500 μM). The final concentration of ANS was 10 μM. The inset plot shows the fluorescence of ANS in water at the absence of peptides. The fluorescence intensity of all samples was normalized to that of water sample at 670 nm (I_s).

4.3.3 Kinetics of adsorption of C6 and C6M1 at the air-water interface

Considering the amphipathic feature of C6 and C6M1, ADSA technique was employed to measure the kinetics of adsorption of peptide at air-water interface. Figure 4.3 shows the change in surface tension of C6 and C6M1 solutions (100 μM) over the time. The surface tension of C6 solution dropped fast initially and reached equilibrium after ~30 min. This indicates fast adsorption of C6 molecules and assemblies at air-water interface. In contrast, the surface tension of C6M1 solution showed no significant decrease at the first ~5 min, followed by a gradual decrease to reach equilibrium in ~90 min. The two different patterns of dynamic surface tension of C6 and C6M1 solutions corresponds to different kinetics of adsorption of peptides molecules

or assemblies at the air-water interface. Due to the more hydrophobic leucine residues, C6 molecules and aggregates diffuse very quickly from bulk to the liquid-air interface to minimize the exposure of hydrophobic residues/regions to the aqueous environment, affecting the surface free energy and decreasing the surface tension. However, the sequence modification in C6M1 enables the assembly of peptide in the bulk and gradual absorption of peptide molecules and assemblies at the interface, resulting in the slower decrease in surface tension of the solution. The lower equilibrium surface tension of C6 (~37 mN/m) compared to that of C6M1 (~41 mN/m) may also reflect the more hydrophobic nature of C6 in comparison to C6M1, confirming the results of ANS fluorescence assay.

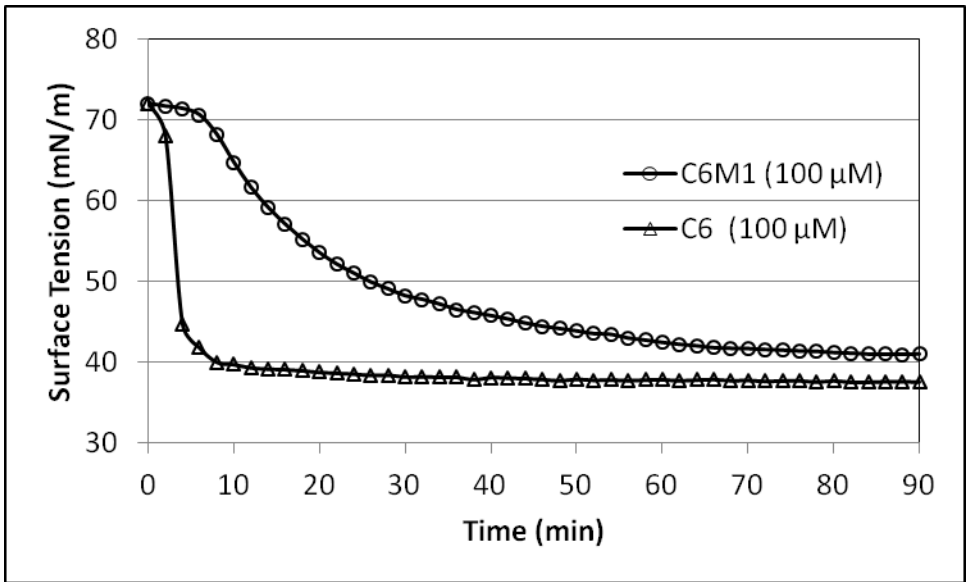

Figure 4.3 Dynamic surface tension of C6 and C6M1 solutions at a concentration of 100 μM.

4.3.4 Effect of complex composition on the adsorption of C6M1 at the air-water interface

The surface activity of C6M1 and its complex with siRNA at different molar ratios was further

studied using ADSA technique. The concentration dependence aggregation/assembly of amphipathic peptides is expected to be analogous to that of surfactants, which have both hydrophilic and hydrophobic moieties. The peptide-induced reduction in surface tension was measured as a function of peptide bulk concentration. The critical aggregation concentration (CAC) is defined as the concentration for which no further change in surface tension was detected. This was shown as the intersection of a diagonal line fitted to low concentration data and a horizontal line fitted to high concentration data point for which the surface tension values were almost constant (Figure 4.4 A). The CAC of C6M1, i.e., ~30 μM, was lower than CACs reported for other amino acid pairing (AAP) peptides (~ 60μM for EAK-16-II) [177,183]. However, the reduction in surface tension at CAC (~30 mN/m) was much higher than those of other reported AAP peptides (~10 mN/m for EAK-16-II), which reflected the stronger surface activity of C6M1.

The adsorption property of C6M1 was changed by its interaction with siRNA. Peptide:siRNA complexes at molar ratios from 0 to 80:1 were obtained using a fixed peptide concentration of 100 μM and varying siRNA concentration. As shown in Figure 4.4B, the surface tension of siRNA solution (20 μM) was as the same as that of water, indicating that siRNA did not have surface active nature. At low molar ratios up to 10:1, the siRNA molecules were enough to interact with whole C6M1 molecules which could eventually trap them in the bulk, resulting in no change in surface tension of the solution. However, at higher molar ratios, *e.g.*, 80:1, the excess of C6M1 molecules could create extra layers on already formed peptide-siRNA complex core through AAP peptide-peptide interactions. The presence of C6M1 molecules on the surface of the complex could regain the ability of complex to be absorbed in air-water interface, resulting in the same drop in surface tension as that of free peptide, i.e., ~30 mN/m. According to Figure 4.4 B, a molar ratio of at least 20:1 was required to gain surface active properties. The surface activity of the complex is required to efficiently interact with cell membrane component and internalize the cells.

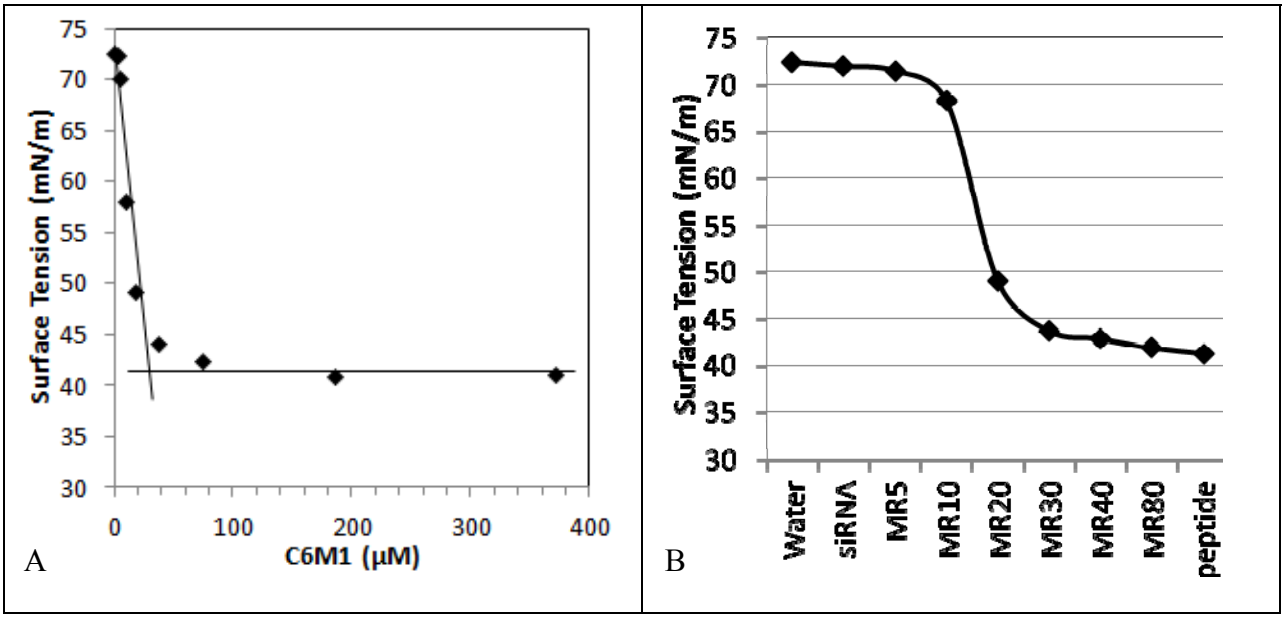

Figure 4.4 A) Equilibrium surface tension of C6M1 solution as a function of peptide concentration. The intersection of two fitted lines indicates the CAC of C6M1 (~30 μM), B) Surface tension of solutions containing C6M1/siRNA complexes at fixed peptide concentration of 100 μM and different molar ratios. The maximum standard deviation of the surface tension values was less than 0.3 mN/m. (MR= peptide:siRNA molar ratio)

4.3.5 Effect of sequence modification on secondary structure of the peptide

The secondary structure of C6 and C6M1 was characterized in water and a membrane-mimicking environment (50% TFE), using CD spectroscopy. As shown in Figure 4.5A, C6 in water showed a mostly random coil structure with only ~9% helical content (Table 4.1). However, C6M1 in water partially (~37%) adapted a helical structure. This increased helicity might be associated with more tryptophan residues in C6M1 which can stabilize the helical structure through π-π stacking of aromatic rings [184]. Both peptides showed a significant increase in helical content in 50% TFE solution (Figure 4.5A). The secondary structure of C6 and C6M1 in 50% TFE solution included 80 and 93% α-helices, respectively, implying that both peptides adapt mainly helical conformation upon interaction with cell membrane. TFE provides a membrane-mimicking environment and has been reported to have similar effect on CPPs

secondary structure as phospholipids do [185]. By changing its conformation, the peptide attains a more stable structure which allows better interaction with cell membranes and enhances cell penetration [186].

Further experiments with C6M1 showed that the helical contents of C6M1 increased with increasing the ionic strength of the media (Figure 4.5B). Changing the media from water to 30 and 100 mM NaCl solutions led to 40 and 50% helical contents in secondary structure of C6M1, respectively (Table 4.1). The presence of anionic components in media can screen the positive charge of arginine residues in one face of helical structure, resulting in decrease in their charge repulsion and adopting a stable helical structure. This finding was further confirmed by FTIR spectroscopy. Figure 4.6 shows the FTIR spectra of C6M1 in the wavenumber range of 1575-1725 cm^{-1}, which corresponds to amide I band. At this band, the peak of ~1650 cm^{-1} is attributed to the formation of α-helices; whereas random coil structures occur at 1640 cm^{-1}. The peaks of ~1630 and ~1690 cm^{-1} represent ß-sheet structures. As shown in Figure 4.6, C6M1 in water showed the peak around 1640 cm^{-1} with a wide shoulder around 1650 cm^{-1}, indicating the presence of a combination of random coil and α-helical structures. On the other hand, C6M1 in 200 mM NaCl solution adapted mainly α-helical structure (main peak at 1650 cm^{-1}) with a shoulder at 1640 cm^{-1} (random coil). These results are in full agreement with those obtained by CD spectroscopy (Figure 4.5 and Table 4.1).

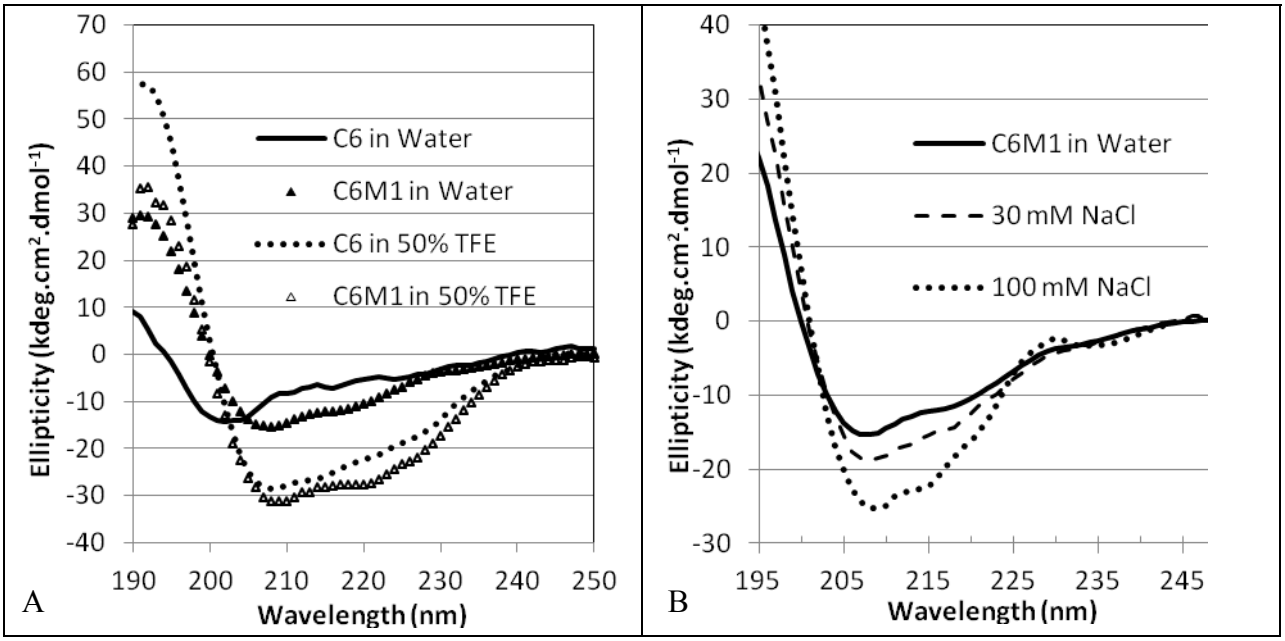

Figure 4.5 A) CD spectra of C6 (80 µM) and C6M1 (80 µM) in water and in 50% TFE. B) CD spectra of C6M1 (80 µM) in water, and saline.

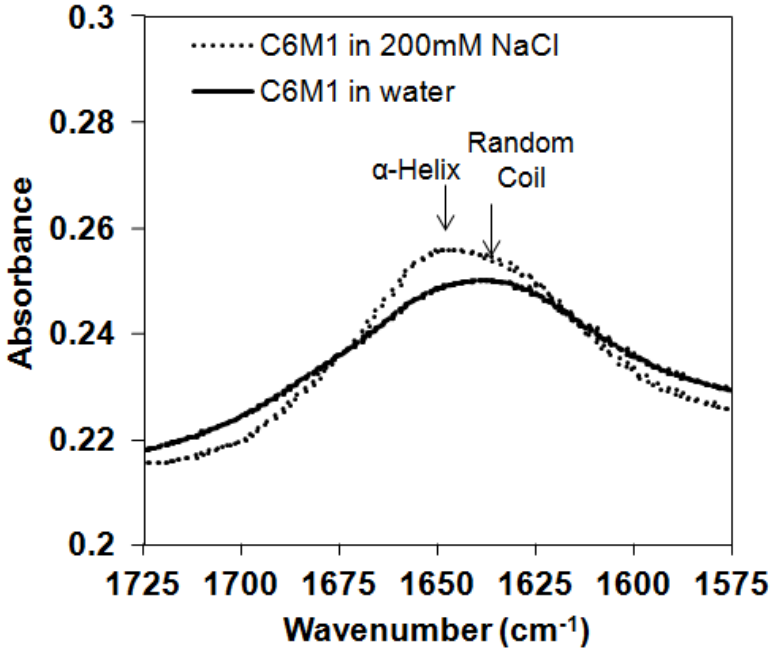

Figure 4.6 FTIR spectra (Amide I region) of C6M1 in water or 200 mM NaCl solution

Table 4.1- Secondary structure composition of C6 and C6M1 at different conditions

Sample	α-helix (%)	r.c. (%)	Other (%)
C6 in water	9	57	34
C6 in 50% TFE	80	20	0
C6M1 in water	37	45	18
C6M1 in 50% TFE	93	7	0
C6M1 in 30mM NaCl	40	44	16
C6M1 in 100mM NaCl	50	38	12

r.c. = random coil, TFE= Trifluoroethanol

4.3.6 Cytotoxicity of C6 and C6M1 peptides

In order to evaluate the cellular toxicity of C6 and C6M1 peptides and whether the modification of C6 peptide could alter its cytotoxicity behavior, dose-response toxicity assay of both peptides at final concentrations, ranging from 0.1 to 100 μg/ml, was performed on A549 cells. As reported in Figure 4.7A, peptide C6M1 showed lower toxicity with an IC50 (the concentration of peptide at 50% cell viability) of 22 μM, compared with C6 with an IC50 of 12 μM. This shows that modification of peptide C6 by replacing three Leucine residues with less hydrophobic tryptophan residues significantly reduced its cytotoxicity. Peptide C6 has shown high membrane perturbing activity and pore formation tendency, leading to cytotoxicity at high concentration above 2 μM (Not published). However, the modification of peptide sequence in C6M1 reduced toxic properties, making this peptide a safer carrier at concentrations used for siRNA delivery (below 4 μM).

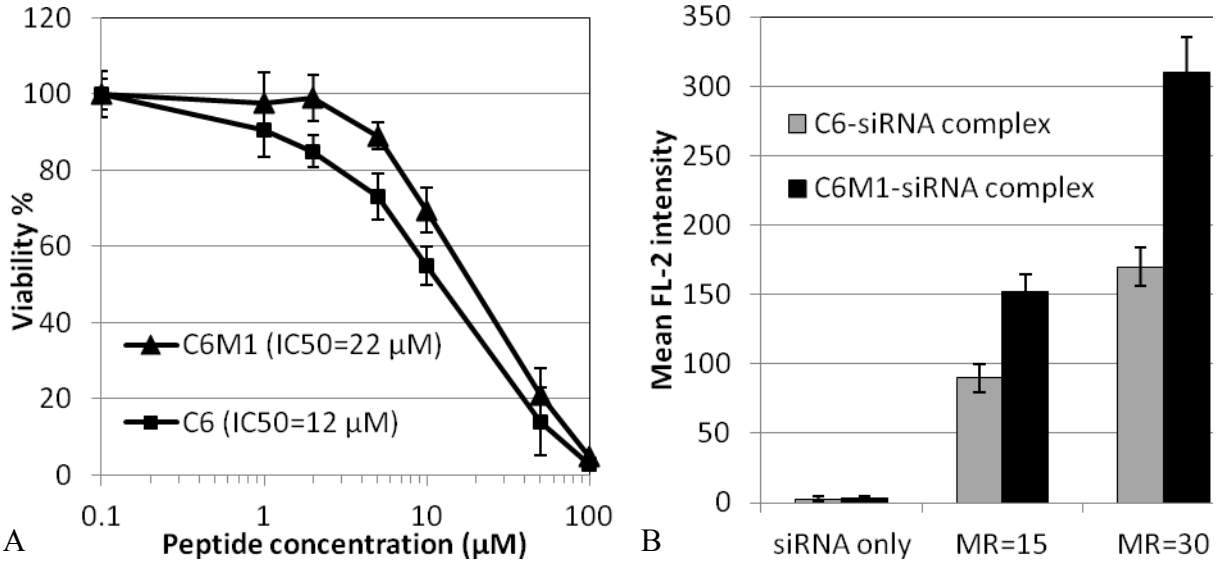

Figure 4.7 A) Effect of C6 and C6M1 peptides on the viability of CHO-K1 cells. Cells were cultivated in F-12K medium with indicated concentrations of peptides for 24 h. The cell viability was measured by CCK-8 assay. B) uptake of Cy3 labeled siRNA alone or in complex with C6 and C6M1 peptides at peptide:siRNA molar ratios (MRs) of 15:1 and 30:1. Fluorescence values were normalized to that of non-treated cells (uptake=0%). Error bars represent standard deviation of three independent experiments in both figures.

4.3.7 Effect of sequence modification on the peptide uptake efficiency

The efficiency of C6 and C6M1 peptides in delivering labeled Cy3-siRNA was evaluated by flow cytometry. This technique determines the quantity of intracellular complexes by measuring the Cy3 fluorescence intensity. Because of high tendency of these peptides to attach to cell membrane surface, a trypsin/heparin washing procedure was employed to ensure detachment of surface-bound complexes. After treatment with C6-siRNA or C6M1-siRNA complexes for 2 h at 37 °C, cells were washed with PBS, trypsin (0.5 mg/ml in PBS for 5 min), and heparin (0.5 mg/ml in PBS for 3×10 min), before flow cytometry analysis.

As shown in Figure 4.7B, siRNA by itself was unable to cross cell membrane; however, the complex of siRNA with C6 or C6M1 showed significant uptake in CHO-K1 cells which was dependent on the molar ratio (MR) of peptide:siRNA. Replacing three leucine (C6) with tryptophan residues (C6M1) led to ~90% increase in uptake efficiency of the peptide at both MR's, implying the role of tryptophan residues in facilitating the uptake of the complex. In a similar study, Bechara *et al.* reported the unique role of tryptophan residues in the interaction of cationic CPP's with cell surface glycosaminoglycans (GAGs), facilitating direct penetration or GAG-dependent endocytosis [187]. It is worth noting that the uptake efficiency of the peptide-siRNA complex does not necessarily reflect its transfection efficiency, as some complexes may trap in endosomes or have difficulties in releasing siRNA in the case of aggregation.

4.4 Conclusions

In this study, a new amphipathic peptide, C6M1, a modified version of already-reported C6 peptide, was introduced as a safer and more efficient carrier for siRNA delivery. The impact of the replacement of three leucine with tryptophan residues in peptide sequence on its solubility, secondary structure, cytotoxicity, and uptake efficiency was investigated. ANS fluorescence assay showed that the sequence modification significantly enhanced the solubility of the peptide in aqueous solutions. C6M1 also showed more helical content in its secondary structure compared with C6. This modification significantly reduced the cytotoxity of the peptide, making it a safer carrier. C6M1 was also found ~90% more efficient than C6 in delivering Cy3 labeled siRNA in CHO-K1 cells.

Chapter 5*

Physicochemical characterization, stability studies, and delivery efficiency of C6M1

The efficient delivery of nucleic acids as therapeutic agents is a major challenge in gene therapy. Peptides have recently emerged as a novel carrier for delivery of drugs and genes. The potential for peptides as vectors for nucleic acid delivery lies in their properties such as efficiency of cell penetration and capacity to bind and deliver. C6M1 is a designed amphipathic peptide with the ability to form stable complexes with short interfering RNA (siRNA). The peptide showed a combination of random coil and helical structure in water but mainly adapted a helical conformation in the presence of anions or siRNA. Revealed by DLS, TEM, and AFM techniques, the interaction of C6M1 and siRNA in water and HEPES led to complexes of ~70 and ~155 nm in size, but showed aggregation as large as ~500 nm in PBS. The time-dependent aggregation of the complex in PBS was studied by DLS and fluorescence spectroscopy. At molar ratio of 15:1, C6M1 was able to completely encapsulate siRNA; however, higher molar ratios were required to obtain stable complexes. Naked siRNA was completely degraded in 4 h in the solution of 50% serum; however C6M1 protected siRNA against serum RNase over the period of 24 h. Western blotting experiment showed ~75% decrease in GAPDH protein level of the cells treated with C6M1-siRNA complexes; while, no significant knockdown was observed for the cells treated with naked siRNA.

---

* This chapter is adapted from a paper draft "M. Jafari, Wen Xu, Ran Pan, C. M. Sweeting, N. Karunaratne, and P. Chen, Physicochemical characterization, stability studies, and delivery efficiency of C6M1 peptide, submitted to *J. Biochimica et Biophysica Acta* 2012".

5.1 Introduction

Over the past two decades, major advances have been made in the field of gene therapy. Since its discovery, RNA interference (RNAi) has provided new perspectives in developing novel nucleic acid (NA)-based therapeutics [2,3,5]. However, their development has been restricted by their poor stability and cellular uptake. NAs are vulnerable to enzymatic degradation in physiological environment, reducing their potency, and lack the ability to cross impermeable barriers of biological membranes. For the clinical advancement of RNAi, the design and development of safe and effective delivery systems is vital. Several viral and non-viral delivery systems, including lipids [41,42], polymers [43,44], and peptides [45,46] have been engineered and developed to obtain desired capabilities to overcome the cellular delivery barriers.

Cell penetrating peptides (CPPs) are short positively-charged peptides, usually less than 30 amino acids, with the ability to cross the cellular plasma membrane. CPPs have been reported to mediate the delivery of a large panel of cargos including siRNA, plasmid DNA, protein, and liposome *in vitro* and *in vivo* [168,188,189].Two different strategies are mainly applied to form peptide-cargo conjugates: either peptides are covalently attached to the cargo, or they interact through non-covalent, mainly electrostatic, interactions to form complexes. Considering the opposite charges of CPPs and NAs, the non-covalent approach has been mostly applied for the formulation of peptide-NA complexes.

Considering the amphiphilic nature of the cell membrane, the majority of protein-derived and designed CPPs are amphipathic. This feature facilitates the interaction of peptide with charged phospholipids or proteoglycans on the surface of cell membrane and hydrophobic core of the bilayer. It also enables peptides to interact with both hydrophilic and hydrophobic drugs. The amphiphilicity of the peptides may evolve from their primary structure, *e.g.*, MPG [72], or secondary structure, *e.g.*, CADY [118], and penetratin [80]. In Primary amphipathic peptides, the hydrophilic and hydrophobic moieties are located in the two opposite ends of the peptide sequence while, secondary amphipathic peptides are required to adapt a helical structure in order

to organize hydrophilic and hydrophobic moieties at opposite sides of the helix [109,176].

In this chapter we characterize the interaction of a designed amphipathic peptide, C6M1, with siRNA, using several spectroscopic and microscopic techniques. The change in the size and charge of the C6M1-siRNA complexes in different media will be discussed. The stability of C6M1-siRNA complexes in the presence of heparin and serum will be examined using gel electrophoresis. The effect of interaction with siRNA and anions on the secondary structure of C6M1 will be also explained.

5.2 Materials and methods

5.2.1 Peptides, siRNA and Chemicals

N-terminal acetylated and C-terminal amidated C6M1 peptide (MW=2689.4 g/mol, purity>98%) were purchased from CanPeptide, Inc. (Quebec, Canada). Glyceraldehyde 3-phosphate dehydrogenase (GAPDH) siRNA were purchased from Ambion (Austin, USA). All chemicals for buffer preparations were obtained from Sigma-Aldrich (Oakville, ON, Canada) and used as received.

5.2.2 Formulation of peptide-siRNA complexes

The peptide solution was prepared by dissolving peptide powder in RNase free water, HEPES (6 mM, pH=7.4), or phosphate buffered saline (PBS, pH=7.4), according to the designed experiment. A stock solution of 1mM was prepared and diluted at required concentrations. The solution was then vortexed for 10 seconds and sonicated for 10 minutes in a tabletop ultrasonic cleaner (Branson, model 2510, USA). siRNA was diluted in RNase free water , HEPES, or PBS, to a concentration of 50 μM. Peptide-siRNA complexes were formed by adding peptide solution into siRNA in proportion according to the designed experiment. The complexes were incubated

for 20 minutes at room temperature before each experiment, unless specified otherwise.

5.2.3 Dynamic Light Scattering (DLS) and Zeta potential

The size of the peptide-siRNA complexes was measured on a Zetasizer Nano ZS (Malvern Instruments, U.K.) equipped with a 4 mW He-Ne laser operating at 633 nm. Samples at molar ratios of 1:1 to 60:1 with final siRNA concentration of 100 nM were prepared as mentioned above. A quartz microcell (45 μL) with a 3 mm light path was used and the scattered light intensities were collected at an angle of 173°. Clear disposable zeta cells were used for Zeta potential measurements. The size distribution and zeta potential values were acquired using the multimodal algorithm CONTIN, Dispersion Technology Software 5.0. Three independent measurements were performed for each sample 20 min after sample preparation at 25°C.

5.2.4 Transmission Electron Microscopy (TEM)

5μl samples of peptide/siRNA complexes at siRNA concentration of 200 nM and molar ratio of 30:1 in water, HEPES, and PBS were deposited onto 400 mesh Formva coated copper grids (Canemco-Marivac, Canada) for 10 minutes. The excess was blotted with a filter paper. The grids were then washed by plunging into an RNase free water bath, followed by drying overnight. The samples were stained with 2% uranyl acetate solution (Electron Microscopy Sciences) and analyzed on TEM (Philips CM10 TEM).

5.2.5 Atomic Force Microscopy (AFM)

The nanostructures of C6M1-siRNA (molar ratio of 30:1) complex were characterized by AFM. The sample solution (10 μl) was placed on a freshly cleaved mica surface, fixed on a glass slide, and incubated for 30 min at room temperature to allow the sample to adhere onto the mica surface. The mica was then rinsed five times with Milli-Q water to remove any unattached particles, followed by air-drying overnight. The mica surface was analyzed by a PicoScanTM AFM (Molecular Imaging, Phoenix, AZ) at room temperature using the tapping mode with

silicon single-crystal tips (NCL type, Molecular Imaging, Phoenix, AZ), with a typical tip radius of 10 nm and resonance frequency of <170 kHz.

5.2.6 Fluorescence spectroscopy

Since C6M1 has four tryptophan residues as intrinsic fluorescent probes, fluorescence spectroscopy was applied to characterize the interaction between siRNA and peptide. The peptide fluorescence was acquired on a Photon Technology International spectrofluorometer (Type LS-100, London, Canada) with a pulsed xenon lamp as the light source. Samples (80 µl) were transferred to a quartz cell (1cm×1cm) and excited at 280 nm and spectra were collected in the range of 300-500 nm. The standard fluorescence intensity I_s was obtained by taking the average of the fluorescence of peptide only sample from 480 to 500 nm.

5.2.7 Circular Dichroism (CD) spectroscopy

C6M1-siRNA complexes in water or HEPES-buffered saline (HBS: 6 mM HEPES, 150 mM NaCl) at molar ratios of 10:1, 20:1, and 40:1 were prepared at fixed C6M1 concentration of 80 µM and varying concentration of siRNA. Spectra from 250 to 190 nm with spectral resolution and pitch of 1 nm and scan speed of 200 nm/min were recorded with a J-810 spectropolarimeter (Jasco, USA). Samples were transferred into 1 mm long quartz cells and maintained at 25 °C. Spectra shown are the average of three replicates. The raw CD ellipticity (in millidegrees) was converted to residue molar ellipticity (deg.cm^2.dmol^{-1}.residue^{-1}): $\theta=\theta_{raw}/ (10\times C\times N\times l)$, where θ_{raw} is the ellipticity in millidegrees, C is the peptide concentration (mol/L), l is the optical path length of the cell (cm) and N is the number of residues. The secondary structure composition of the peptide was estimated from CD spectra using K2D3 program [178].

5.2.8 Gel electrophoresis

To study the ability of C6M1 to co-assemble with siRNA, the agarose gel electrophoresis was carried out at 50 V for 60 min in TBE buffer (4.45 mM Tris–base, 1 mM sodium EDTA, 4.45

mM boric acid, pH 8.3). C6M1 and siRNA were mixed at different molar ratios ranging from 1:1 to 40:1 and incubated at 37 ^{o}C for 20 min, to form complexes. Samples were analyzed on a 0.8% wt/vol agarose gel, stained with 0.5 μg/ml ethidium bromide and revealed by UV illumination.

To evaluate the stability of the complexes at different molar ratios, the heparin completion assay was performed. Different amounts of heparin corresponding to final concentrations from 0.5 to 10μg heparin per 10 μl of the complex were added to C6M1/siRNA complexes at molar ratios of 15:1, 40:1, 60:1, and 80:1. Ten microliters of each sample, corresponding to 50 pmol of siRNA, was then analyzed by electrophoresis on agarose gel (1.2% wt/vol) stained with ethidium bromide.

5.2.9 Stability of naked siRNA and complexes in the presence of serum

The ability of C6M1 in protecting siRNA against degradation by serum components was studied by agarose gel electrophoresis. C6M1-siRNA complexes at molar ratio of 30:1 were incubated with equal volume of fetal bovine serum (FBS) (final concentration of 50% v/v) at 37 °C. The inactivated serum, treated with 0.5M EDTA, was used as a control. 20 μl aliquots were taken at 30min, 2h, 4h, 6h, 18h and 24h. 1μl of 0.5M EDTA was immediately added to stop the degradation. After the addition of 1% heparin to displace siRNA from the complex, aliquots were analyzed by 0.8% agarose gel electrophoresis.

5.2.10 C6M1-mediated siRNA knock down analysis by Western blotting

CHO cells were cultured in 12-well cell culture plates at a concentration of 80000 cell/ml to reach ~60% confluency the next day. 24 h later, the medium was replaced with Opti-MEM. The complexes of C6M1 with GAPDH siRNA or scrambled (negative control) siRNA at molar ratio of 30:1 were prepared in Opti-MEM and incubated in 37°C for 20 min. The complexes or naked siRNA were then added to the cells and incubated at 37 °C humidified atmosphere containing 5% CO2. 3 hours later, growth medium with 20% FBS was added. 24 h post-treatment, the cells were washed with PBS. Cells were detached by adding trypsin 48 hours after transfection,

incubated with ice-cold lysis buffer 50 mM Tris-base, 150 mM NaCl, pH 8.0, 1% Triton X-100) containing Protease Inhibitor Cocktail (Cell Signaling Tech.) for 20 min, mixed every 5 min and then centrifuged at 4°C for 10 min at 13000 g. The supernatants were collected and total protein concentration was measured using BCA protein assay kit (Pierce) (Appendix A). 15 mg cell extract proteins were separated by 12% SDS-PAGE and transferred onto a nitrocellulose membrane, blocked with TBS containing 5% dried skimmed milk for 1 h, followed by overnight incubation at 4°C with mouse anti-ß-actin (AM4302, Ambion) and mouse anti-GAPDH (AM4300, Ambion). After washes in 0.05% Tween in PBS, the membrane was incubated with anti-mouse-HRP secondary antibody (Sigma-Aldrich). The blots were exposed by ECL Plus substrate and developed on X-Ray film (Fisher Scientific).

5.3 Results

5.3.1 Peptide structure

Considering several factors, including peptide self assembly, peptide-siRNA co-assembly, siRNA loading and protection capability, peptide C6M1 was designed. Figure 5.1 shows the sequence, helical structure, and helical wheel projection of C6M1. The distribution of amino acids in C6M1 sequence enables the appearance of the same residues on the same face of the helix, inducing the amphiphilicity to the peptide. This arrangement facilitates the interaction of the peptide with siRNA and cell membrane and mediates the internalization of the peptide and its associated complex.

It is generally believed that the hydrogen bonding between N-H and C=O groups in the backbone of the peptide is involved in the formation of the helical structure. However, the role of hydrophobic, hydrogen bonding, π-π stacking, and electrostatic interactions between side chains in stabilizing the helices has also been revealed [190,191]. Considering the unique arrangement

of amino acids in C6M1 helical structure, hydrophobic interaction between leucine residues, π-π stacking interaction between tryptophan residues, and hydrogen bonding between arginine residues are expected to stabilize the helical conformation of the peptide (Figure 5.1).

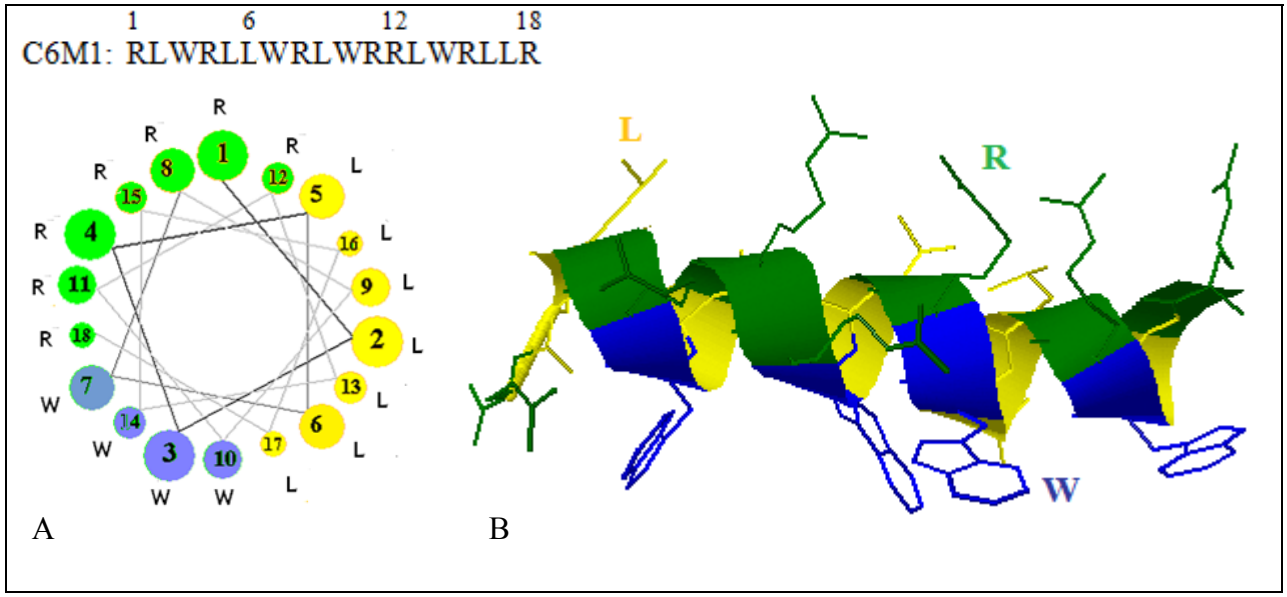

Figure 5.1 Helical structure and helical wheels representation of C6M1. A) A downward cross-sectional view of the helix axis is shown. The axis of the alpha helix is orthogonal to the paper plane. The bigger the circle is, the upper turn the residue is located in, when viewing from the top, B) In helical structure, same amino acids (side chains) face the same side of the helix. The schematic was generated using RaptorX web server [192]. R (green), L (yellow), and W (blue) represent arginine, leucine and tryptophan residues, respectively.

5.3.2 Size and surface charge of the C6M1-siRNA complexes in different media

The size of the C6M1-siRNA complexes at molar ratio of 30:1 was measured by dynamic light scattering. The complexes were incubated for 20 min in water, HEPES, or PBS prior to size measurement. As shown in Figure 5.2A, complexes in water and HEPES buffer showed an average size of ~70 and ~155 nm, respectively; however, the incubation in PBS led to the aggregation of the complex (~460 nm). As the surface charge of the complex has been reported to affect its size, bio-distribution, and cellular uptake [193], zeta potential experiments were

carried out for the complexes in water, HEPES, and PBS at molar ratios from 5:1 to 30:1. As shown in Figure 5.2B, Complexes in all three media at MR of 5:1 showed a negative zeta potential, implying that the peptide molecules were not enough to cover all negatively-charged siRNA molecules. At MR of 10, complexes in water and HEPES showed positive zeta potential; while those in PBS possessed negative surface charge. This indicated that the ions in PBS may interfere with the electrostatic interaction between the peptide and siRNA, leading to mostly uncovered siRNAs. Increasing the MR to 30:1 led to zeta potential of + 57, +31 and +5 mV in water, HEPES, and PBS, respectively. The charge repulsion in highly-charged complexes in water prevented their aggregation, keeping the size around 70 nm. HEPES, as a zwitterionic buffering agent, can maintain the physiological pH without significant contribution to the ionic strength of the solution and is a commonly-applied buffer in cell culture media. The low ionic strength of HEPES only slightly increased the size of the complex to ~155 nm, considering the zeta potential of +31 mV. In contrast, the high concentration of phosphate and chloride anions in PBS mainly neutralized the positive charge of the complex surface, as arginine residues on the surface of the complexes could act as phosphate and chloride binding sites [194]. This promoted the aggregation of the almost neutral particles mainly through hydrophobic interaction of leucine residues.

In a similar study, Hao *et al.* reported the dependency of size and charge of a cationic polymer-DNA complex on the nature of the media [195]. In their experiments, the complex had a high zeta potential and low particle size in water and 5% glucose solution. In contrast, PBS, DMEM or saline, lowered the zeta potential and mediated the aggregation of the particles. This is in accord with our observation and indicates that the ions in the medium could alter the size and charge of the complexes of cationic peptides/polymers with NAs.

These findings were confirmed by microscopic approaches. Figure 5.3 shows the TEM images of C6M1-siRNA complexes in water, HEPES and PBS. The sample in water and HEPES showed nanoparticles of irregular shape with less than 100 and 200 nm, respectively; whereas, those in

PBS showed aggregates of larger than 700 nm. The AFM images confirmed a size distribution of 20-200 nm for the complex in water (Figure 5.4A); while, the image of the sample in PBS proved the presence of large aggregation (Figure 5.4B).

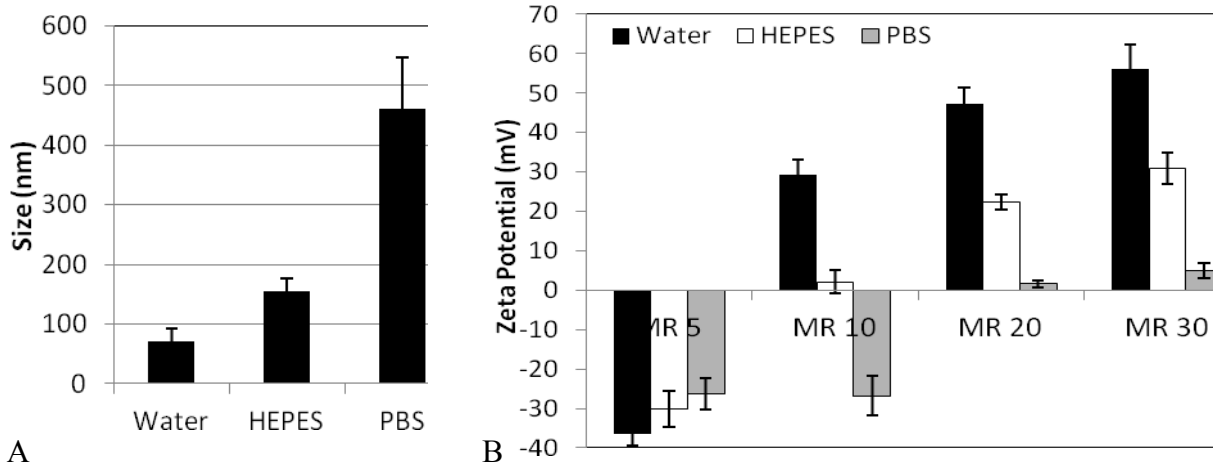

Figure 5.2 A) Size of the C6M1-siRNA complexes in water, HEPES, and PBS, B) Zeta potential of C6M1-siRNA complexes at different molar ratios in water (black bars), HEPES (white bars), and PBS (grey bars). Error bars represent standard deviation of triplicates. (MR= C6M1:siRNA molar ratio)

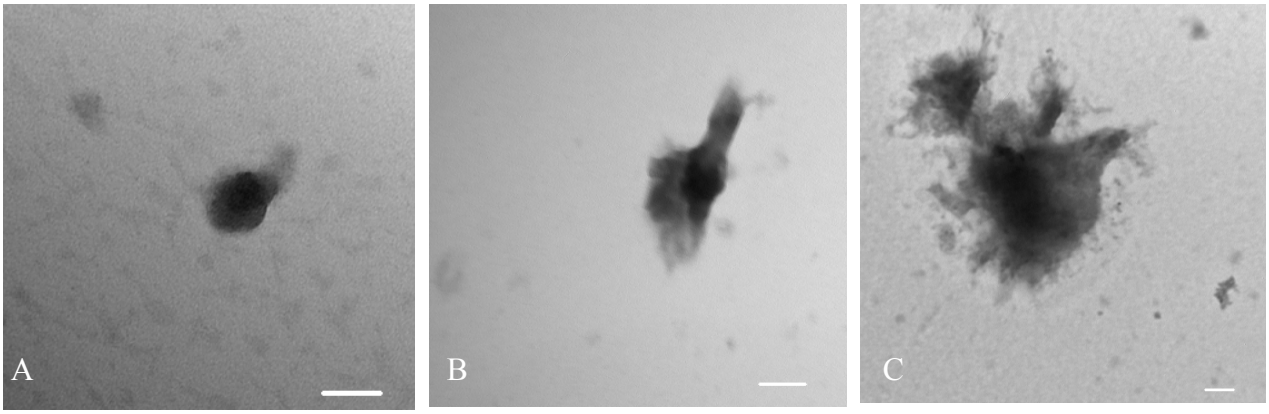

Figure 5.3 Transmission electron microscope images of C6M1-siRNA complexes (MR=30:1) in water (A), HEPES buffer (B), and PBS (C). Scale bars are 100 nm.

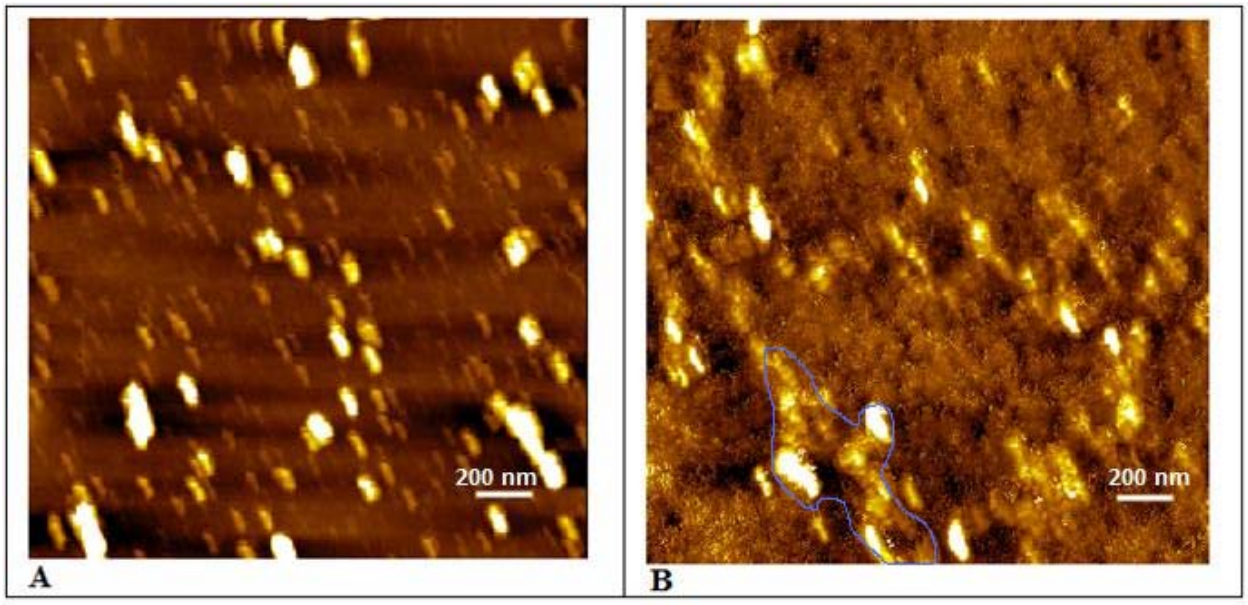

Figure 5.4 AFM images of C6M1-siRNA complex (MR=30:1) in water (A) and PBS (B). The sample solution (10 µl) was placed on the mica surface, and incubated for 30 min at room temperature. The mica was then rinsed with Milli-Q water, followed by air-drying overnight. The blue curve shows the border of an aggregate in PBS. The scan size of the images is 2 × 2 μm^2.

5.3.3 Time-dependant aggregation of C6M1-siRNA in PBS

The size of the C6M1-siRNA complex formed in PBS varied with time and the peptide:siRNA molar ratio (MR). As shown in Figure 5.5, the size of the complex remained unchanged at the MR of 1:1. At the MR of 5:1, the size of the complex changed from 50 to 120 nm over a time period of 3 h. When the ratio was increased to 20:1, a larger aggregation (~500 nm) was observed in a short time of 30 min. Further investigation showed that the size of the complex could grow up to 1 µm at higher MRs (Figure 5.5). It should be noted that change in the size of the complexes was only observed in PBS and the size of the complexes in water and HEPES remained below 100 and 200 nm, respectively, even after 24 h incubation. These results show the importance of choosing suitable media especially during the formulation process, to avoid the aggregation or degradation of the complex which can greatly affect its functionality. Considering the buffering capabilities and "salt free" nature, HEPES was suggested as the solution for

peptide-siRNA formulation.

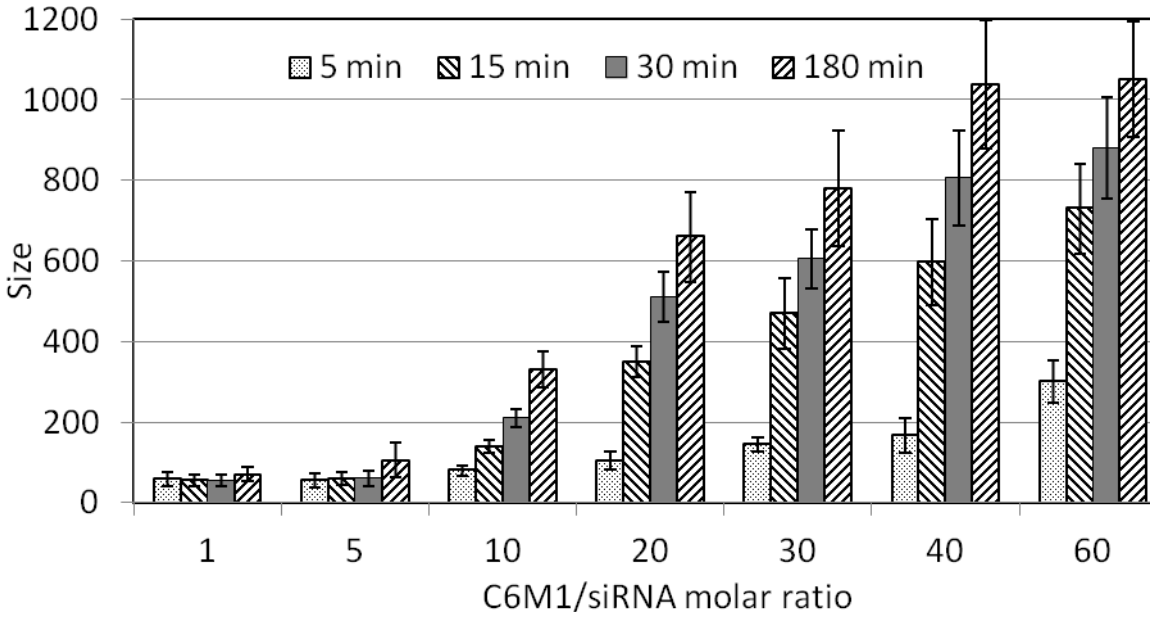

Figure 5.5 Size of C6M1/siRNA complexes at different molar ratios in PBS solution over time. Error bars represent standard deviation of three independent experiments.

5.3.4 Change in fluorescence spectra over time

Using tryptophan residues in C6M1 as internal fluorescent probes, the change in fluorescence spectra of C6M1-siRNA complexes at MR of 20:1 was measured over a time period of 70 min. As tryptophan fluorescence is sensitive to the local environment, changes in the fluorescence emission spectra provide information on the conformation and aggregation of the peptide [196]. As shown in Figure 5.6, a decrease in the fluorescence intensity of the complex was observed over time until it reached a plateau at ~60 min. This change in fluorescence intensity could only correlate to the change in the particle size as no other physicochemical parameter was changed during the experiment. Increasing the size of the complexes minimized the total surface area and number of tryptophan residues on the surface of the complexes, compared to smaller complexes, leading to decrease in the fluorescence intensity. The DLS experiment also revealed that there was no significant change in size of the complexes after ~60 min (not shown). The change in the

fluorescence of the complex in water was negligible since there was no significant aggregation of the complex (Figure 5.6, inset).

5.3.5 Conformational Changes of C6M1 upon interacting with siRNA

The impact of siRNA on the secondary structure of C6M1 in water and HBS (6 mM HEPES, 150 mM NaCl) was evaluated by CD spectroscopy. As shown in Figure 5.7A and Table 5.1, C6M1 in water showed a combination of helical structure (37%) and random coil (45%) in its secondary structure. Introducing small amount of siRNA (MR of 40:1) increased the absolute values in spectrum minima at 208 and 222 nm, and the maximum around 190 nm, which represent the helical structure. The helical content of C6M1 secondary structure increased to 81% at higher concentration of siRNA (MR of 10:1). The secondary structure of C6M1 did not change by introducing more peptides, indicating a saturation point at MR of 10:1. Considering the arrangement of amino acids in C6M1 (Figure 5.1), the ionic interaction between siRNA and arginine residues may stabilize C6M1 helical structure by neutralizing positive charge of arginine residues and reducing the charge repulsion between them. In HBS, however, the MRs of 20:1 and 40:1 showed the highest helical contents (69%) (Figure 5.7B and Table 5.1). Interestingly at MR of 10:1, the presence of high amount of oligonucleotide and chloride anions led to a deformation of the CD spectra with a decrease in helical structure. This might be related to helix aggregation at high anion and RNA concentrations as also reported for CADY peptide [150].

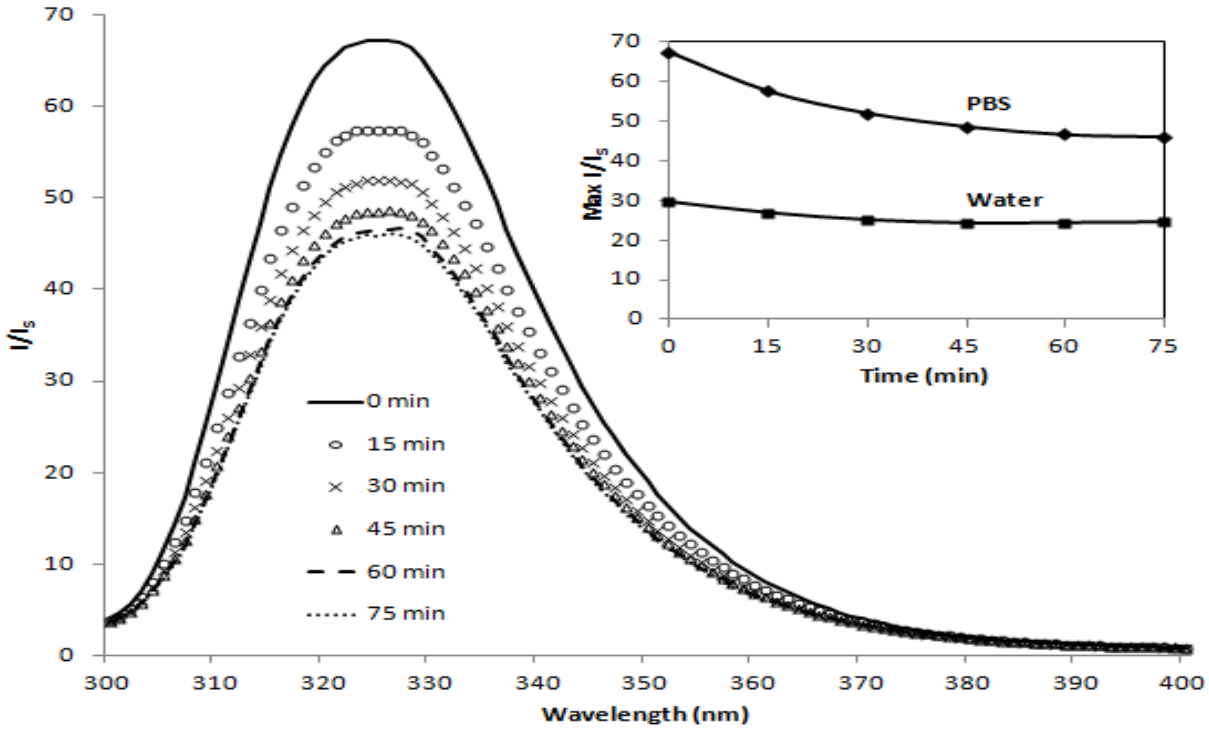

Figure 5.6 Change in fluorescence intensity of C6M1-siRNA complex (MR=20:1) over time in PBS. Inset Plot shows the change in maximum fluorescence intensity of the complex in PBS and water over time.

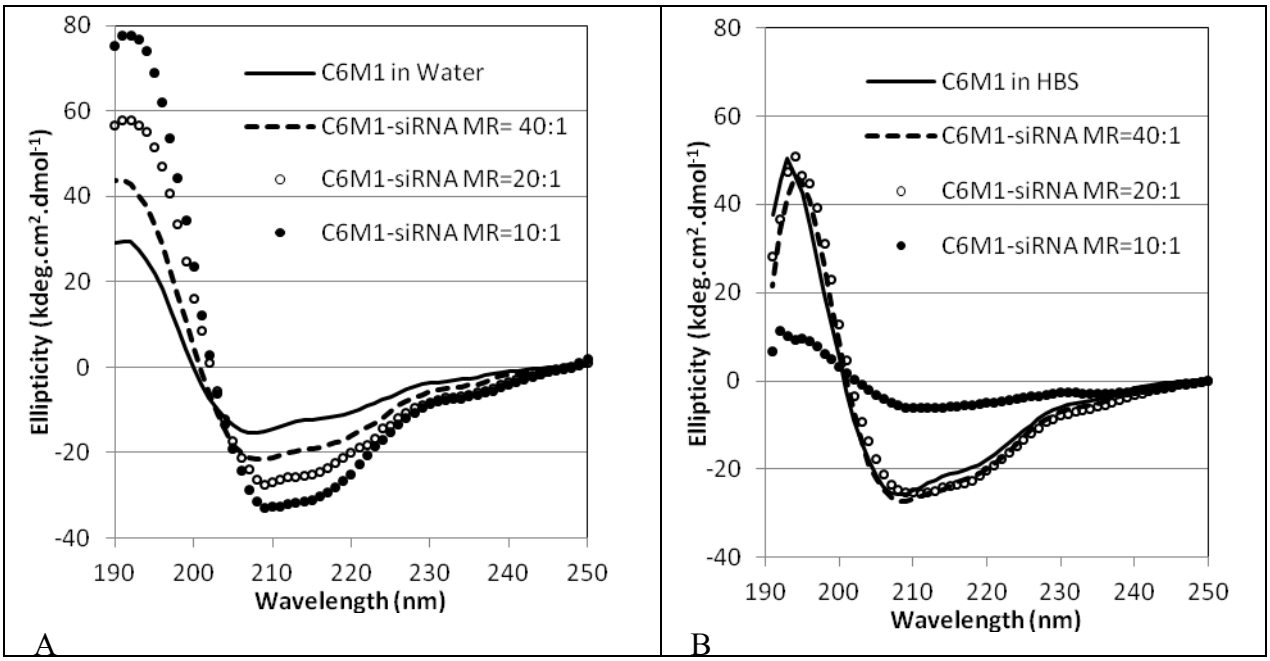

Figure 5.7 CD spectra of C6M1 peptide (80 μM) with varying amounts of siRNA in water (A) and in HBS (B). (MR= C6M1:siRNA molar ratio).

Table 5.1 Secondary structure composition of C6M1 at different conditions

Sample	α-helix (%)	r.c. (%)	Other (%)
C6M1 in water	37	45	18
C6M1-si MR=40 in water	54	36	10
C6M1-si MR=20 in Water	74	24	2
C6M1-si MR=10 in Water	81	19	0
C6M1 in HBS	63	31	6
C6M1-si MR=40 in HBS	69	27	4
C6M1-si MR=20 in HBS	69	27	4
C6M1-si MR=10 in HBS	26	50	24

r.c. = random coil
MR= peptide:siRNA molar ratio

5.3.6 Agarose gel shift assay to characterize the interaction of C6M1 with siRNA and stability of the complex

Agarose gel shift assay was applied to evaluate the interaction between siRNA and C6M1 molecules, the stability of the formed complex in the presence of heparin and serum. Positively-charged peptides interact with siRNA mainly electrostatic interaction between basic residues and phosphate groups in siRNA backbone. Free negatively-charged siRNA molecules could move toward the positive electrode when the voltage is applied; while, stable peptide-siRNA complexes prevent the internalization of siRNA molecules to agarose gel, suggesting that there is no free siRNA to appear in siRNA bands.

Figure 5.8B shows the agarose gel shift assay of C6M1-siRNA complexes at different MRs. As shown, at MR of 1:1, there was no significant difference between siRNA bands of free "siRNA only" and "MR=1:1" samples, suggesting that this MR was not enough to encapsulate the majority of siRNA molecules. The siRNA band in MR of 5:1 was less bright than that of "siRNA only" sample, implying an effective interaction between C6M1 and siRNA molecules at this ratio. At the molar ratio of 10:1, very small amount of free siRNA was observed on siRNA band, indicating that siRNA molecules were almost completely complexed with C6M1. The siRNA band was completely disappeared at the MR of 15:1. Considering 7 arginine residues in C6M1 and 42 nucleotides in an siRNA molecule, 6 molecules of C6M1 should theoretically be enough to encapsulate one siRNA molecule; however, this finding suggests that excess C6M1 molecules are needed to achieve stable complexes.

Gel electrophoresis was also applied to study the stability of C6M1-siRNA complexes at different MRs in the presence of heparin. Heparin is an anionic competitive binding agent and a chemical analog of heparan sulphate proteoglycans (HSPG). The complex is expected to be stable at low concentration of heparin, as HSPG are abundantly found in the extracellular matrix and can dissociate the complex in extracellular environment. On the other hand, the complex should be able to dissociate and release siRNA easily, following cellular entry. As shown in

Figure 5.8 B, C6-siRNA complexes were stable in the absence of heparin (second well from left) and no free siRNA was shown in siRNA bands at all MRs. The complex at MR of 15:1 was dissociated at heparin concentration of 2.5 µg per 10 µl of sample and higher. The minimum concentration of heparin required for dissociation of the complex increased by increasing the MR, indicating that higher amount of peptide could protect siRNA against dissociation from the complex. Interestingly, the complex at molar ratio of as high as 80:1released siRNA at high concentration of heparin, implying its ability to release siRNA even at high MR.

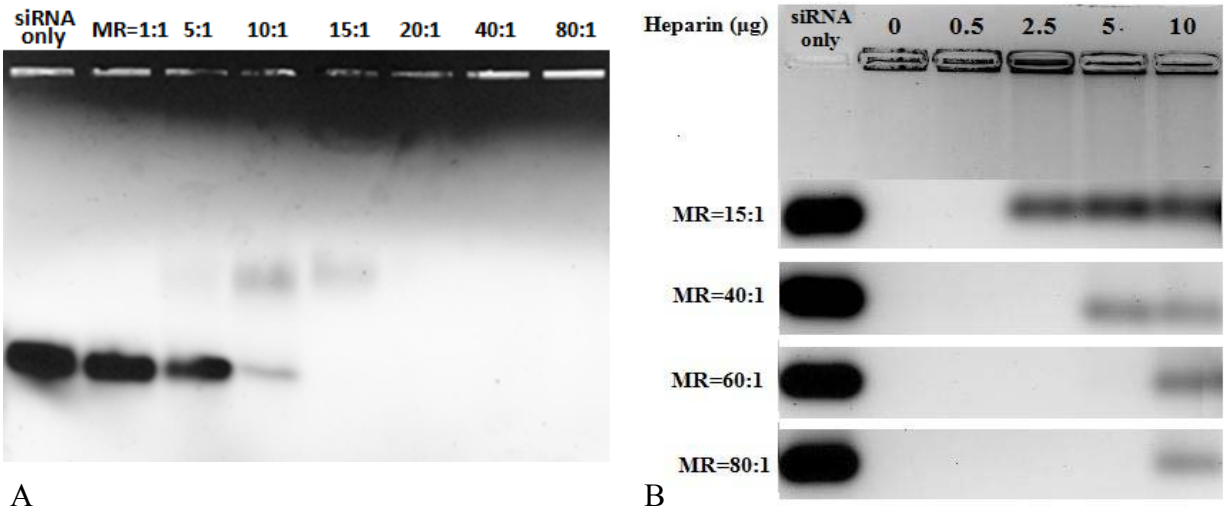

A B

Figure 5.8 A) The formation of siRNA-C6M1 complex indicated by agarose gel, B) The stability of C6M1-siRNA complex indicated by heparin competition assay. Different amounts of heparin corresponding to final concentrations of 0.5 to 10µg heparin per 10 µl of complex were added to C6M1-siRNA complexes at different molar ratios. The stability of complexes were analyzed by electrophoresis on agarose gel (1.2% wt/vol) stained with ethidium bromide. For better comparison, the siRNA bands of four independent gels were put in the same image.

5.3.7 Stability of the complex to serum RNase degradation

Naked siRNAs are vulnerable to RNase degradation. In our study, we were interested in

measuring the protection afforded by the peptide against serum RNase. Naked siRNA and C6M1-siRNA complexes at MR of 30:1 were incubated in the presence of 50% active fetal bovin serum (FBS) and aliquots were taken at determined time intervals. Heparin was added to the complex after incubation with serum to release siRNA from the serum associated complexes.

As shown in Figure 5.9A, Naked siRNA was completely degraded after 4 h incubation with active serum; however, it was stable in the presence of inactive serum. In contrast, C6M1 was able to protect siRNA even after 24 h incubation with high concentrations of serum, showing the ability of C6M1 in protecting siRNA against serum RNase.

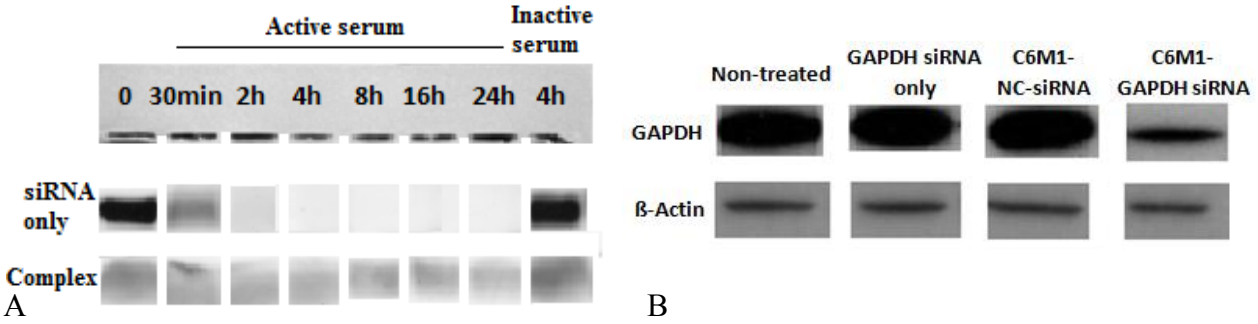

Figure 5.9 Stability of the C6M1-siRNA complexes to serum RNase degradation over time. Naked siRNA or C6M1-siRNA complex at molar ratio of 30:1 were incubated in the presence of 50% active serum (FBS) over the period of 24 h or 50% heat-inactive serum (control) for 4 h. Aliquots (20 µl) were taken at 30min, 2h, 4h, 6h, 18h and 24h and EDTA (1 µl) was immediately added to stop the degradation. After the addition of 1% heparin to displace siRNA from the complex, aliquots were analyzed by 0.8% agarose gel electrophoresis. For better comparison, the siRNA bands of three independent gels were put in the same image. B) GAPDH protein levels were determined by western blotting using ß-actin as a control for quantification. CHO-K1 cells were treated with naked GAPDH siRNA or the complex of C6M1 with GAPDH siRNA (or negative control NC-siRNA) at MR of 30:1 at 50 nM siRNA final concentration. 24 h post-treatment, the cells were lysed and analyzed by western blotting for the GAPDH protein levels as described in "Materials and Methods" section.

5.3.8 Knock-down efficiency of C6M1-siRNA complexes

The efficiency of C6M1 in intracellular delivery of siRNA and the knock-down of GAPDH gene were analyzed in protein level by Western blotting technique. As shown in Figure 5.9B, the treatment of CHO-K1 cells with naked GAPDH siRNA did not change the level of this protein, implying that siRNA without an efficient carrier was not able to gain access to intracellular environment. However, the C6M1-siRNA complexes significantly decreased the level of GAPDH protein. Analysis of the gel images by ImageJ software showed ~75% decrease in the GAPDH protein level in the cells treated with C6M1-GAPDH siRNA complexes compared to non-treated cells; while, those treated with naked siRNA or C6M1-NC siRNA showed no significant knockdown. ß-actin protein was used in this experiment as an internal control for quantification.

5.4 Conclusions

Understanding the properties of peptides is necessary for their effective use as siRNA delivery systems. C6M1, an 18-mer amphipathic peptide, formed small complexes in water and HEPES (<200 nm), but aggregated to larger particles in PBS. Using DLS and fluorescence spectroscopy, the study of the aggregation kinetics of complex in PBS revealed that the size of the complex remained almost constant after 1 h incubation. The secondary structure of C6M1 in water involved a combination of helical and random coil structures; however, upon binding to siRNA or in the presence of anions, C6M1 adapted mainly an α-helical structure. Agarose gel experiments showed that C6M1 was able to completely encapsulate siRNA molecules at molar ratio of 15:1; however, higher molar ratios were required to achieve stable complexes. C6M1 showed high capability in protecting siRNA against serum nuclease over the period of 24 h; while naked siRNA was completely degraded in 4 h. Western blotting experiment showed ~75% decrease in GAPDH protein content of the cells treated with C6M1-siRNA complexes.

Chapter 6*

Size-dependent internalization pathways of peptide C6M1

Understanding the mechanisms of cellular attachment, uptake, and intracellular pathways facilitates the development of safe and efficient gene delivery vectors. Cell penetrating peptides (CPPs) have been recently applied for intracellular delivery of a variety of therapeutic agents; however, their uptake mechanism is still a matter of debate. In this work, we investigated the interaction of a novel amphipathic peptide, C6M1, in complex with short interfering RNA (siRNA), with cell surface and the mechanisms involved in the internalization of the complex at different size ranges. Heparin and chlorate treatments revealed that the electrostatic interaction of the C6M1-siRNA complex with heparan sulphate proteoglycans (HSPGs) at the cell surface is required to trigger the uptake process. Using physical and chemical endocytic inhibitors, we also found that small C6M1-siRNA complexes (mean ~155 nm) mainly enter Chinese hamster ovary (CHO-K1) cells through an energy-independent mechanism, most likely involving direct translocation. In contrast, large complexes (mean ~460 nm) internalize CHO-K1 cells mainly through a lipid raft-dependant macropinocytosis. The integrity of the cytoskeletal components, *e.g.*, actin filaments, and microtubules, also showed significant impact on the efficient internalization of the C6M1-siRNA complex. The kinetics experiments also confirmed the fast internalization of small complexes (with uptake half-time of 25 min) in comparison to large complexes (70 min).

---

* This chapter is adapted from a paper "M. Jafari, S. Naahidi, R. Pan, and P. Chen, Size-dependent internalization pathways of a novel amphipathic cell penetrating peptide, submitted to *J. Nanomedicine* 2012".

6.1 Introduction

Cell-penetrating peptides (CPPs), net positively charged peptides of 8-30 amino acids, have recently gained increasing attention due to their ability to cross biological membranes and mediate intracellular delivery of various types of cargos [66,154,188]. Despite their widespread use as delivery systems, the mechanism through which CPPs internalize the cells is still under debate. A combination of both direct translocation and endocytosis has been suggested as the uptake mechanism for CPPs [197,198]. Earlier observation in which CPPs could internalize into the cells even at low temperature (4 °C) suggested direct translocation as the main uptake mechanism as endocytosis is suppressed at this temperature [79,103]. However later studies showed that high cell surface binding properties of most CPPs might have led to experimental artifacts by overestimation of internalization [199]. Recent studies revealed that several factors including the experimental conditions, peptide concentration, particle size, nature of the cargo, and cell type have significant effects on the uptake mechanism of CPPs [200].

As the most common mechanism of cellular uptake for gene delivery vectors, endocytosis is an energy-dependent process by which cells take up material by engulfing them in membrane invaginations. It could be subdivided into four distinguished and well-characterized pathways (Figure 6.1). (i) Phagocytosis is limited to some specialized cells such as macrophages, monocytes, dendritic cells, and neutrophils and is not covered in this study. Phygocytes have been reported to take up particles as large as 20 μm [201]. (ii) Clathrin-dependent endocytosis (CDE) is the most studied pathway among all endocytosis pathways. It occurs through formation of clathrin-coated pits, resulting from the assembly of clathrin on the cell membrane and has been reported to be the preferred pathway for particles up to 200 nm in size. Using a number of accessory signaling molecules, *e.g.*, adaptor protein AP2, and GTPase, to regulate its function, CDE is a receptor-mediated pathway and is involved in the uptake of various ligands, *e.g.*, transferrin, antibodies, and growth factors [202]. (iii) Caveolae-mediated endocytosis (Cav-ME) is the most reported and well-characterized pathway among clathrin-independent (CIE) pathways. Cav-ME involves the invagination of cholesterol-enriched domains on the cell membrane, forming flask-

shaped structures, caveolae (50-100 nm), which contain the hairpin-like membrane protein, caveolin. This pathway is particularly of importance for development of nanomedicine as it has been shown to bypass lysosomes, preventing the degradation of the cargo [202]. (iv) Macropinocytosis involves formation of membrane ruffles and large vacuoles (0.5-5 μm), coated with F-actin, and is responsible for uptake of material from/with the extracellular fluid. Unlike phagocytosis, macropinocytosis can be stimulated on many cell types and regulated by actin polymerization protein/enzymes present in cells. It has been reported as the uptake pathway for some bacteria (*e.g.*, Salmonella) [203], viruses (*e.g.*, HIV type I) [204] and CPPs (*e.g.*, Tat) [205]. Exploring new endocytosis pathways is still an active and evolving field of research and new clathrin- and caveolae-independent pathways, *e.g.*, flotillin-dependent endocytosis, Arf6-dependent endocytosis, are being introduced and studied.[206,207] The focus in this study will be on the mentioned major pathways.

Among CPPs, several cationic, amphipathic peptides have been designed and employed as delivery vectors for short interfering RNAs (siRNAs) [118,146,150]. In chapter 4, the modified amphipathic, amino acid-paring peptide, C6M1, was introduced as siRNA delivery carrier [176]. In this chapter, the penetration mechanism of C6M1 and its complex with siRNA will be studied using several endocytic chemical inhibitors. The specificity and toxicity of each inhibitor on Chinese hamster ovary (CHO-K1) cells and the effect of size of the complex in the uptake pathway and kinetics will be also discussed.

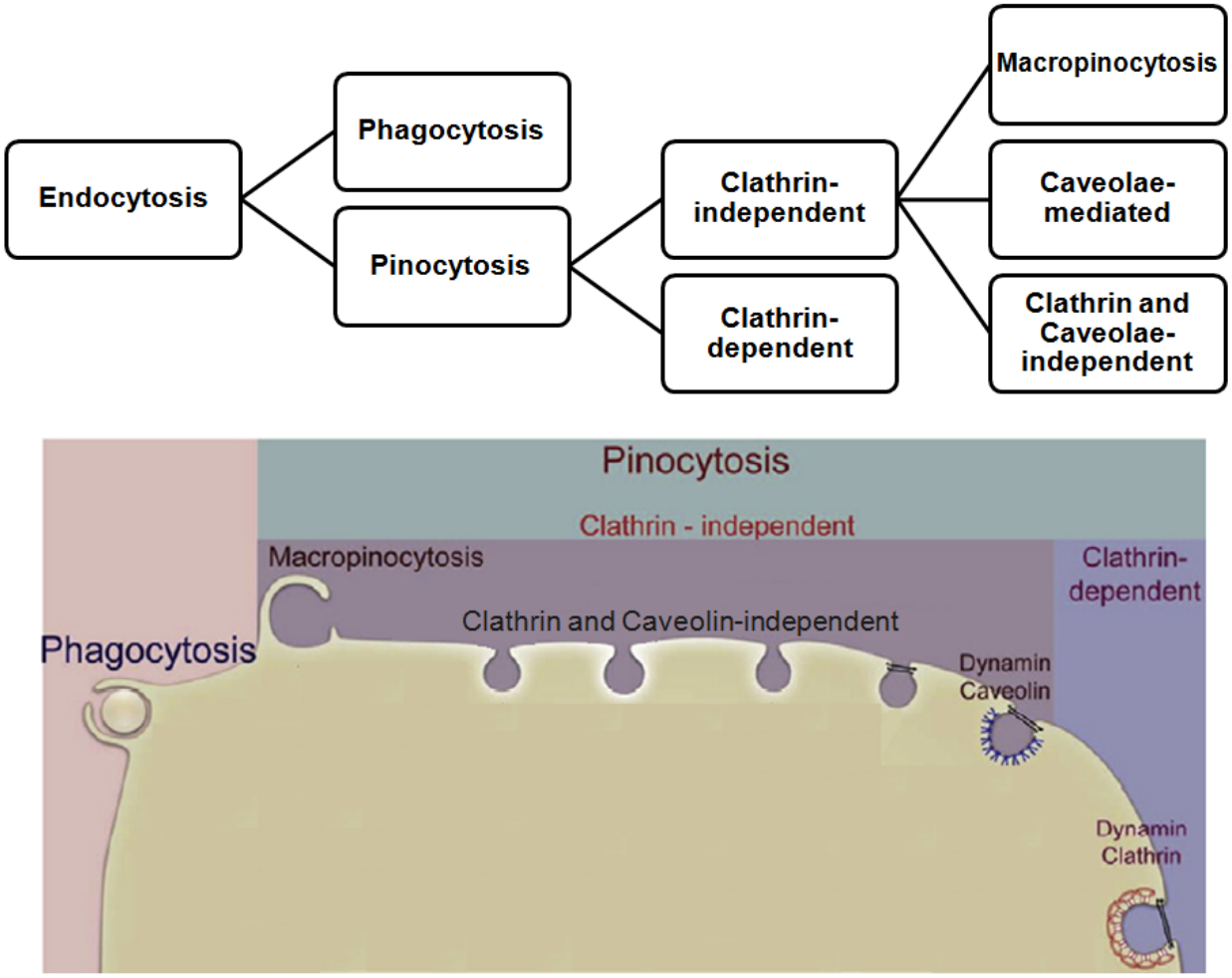

Figure 6.1 Different mechanisms of endocytosis (adapted from Ref [202]).

6.2 Materials and methods

6.2.1 Materials

Heparin, sodium chlorate, and all chemical inhibitors (Table 6.1) were purchased from Sigma-Aldrich (Oakville, Canada). Alexa Fluor-488 labeled human Transferrin, Oregon Green-514

labeled dextran (70 kDa), and BODIPY FL C_5- Lactosylceramide (LacCer) complexed to bovine serum albumin (BSA) were purchased from Invitrogen (Burlington, Canada). The C6M1 peptide (Ac-RLWRLLWRLWRRLWRLLR-NH_2, MW=2689.4 g/mol, purity>98%) was purchased from CanPeptide, Inc. (Quebec, Canada). Cy3-labeled glyceraldehyde 3-phosphate dehydrogenase (GAPDH) siRNA (AM4649) were purchased from Ambion (Austin, USA). All chemicals for buffer preparations were obtained from Sigma-Aldrich (Oakville, Canada) and used as received.

6.2.2 Formulation of peptide-siRNA complexes

A stock solution (1 mM) of C6M1 peptide was prepared by dissolving peptide powder in HEPES (5 mM, pH=7.4) or phosphate buffered saline (PBS, pH=7.4). The solution was vortexed for 10 seconds and sonicated for 10 minutes in a tabletop ultrasonic cleaner (Branson, model 2510, USA). siRNA was diluted in HEPES or PBS to a stock concentration of 50 μM. Peptide-siRNA complexes were formed by adding peptide solution into siRNA in proportion according to the designed experiment. The complexes were incubated for 20 minutes at room temperature before each experiment.

6.2.3 Dynamic Light Scattering (DLS) and Zeta potential

The hydrodynamic diameter of the C6M1-siRNA complexes in HEPES and PBS at a molar ratio of 30:1 with final siRNA concentration of 100nM were measured on a Zetasizer Nano ZS (Malvern Instruments, U.K.) equipped with a 4 mW He-Ne laser operating at 633 nm. A quartz microcell (45 μL) with a 3 mm light path was used and the scattered light intensities were collected at an angle of 173°. Clear disposable zeta cells were used for Zeta potential measurements. The intensity-based size distribution and zeta potential values were acquired using the multimodal algorithm CONTIN, Dispersion Technology Software 5.0. Three independent measurements were performed for each sample 20 min after sample preparation at 25 °C.

6.2.4 Cytotoxicity analysis of chemical inhibitors

CHO-K1 cells (Chinese hamster ovary, ATCC CCL-61) were cultured in F-12K medium (Invitrogen, Burlington, Canada) supplemented with 10% fetal bovine serum (Sigma-Aldrich, Oakville, Canada). Cells were incubated at 37 °C with 5% CO_2. Cells were detached from the flasks by adding trypsin-EDTA 0.25% (Sigma-Aldrich, Oakville, Canada) and incubating for 5 min, and resuspended in fresh media at a concentration of 6×10^4 cells per mL. 100 µL of cell suspension was added into each well of a flat bottom, 96-well plate and incubated for 24 h. The media was then replaced with fresh optiMEM with different final concentrations of chemical inhibitors (Figure 6.3) for 3 h. 48 h after inhibitor treatment, the cell counting kit-8 (CCK-8) (Dojindo, Japan) was used to perform cytotoxicity assays. 10µl of CCK-8 substrate was added to each well and incubated for an additional 2 h at 37 °C in the dark. Absorbance was measured at a wavelength of 450 nm with a reference wavelength of 620 nm using a microplate reader (FLUOstar OPTIMA, BMG, NC).

6.2.5 Treatments of the cells with endocytic inhibitors, markers and C6M1-siRNA complex

Approximately 50,000 cells per well were seeded in a 24-well cell culture plate to reach 60-70% confluency 24 hours later. The media was then discarded and cells were treated with fresh chemical inhibitors in optiMEM at concentrations listed in Table 6.1 for 1 h. The cells were subsequently treated with the C6M1-siRNA complex for 2 h, followed by discarding the media and washing the cells with trypsin (0.5 mg/ml in PBS for 5 min), and heparin (0.5 mg/ml in PBS for 3×10 min) to remove surface-bound complexes. Alternatively, cells were treated with transferrin 18 µg/ml for 15 min, dextran 0.5 mg/ml for 3 h, or LacCer 0.75 µM for 15 min. To remove cell surface-associated transferrin and LacCer, cells were washed three times with ice-cold F-12K medium, followed by 2 min incubation in ice-cold acid wash buffer (0.2 M acetic acid and 0.2 M NaCl) or four times for 10 min in ice-cold 5% defatted BSA at 4 °C, respectively. The cells were then washed twice with ice-cold F-12K. For Oregon Green-514 labeled dextran,

the cells were incubated with 0.2% trypan blue in PBS to quench extracellular fluorescence. For low temperature experiments, cells were kept at 4 °C for 1 h before treatment. All buffers, chemicals, and complexes were also kept in ice-cold water to avoid any temperature rise during the treatment. Cells were then again kept at 4 °C before fixation.

6.2.6 Flow cytometry to quantify intracellular complexes or endocytic markers

The amount of intracellular Cy-3 labeled siRNA and fluorescently labeled markers was quantified by Flow Cytometry (type BD Biosciences, BD FACSVantage SE Cell Sorter, San Jose, USA). After washing, the cells were detached from the plate by adding trypsin-EDTA and re-suspended in fresh 4% paraformaldehyde (PFA) in PBS and collected in FACS tubes for analysis. The fluorescence of Cy-3 siRNA was detected by FL2 channel (585/42 nm bandpass filter); while, those of labeled markers was detected by FL1 channel (530/30 nm). At least 10000 events were recorded for each sample.

6.3 Results and Discussion

6.3.1 Washing procedure to remove cell surface bound complexes

The flow cytometry technique, used in this study to quantify the complex uptake, cannot distinguish between cell surface-bound and intracellular fluorescence. Because of the strong cell surface binding tendency of poly-arginine peptides, the washing procedure is crucial to remove the non-internalized complexes from the cell surface to avoid any overestimation of the quantity of intracellular complexes. After treatment with the C6M1-siRNA complexes for two hours at 37 °C, cells were washed with PBS, trypsin (0.5 mg/ml in PBS for 5 min), heparin (0.5 mg/ml in PBS for 3×10 min), or a combination of trypsin/heparin (T/H).

As shown in Figure 6.2A, washing the cells with trypsin, heparin or their combination

significantly decreased the mean fluorescence of the cells compared with that of cells washed with only PBS (control), indicated by flow cytometry analysis. The trypsin treatment caused an almost 30% decrease in total fluorescence. However, a treatment with heparin decreased 40% of cells' mean fluorescence. This indicates the suitability of heparin washing compared with trypsin treatment to remove surface-bound complexes, probably due to the smaller size of heparin molecules. The large size of trypsin protease may limit its access to smaller complexes, associated with cell surface, resulting in incomplete removal of external bound complexes [199]. We also reported that heparin at this concentration could dissociate extracellular peptide-siRNA complexes, releasing labeled siRNA in extracellular media which could be easily washed away [176]. It is worth reminding that the fluorescence of Cy3-siRNA was measured by flow cytometry. A combination of T/H treatment resulted in an almost 50% decrease in the cells mean fluorescence and complete removal of surface-bound complexes. The remaining represents the fluorescence of intracellular complexes as further treatment did not significantly reduced the cellular fluorescence.

6.3.2 The role of cell surface proteoglycans in cellular attachment and uptake of C6M1-siRNA complexes

The first step in transduction of the complex is the interaction of the complex with extracellular matrix and cell membrane components. There are several reports that cell surface associated anionic heparan sulphate proteoglycans (HSPGs) play an important role in the internalization of arginine-rich cell penetrating peptides [148,155,208]. In order to examine the involvement of HSPGs in the cellular uptake of C6M1-siRNA, cells were co-treated with heparin (1 mg/ml) and the complex for 2 h. As a chemical analog of HSPG, anionic heparin could compete with the cell surface associated HSPG for binding to cationic complex. After 2h treatment, cells washed with PBS (Figure 6.2B, black bars) or T/H (grey bars). As shown in Figure 6.2B, co-treatment with heparin completely abolished the cellular attachment and uptake of the complex. One may argue that co-incubation of C6M1-siRNA complex with heparin could dissociate the complex. As the

fluorescence of labeled siRNA was measured for this study, this may have led to a misconclusion about the attachment and internalization of peptide itself. To address this, cells were co-treated with labeled peptide and heparin; no attachment and internalization of peptide assemblies was observed (not shown).

As the sulfated region of HS chains were reported as the main site of interaction for cationic peptides, we attempted to alter the sulfate constituent of HSPG. For this purpose, cells were pre-incubated with sodium chlorate (60 mM) for 48 h and then incubated with C6M1-siRNA complex for 2 h. Sodium chlorate pre-treatment has been reported to result in remarkable reduction of the sulfation of the HSPG, by inhibiting ATP-sulfurylase, which catalyzes the transfer of sulfate to polysaccharides [209]. As shown in Figure 6.2B, pre-treatment of cells with sodium chlorate resulted in significant decrease of both attached and internalized complexes, implying that highly anionic sulfated region of HSPG was the major site to interact with positively-charged guanidinium group in arginine residues. Overall, the results of heparin and sodium chlorate treatments indicated that the electrostatic interaction between the anionic HSPG and positively charged C6M1-siRNA complex initiated the cellular attachment and internalization of the complex.

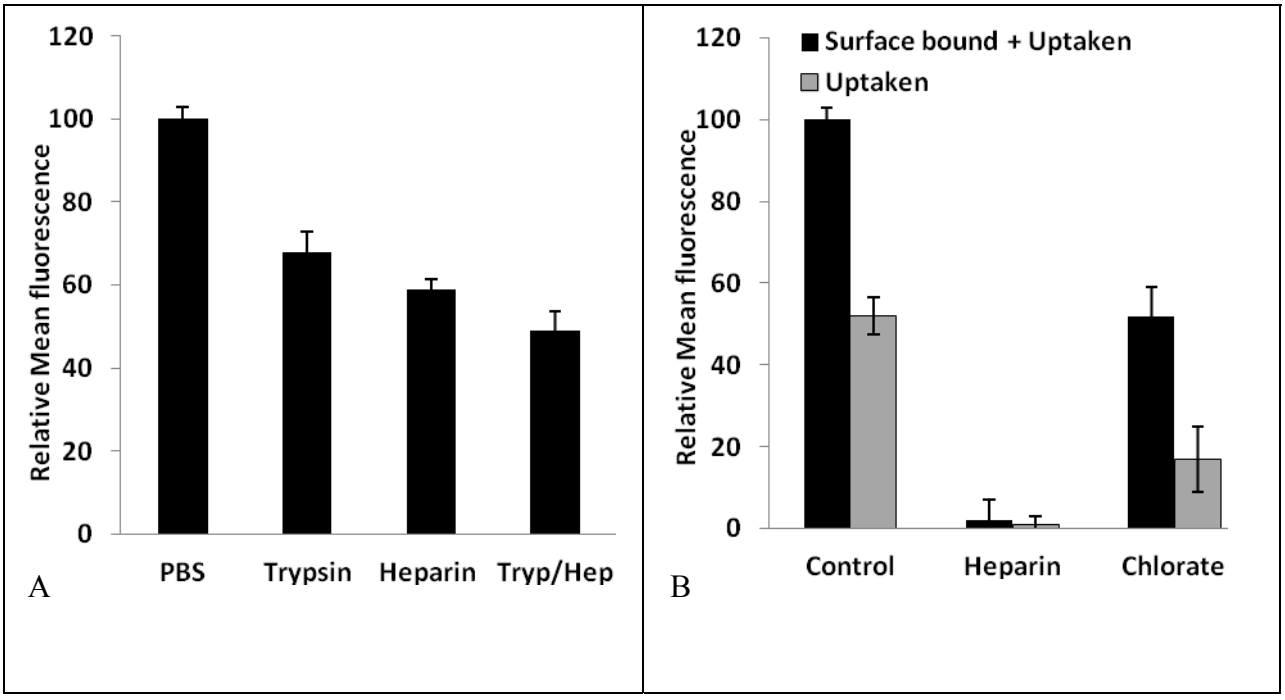

Figure 6.2 A) Effect of different washing procedures on the removal of surface bound complexes, B) Role of cell surface proteoglycans in cellular attachment and uptake of C6M1-siRNA complexes in CHO-K1 cells. Cells were co-treated with the complex and heparin (1 mg/ml) for 2 h or pre-treated with sodium chlorate (60 mM) for 48 h, then treated with the complex for 2 h. Error bars in both figures represent standard deviation of triplicates.

6.3.3 Chemical inhibitors and their cytotoxicity

In order to cover all known major endocytosis pathways, seven different chemical inhibitors were used in this study (Table 6.1). It should be noted that phagocytosis was not studied here as it was an irrelevant study for non-phagocytic CHO-K1 cells.

Chlorpromazine (Cpz) was used to specifically inhibit clathrin-mediated endocytosis (CDE) by translocation of clathrin and AP2 adaptor from cell membrane to intracellular vesicles and preventing the formation of clathrin-coated pits. There is no report on inhibiting lipid raft endocytosis by Cpz; however, this drug may partially inhibit macropinocytosis by increasing the fluidity of cell membrane [210]. EIPA (5-(N-ethyl-N-isopropyl) amiloride) has been reported to

block macropinocytosis and phagocytosis in a large selection of mammalian cell types by blocking the Na^+/H^+ exchanger. Some studies have concluded inhibitory activity of EIPA towards clathrin-mediated pathway [211]. Methyl-β-cyclo- dextrin (MBCD) depletes cholesterol from the cell membrane and was primarily employed to determine whether the uptake mechanism was dependent on the integrity of lipid rafts. As caveolae-mediated endocytosis and macropinocytosis require lipid rafts, MBCD was applied to inhibit those pathways [212]. Cytochalasin D (CytoD) inhibits F-actin polymerization and elongation by attaching to the growing ends of actin filaments. Actin polymerization has been reported as a requirement for phagocytosis, macropinocytosis and to some extend for caveolin-mediated endocytosis [213]. Nocodazole triggers the depolymerization of the microtubules and eventually disrupts the structure of cytoskeleton [214]. Nystatin and fillipin, polyene antibiotics, were used to inhibit lipid raft/caveolin-mediated endocytosis. Both drugs have been reported to interact with lipid cholesterol thereby creating large aggregates of cholesterol to sequester membrane from this steroid. This distortion of cholesterol rich domains is thought to inhibit caveolin-mediated endocytosis. Unlike MBCD, these chemicals show relatively high specificity for inhibiting this pathway.

Table 6.1. Endocytosis inhibitors used in this study

Inhibitor	Inhibition or effect	Concentration
Chlorpromazine	CDE	5 μg/ml
EIPA	MPC	20 μg/ml
MBCD	MPC, Cav-ME	5 mg/ml
Cyto D	Actin depolymerization	3 μg/ml
Nocodazole	Microtubule disruption	5 μg/ml
Nystatin	Cav-ME	40 μg/ml
Fillipin	Cav-ME	4 μg/ml

CDE: clathrine-mediated endocytosis; Cav-ME: caveolin-mediated endocytosis, MPC: macropinocytosis, EIPA: ethyl-isopropyl amiloride, MBCD: methyl-ß-cyclodextrin, CytoD: cytochalasin D

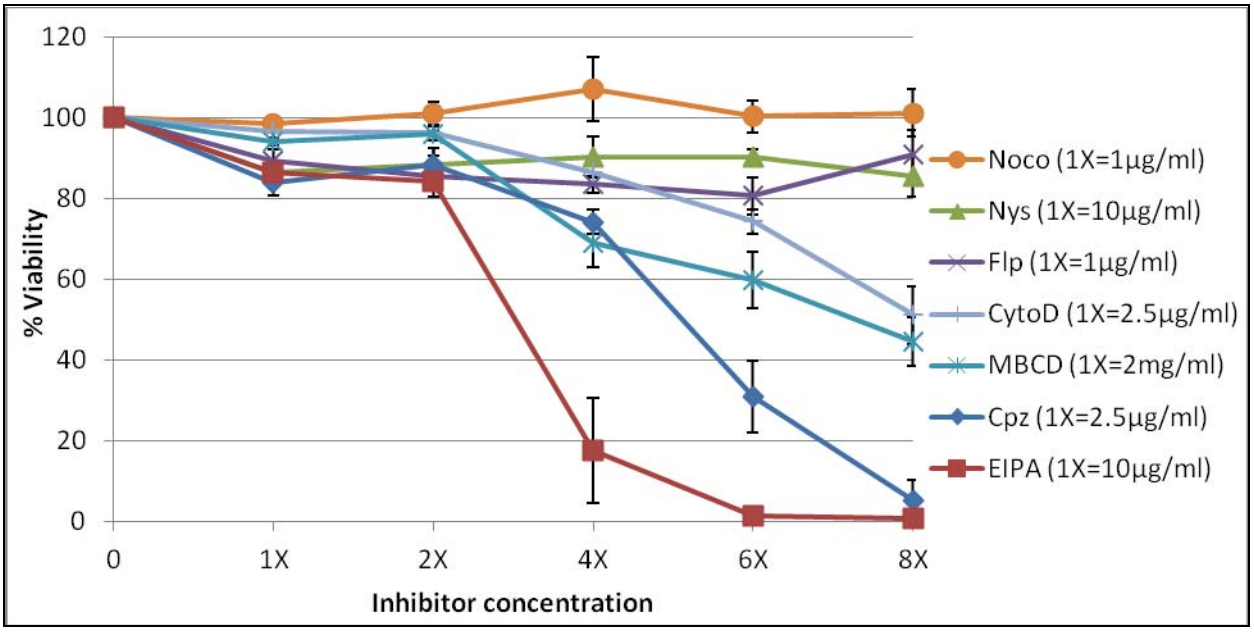

Figure 6.3 Cytotoxicity of chemical endocytosis inhibitors on CHO-K1 cells. Cells were treated with different concentrations of inhibitors for 3 h and viability of the cells was assessed using CCK-8 assay. Error bars represent standard deviation of quadruplicates. (Noco: nocodazole, Nys: nystatin, Flp: fillipin, CytoD: cytochalasin D, MBCD: methyl-ß-cyclodextrin, Cpz: chlorpromazine, EIPA: ethyl-isopropyl amiloride)

To minimize the influence of toxicity of chemical inhibitors on their performance and optimize the inhibition protocol, cellular toxicity of inhibitors at a range of concentrations was evaluated. CHO-K1 cells were incubated with five different concentrations of each inhibitor in OptiMEM for 3 h and the viability of the cells was measured using CCK-8 assay. As shown in Figure 6.3, nocodazole, nystatin, and fillipin showed no acute toxicity at the concentrations tested. Chlorpromazine and EIPA exhibited strong toxicity at concentrations above 5 and 20 µg/ml, respectively. For all inhibitors, concentrations with cell viability of 80% or higher were considered safe. It should be noted that the final suitable concentrations of inhibitors, listed in Table 6.1, were selected considering both cytotoxicity data and microscopic images. For

instance, CCK-8 assay did not show any significant toxicity for cytoD at a concentration as high as10 μg/ml; however, the cells treated with cytoD at this concentration underwent strong morphological changes (not shown).

6.3.4 Size of the peptide-siRNA complexes in HEPES and PBS

In addition to the shape and surface chemistry, and concentration, the particle size has been reported to influence the cellular uptake pathway and intracellular trafficking of particles [161,179]. Particles as large as 1 μm can internalize into non-phagocytic eukaryotic cells; however, in tumor therapy, particle size of 100-500 nm is ideal for passive targeting through the enhanced permeability and retention effect [159,160].

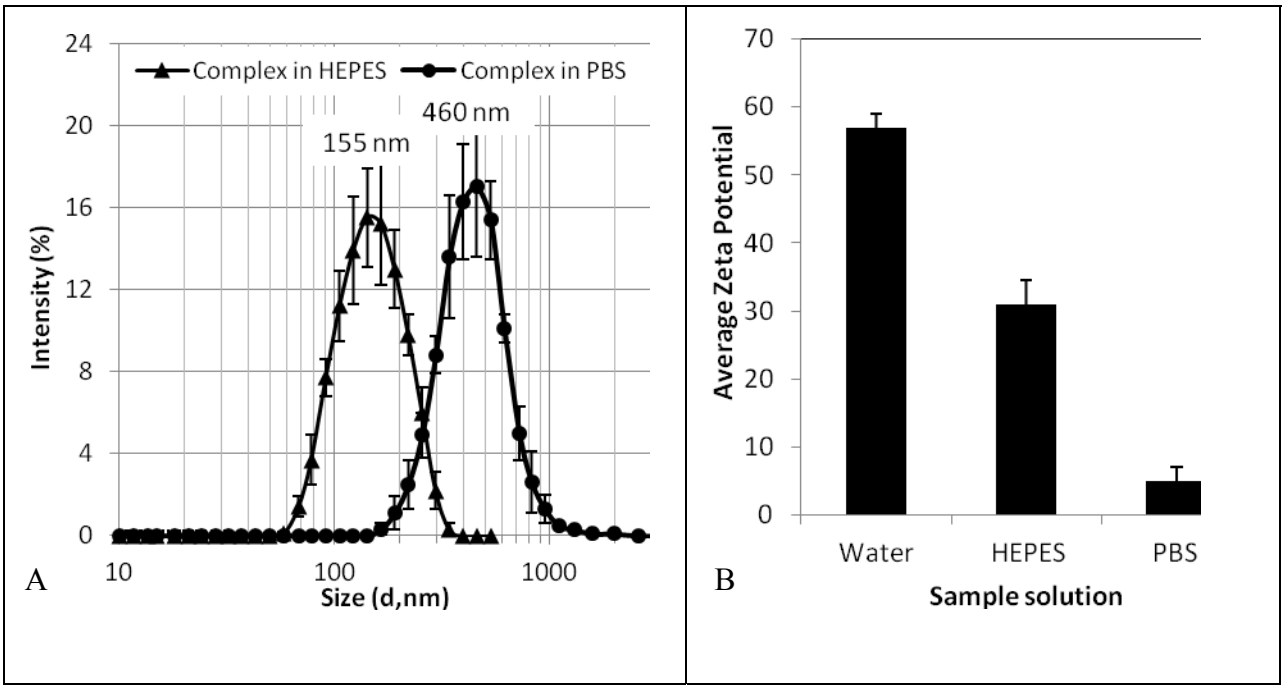

Figure 6.4 A) Size distribution of C6M1-siRNA complexes (molar ratio of 30:1) in HEPES and PBS buffers, determined by DLS. The numbers at the top of each curve show the average diameter. B) Zeta potential of C6M1-siRNA complexes in water, HEPES and BPS. Error bars in both figures represent standard deviation of triplicates.

As presented in Figure 6.4A, C6M1-siRNA complexes in HEPES showed a size distribution from 50 to 300 nm with an average size of 155 nm. In PBS, however, the particles aggregated to a size range of 140-1100 nm with an average of 460 nm. The surface of peptide-siRNA complexes at molar ratio of 30:1 was mainly covered by hydrophilic arginine residues, leading to positively-charged surfaces (Figure 6.4B). Complexes in water showed an average zeta potential of + 57 mV. This value dropped to +31 and +5 mV in HEPES and PBS, respectively, due to different level of ionic strength of these buffers. The high surface charge of the particles in water prevented their aggregation due to the charge repulsion, keeping the particles size below 70 nm (not shown). As a zwitterionic buffering agent, HEPES can maintain the physiological pH without significant contribution to the ionic strength of the solution and is commonly used for buffering the cell culture media. In contrast, the high concentration of phosphate anions in PBS mainly neutralized the positive charge of the complex surface, as arginine residues could act as sites for phosphate binding [194]. This facilitated the aggregation of the particles mainly through hydrophobic interaction of leucine residues.

6.3.5 Size-dependent uptake mechanism of C6M1-siRNA complex

Taking advantages of different size distributions of C6M1-siRNA complexes in HEPES and PBS, the size-dependency of complex internalization mechanism was studied. Flow cytometry was employed as a technique to quantify the intracellular complexes by measuring the intensity of fluorescence of labeled Cy3-siRNA. As an example, Figure 6.5A shows fluorescence distribution histogram of untreated cells or cells treated with complex (in PBS) for 2h with or without pre-incubation with a chemical inhibitor (EIPA). As shown, pretreatment of cells with EIPA caused a left-shift in intensity peak, implying that EIPA significantly reduced the quantity of intracellular complexes by inhibiting the uptake pathway.

Several studies suggest that CPPs use both energy-independent direct translocation and energy-dependent endocytosis to enter cells. To elucidate whether the complex uptake was energy-dependent, uptake experiments were performed at 4 °C and 37 °C. Assuming that all intracellular

activities including endocytosis are inhibited at low temperature (4 °C), the complex internalization at this temperature likely reflects direct penetration [198]. As shown in Figure 6.5B, complexes with different sizes showed different behavior when treated at 4 °C. The uptake of larger complexes (formed in PBS) was significantly decreased at 4 °C in comparison with that at 37 °C; while the uptake of smaller complexes (formed in HEPES) only slightly affected by the temperature. This clearly suggested that the major penetration mechanism for small complexes was direct translocation while the energy-dependent endocytosis was responsible for only ~20% of the total complex uptake. In contrast, endocytosis contributed the most (~80%) to the uptake of larger complexes.

In order to provide further evidence to support our observation in a physical inhibition experiment (4 °C), chemical inhibitors were employed to block specific endocytosis pathways. The experiments were performed using chlorpromazine, EIPA, and nystatin, inhibitors of CDE, MPC and Cav-ME, respectively. As revealed in Figure 6.5B, none of the inhibitors caused significant inhibition to the uptake of small complexes (black bars). In the presence of chlorpromazine, internalization of large complexes was partially inhibited, implying that CDE might be involved in the uptake process. Pre-incubation of the cells with EIPA, an inhibitor of MPC, strongly inhibited the uptake of large complexes with no effect on the uptake of small complexes. Pre-treatment of the cells with nystatin even increased the uptake of complexes by 40-50%. As a side-effect, nystatine has been reported to increase cell membrane permeability by interacting with membrane phospholipids, which may account for the increased complex uptake. Overall, we found that the uptake of small complexes was not inhibited by physical or chemical endocytic inhibitors, implying that C6M1-siRNA complexes at this size range (mean 155 nm) internalized into the cells through the energy-independent direct translocation; however, large complexes with a mean size of 460 nm were mainly taken up by endocytosis which will be discussed in detail in the next section.

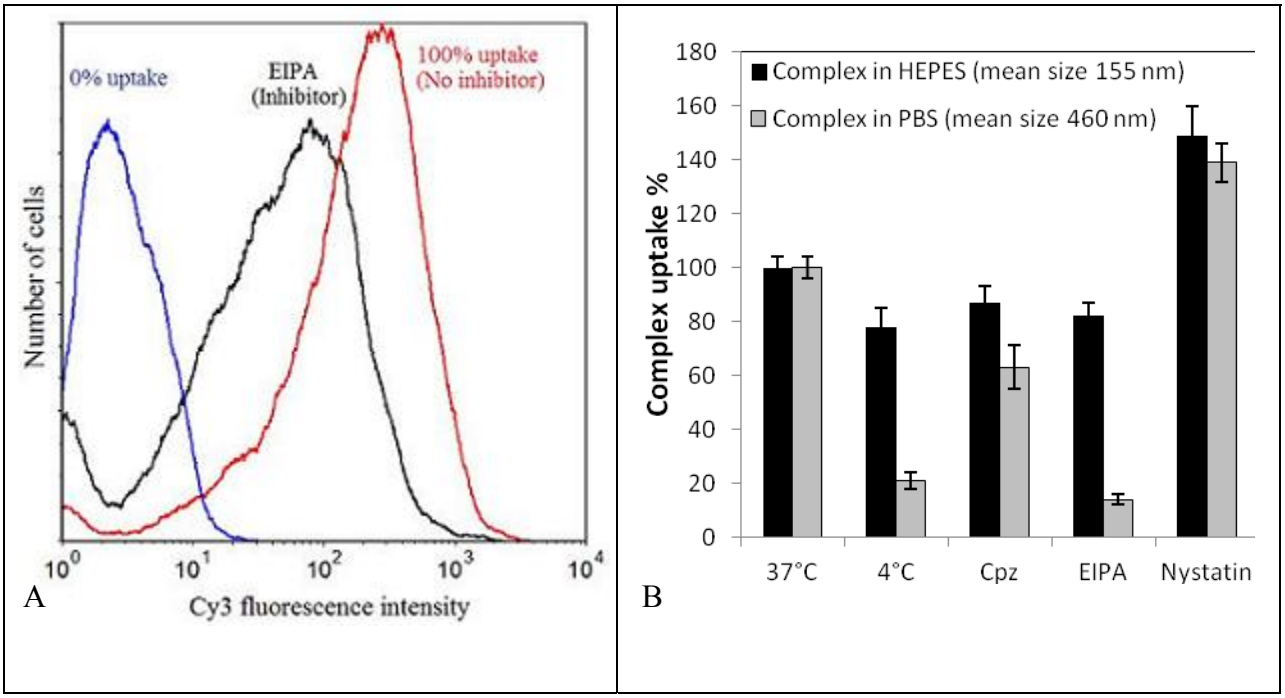

Figure 6.5 A) Cy3 fluorescence intensity histograms of CHO-K1 cells, nontreated (blue), treated with C6M1-Cy3siRNA (formed in PBS) for 2h (red), or preincubated with EIPA for 1 h and then treated with C6M1-Cy3siRNA for 2h (black), obtained by flow cytometry. B) Effects of endocytic inhibitors on cellular uptake of C6M1-siRNA complexes, prepared in HEPES (black bars) or PBS (grey bars). Cells were treated with C6M1-siRNA complex in the absence (control) or presence of chemical or physical (4 °C) endocytic inhibitors. Error bars represent standard deviation of triplicates. (Cpz: chlorpromazine)

6.3.6 Studying the involvement of different endocytosis pathways in the complex uptake

As the C6M1-siRNA complex, formed in PBS, showed a strong reduction in cellular uptake when treated at 4 °C, we used a more comprehensive set of chemical inhibitors to unravel the role of each endocytic pathway in the complex uptake by CHO-K1 cells. In order to ensure the specificity and efficiency of each inhibitor, at the concentrations used, three fluorescently-labeled endocytic markers were employed. Human transferrin is a ligand which exclusively uses CDE to enter the cells and was used as the marker of this pathway [215]. Dextran 70 kDa is a

hydrophilic polysaccharide which internalizes into the cells specifically via macropinocytosis and was used to adjust the concentrations and evaluate the specificity of inhibitors employed to block this pathway [199]. Lactosylceramide (LacCer) is a glycosphingolipid which traffics through CIE [216] and was used here as a probe for lipid raft/cav-ME.

6.3.6.1 Role of clathrin-dependent endocytosis in the complex uptake

To study the possible role of CDE in the uptake process, chlorpromazine was used to inhibit this pathway by interfering with the formation of clathrin-coated pits. As shown in Figure 6.6, chlorpromazine significantly reduced the uptake of transferrin, the marker of CDE. However, pre-treatment of the cells with chlorpromazine did not alter the internalization of LacCer, indicating that chlorpromazine did not inhibit cav-ME. This drug slightly inhibited the uptake of Dextran, the marker of macropinocytosis, by most likely increasing the fluidity of cell membrane. The uptake of the complex was also partially (~32%) inhibited by chlorpromazine, implying that CDE might have a role in the cellular uptake of the complex specifically at the lower size range (<200 nm). However, one may argue that the partial inhibition of macropinocytosis might have caused the partial reduction in the complex uptake, when treated with chlorpromazine.

6.3.6.2 Role of macropinocytosis in the complex uptake

EIPA has been widely used as a specific inhibitor of macropinocytosis. As expected, the internalization of Dextran was remarkably reduced by EIPA treatment (Figure 6.6). In contrast, it had no significant effect on the uptake of transferrin and LacCer. This indicates the specificity and efficiency of EIPA, at the concentration used, to exclusively block macropinocytosis pathway in CHO-K1 cells. The uptake of the complex was also dramatically inhibited in the presence of EIPA, implying that macropinocytosis is the main route of complex internalization. To further confirm this finding, we also used MBCD which has been reported as an inhibitor for macropinocytosis and lipid raft/cav-ME, by depleting the cholesterol from the cell membrane [212]. As shown, MBCD treatment had only slight effect on transferrin uptake but almost

abolished the uptake of Dextran and significantly decreased that of LacCer, showing strong inhibition effect of MBCD on macropinocytosis and cav-ME. This treatment also caused a substantial decrease in the complex uptake, confirming the observation upon EIPA treatment. This also indicates the dependency of the complex uptake on the integrity of lipid raft. CytoD has also been reported as a macropinoytosis inhibitor in some studies; however its primary action is to inhibit actin polymerization which could eventually affect all the pathways. This highlights the non-specificity of this inhibitor and care should be taken when analyzing its inhibitory effects. As shown in Figure 6.6, treatment of CHO-K1 cells with CytoD partially inhibited the uptake of CDE, macropinocytosis, and cav-ME markers, suggesting the non-specificity of this inhibitor in exclusively blocking any of pathways in CHO-K1 cells at the concentration used. The uptake of the complex was also partially inhibited by actin disruption.

6.3.6.3 Role of caveolin-mediated endocytosis in the complex uptake

Filipin and Nystatin have been regularly used for inhibition of lipid raft/cav-ME. Both chemicals have been reported to interact with lipid cholesterol, creating large aggregates to sequester this lipid from the membrane structure [217]. As reported in Figure 6.6, both inhibitors had no inhibitory effect on the uptake of CDE and macropinocytosis markers; however, they exhibited a pronounced inhibition of LacCer, indicating the specificity of both inhibitors, unlike MBCD, for lipid raft/cav-ME. Interestingly, the complex uptake was increased by ~40% in the presence of nystatin, mainly due to the increased cell membrane permeability as a side-effect of nystatin treatment. In the case of fillipin, the complex uptake did not change. Overall, these results suggest that cav-ME was not involved in C6M1-siRNA complex cellular uptake.

6.3.6.4 Importance of cell structural integrity in the complex uptake

As reported, pre-treatment of CHO-K1 cells with MBCD which extracts cholesterol out of the cell membrane led to a pronounced inhibition of the complex uptake. This clearly suggests the importance of lipid raft integrity in the uptake process. We also confirmed the contribution of

actin filaments to the uptake of all endocytic markers and the complex by treating the cells with CytoD. Microtubules are other major components of cytoskeleton which play important role in some endocytic processes [218,219]. To investigate whether the complex uptake was microtubule-dependent, the cells were treated with nocodazole to induce depolymerization of microtubules. As shown in Figure 6.6, nocodazole had only minor effect on the uptake of chlorpromazine and LacCer; but significantly reduced the uptake of dextran, implying the dependency of macropinocytosis to microtubules polymerization. The internalization of the complex was also decreased by ~25%. Overall, the integrity of the cytoskeletal structures is important for efficient internalization of the C6M1-siRNA complex.

Considering the results collectively, lipid raft-dependent HSPG-mediated macropinocytosis plays the major role in internalization of large C6M1-siRNA complexes. The mechanism of how the interaction of the complex with cell surface proteoglycans induces macropinocytosis or facilitates direct penetration needs to be elucidated. Recent studies have shown that high local concentration of arginine-rich peptides in contact with proteoglycans could activate intracellular signaling via Rac1 protein which could eventually lead to remodeling of the actin network, triggering macropinocytosis or increasing the fluidity of the membrane for direct penetration of the peptide [220]. The unique amino acid pairing feature of C6M1 enables high local clustering of peptide at the cell surface even at low bulk concentrations, facilitating its entry into the cell.

6.3.7 Kinetics of the complex uptake

Figure 6.7 shows the kinetics of uptake of C6M1-siRNA complexes at different size ranges. As reported, complexes at smaller size range internalized the cells through mainly temperature-insensitive direct translocation; while the major route for the uptake of larger complexes was endocytosis. In order to evaluate the effect of internalization route on the kinetics of uptake and determine the optimal complex treatment time, the uptake of the complex was quantified over the time. As shown in Figure 6.7, smaller complexes internalized the cells faster than larger complexes with uptake half-times of 25 and 70 min, respectively.

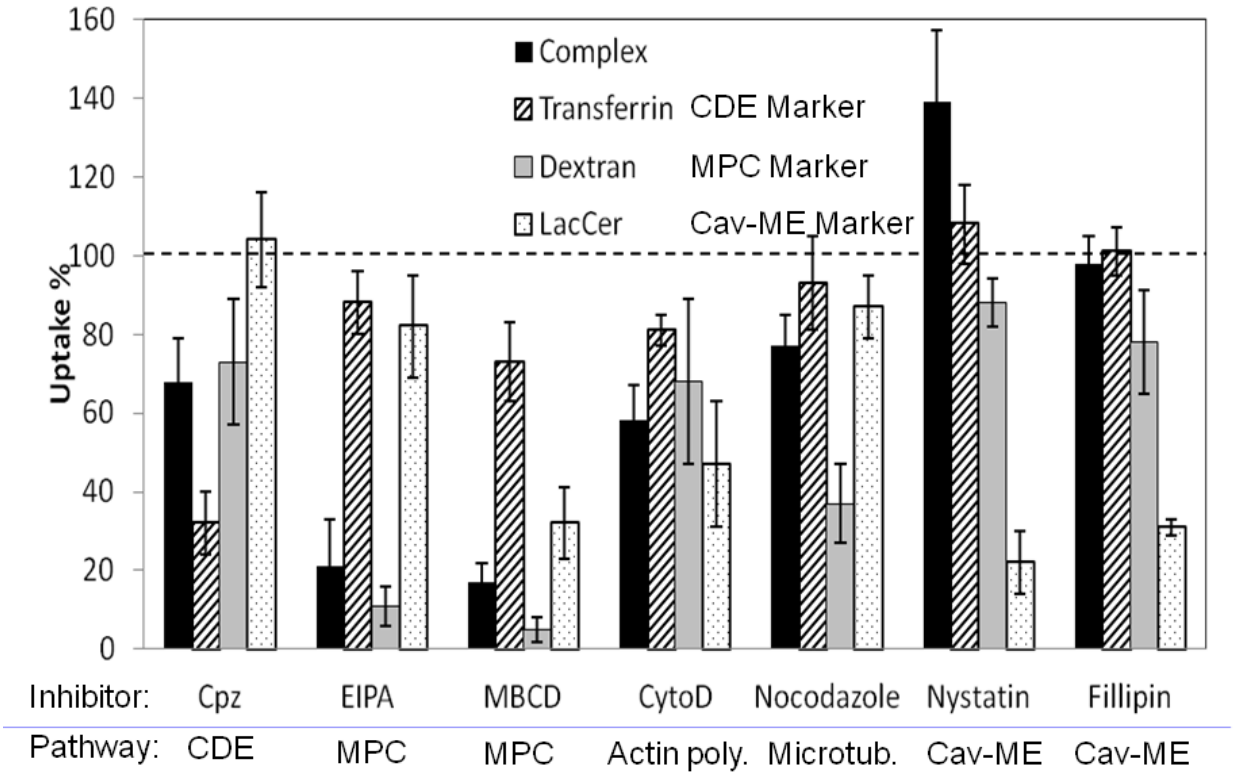

Figure 6.6 Uptake of the complex and labeled endocytic markers following the pre-treatment of CHO-K1 cells with different endocytic chemical inhibitors. Cells were pre-incubated with chemical inhibitors at the concentrations listed in Table 6.1 for 1 h, followed by treatment with either C6M1-siRNA complex or endocytic markers (transferrin, dextran 70 kDa, and LacCer) at the concentrations and durations mentioned in Materials and Methods section. The intracellular fluorescence of the cells was measured by flow cytometry and the values were normalized considering 0% uptake for non-treated cells and 100% uptake for the cells treated with the complex or the markers without inhibitors at 37 °C. Error bars represent standard deviation of quadruplicates. (CytoD: cytochalasin D, MBCD: methyl-ß-cyclodextrin, Cpz: chlorpromazine, EIPA: ethyl-isopropyl amiloride, CDE: Clathrin-dependent endocytosis, MPC: Macropinocytosis, Cav-ME: Caveolae-mediated endocytosis).

The internalization of small complexes was almost saturated after 1 h; while that of large complexes occurred after 3 h. The uptake of large complexes followed an interesting pattern. For the first 60 min, the uptake pattern was similar to that of small complexes. This might be

associated with the direct penetration of the fraction of complex with size smaller than 300 nm, considering the polydispersity of the samples and the overlap of size distributions of complexes formed in PBS and HEPES (Figure 6.4A). This may also explains partial uptake of large complexes at 4 °C (Figure 6.5B). After 60 min, the uptake kinetics followed a typical endocytosis pattern (S-shape), reported for some CPPs [221]. The relatively slow uptake of large complexes also suggests macropinocytosis as the main pathway, as the internalization through this pathway has been reported to be slower than that of the receptor-mediated endocytosis.

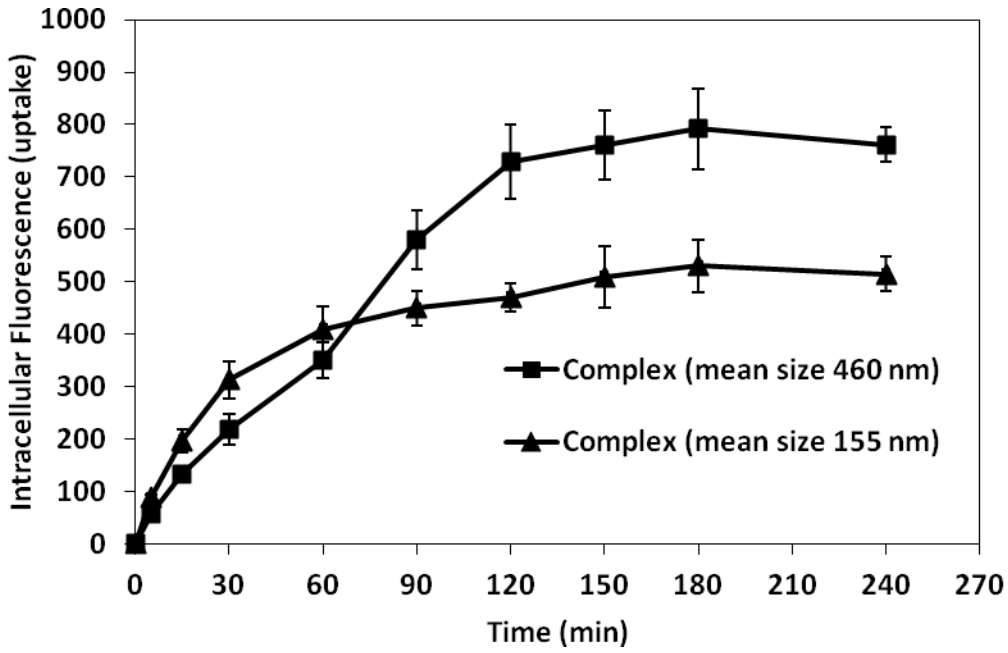

Figure 6.7 Effect of complex size on the kinetics of its uptake. CHO-K1 cells were treated with C6M1-Cy3siRNA complexes and the intracellular complexes were quantified by flow cytometry over the time. Experiments were performed in triplicates and error bars represent standard deviations.

6.3.8 Model for cellular uptake mechanism of C6M1-siRNA complexes

Based on the results of physical (4 °C) and chemical inhibition experiments, the following model is proposed for cellular uptake of C6M1-siRNA complexes (Figure 6.8).

1) C6M1-siRNA complexes bind to cell surface proteoglycans through electrostatic interaction. As revealed in heparin and sodium chlorate experiments, this interaction is required to trigger the next steps of cellular uptake of the complex.

2) Interaction with proteoglycans increases the fluidity of cell membrane, leading to direct translocation of small complexes.

3) Interaction with proteoglycans triggers the remodeling of cytoskeletal network, in particular F-actin, resulting in macropinocytosis of large complexes.

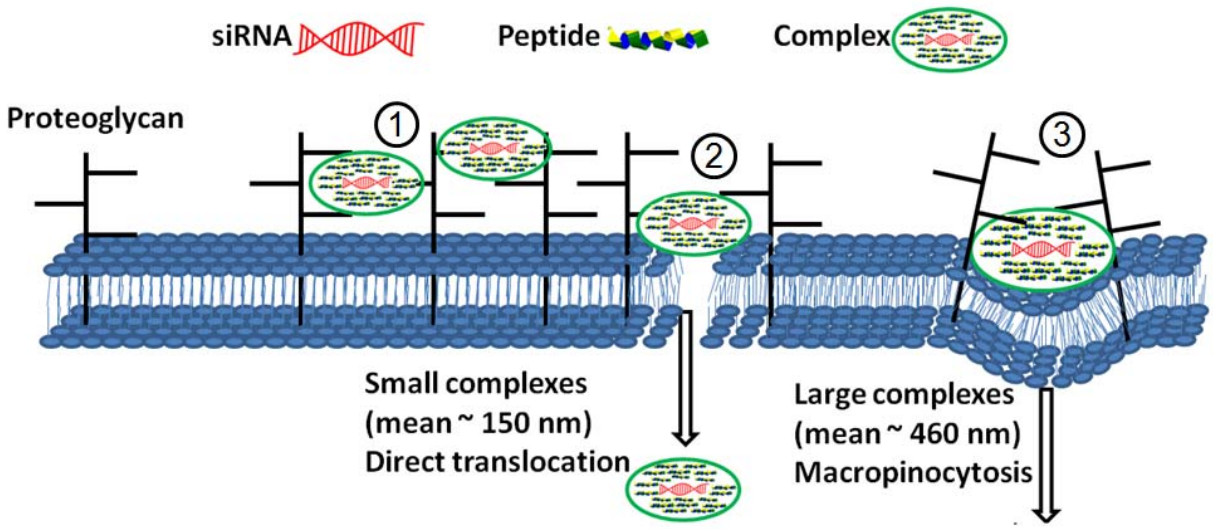

Figure 6.8 Proposed model for cellular uptake of C6M1-siRNA complexes. First step is the interaction of the complex with cell surface proteoglycans (1), followed by direct penetration of small complexes (2) or macropinocytosis of larger complexes (3).

6.4 Conclusions

In this study, the attachment and uptake of C6M1-siRNA complexes in CHO-K1 cells were investigated. Heparin and sodium chlorate treatment unraveled the importance of cell surface proteoglycans in the attachment and uptake of the complex. Applying physical and chemical endocytic inhibitors, the uptake mechanism of the complexes at different size ranges were studied. It was shown that small complexes (mean ~155 nm) internalized the cells via energy-independent non-endocytic mechanism, most likely involving direct translocation; however, larger complexes (mean ~460 nm) mainly utilized endocytosis for cellular uptake. A detailed study using the inhibitors of different pathways identified cholesterol-dependent macropinocytosis as the main pathway of the complex uptake. Using endocytic markers, the poor specificity of some inhibitors in exclusively blocking a specific pathway was revealed; thus, care should be taken when evaluating the inhibitory effects of chemical inhibitors. The internalization kinetics of large complexes followed a typical endocytosis pattern with an uptake half-time of 70 min compared with 25 min for direct penetration of small complexes.

Chapter 7
Original Contributions and Recommendations

7.1 Original contributions to research

This thesis presented the potential of designed amphipathic peptides as carriers for siRNA delivery. A special class of secondary amphipathic peptides was designed, their interaction with siRNA was characterized, and their potency in siRNA delivery and the mechanism of cellular internalization was explored. The thesis includes the following parts: (i) design and characterization of an amphipathic, amino acid pairing peptide, C6, for siRNA delivery in CHO-K1 cells; (ii) sequence modification of C6 and its effect on solubility, secondary structure, cytotoxicity and cellular internalization of the modified peptide, C6M1; (iii) investigation of the effect of ionic strength of the solution and complexation with siRNA on size, charge, and secondary structure of C6M1; (iv) study of the stability of C6M1-siRNA complexes against serum nuclease degradation and the knockdown efficiency of C6M1-GAPDH siRNA complexes in CHO-K1 cells; (v) investigation of cellular internalization mechanism and kinetics of C6M1-siRNA complex in CHO-K1 cells and studying the cytotoxicity and specificity of common chemical endocytosis inhibitors. The major outcomes of each part are summarized in the following sections.

Design and characterization of an amphipathic peptide, C6, for siRNA delivery

C6, a secondary amphipathic peptide, was designed and introduced as a safe and efficient carrier for siRNA delivery *in vitro*. The physicochemical features of the non-covalent interaction between C6 and siRNA were characterized. Upon binding to siRNA, C6 adopted a helical conformation; while C6 alone showed a random coil structure in water. The fluorescence

spectroscopy, DLS, AFM, ITC, and gel electrophoresis results confirmed the formation of stable C6-siRNA complex. The fluorescence microscopy images and flow cytometry data also indicated the high cellular uptake and cytoplasmic localization of siRNA delivered by C6. This study demonstrated the potential of C6 as an efficient carrier for siRNA delivery.

Sequence modification of C6 and its effect on solubility, secondary structure, cytotoxicity and cellular internalization

By sequence modification of C6 peptide, C6M1 was designed and introduced as a safer and more efficient carrier for siRNA delivery. The impact of the replacement of three leucine with tryptophan residues in peptide sequence on its solubility, secondary structure, cytotoxicity, and uptake efficiency was reported. The sequence modification significantly enhanced the solubility of the peptide in aqueous solutions, confirmed by ANS fluorescence assay and surface tension experiments. C6M1 also demonstrated more helical contents in its secondary structure compared with C6. The modification significantly enhanced the efficiency of peptide in intracellular delivery of Cy3-labeled siRNA in CHO-K1 cells and reduced the cytotoxity of the peptide.

Effect of ionic strength of the solution and interaction with siRNA on size and charge of the complex, and secondary structure of C6M1

In this study, solvents with different ionic strength, i.e, water, HEPES, and PBS were used to study the media effect on physicochemical properties of C6M1 and its complex with siRNA. C6M1 formed small complexes with siRNA in water and HEPES (<200 nm), but aggregated to larger particles in PBS. DLS and fluorescence spectroscopy revealed that the aggregation was saturated after 1 h. C6M1 in water showed a combination of helical and random coil structures; while, it adapted mainly an α-helical structure in the presence of anions or upon binding to siRNA.

Serum stability and knockdown efficiency of C6M1-siRNA complexes in CHO-K1 cells

The stability of C6M1-siRNA complexes at different molar ratios in the presence of serum

nuclease or heparin, an anionic competitor, was investigated in this study. Agarose gel experiments showed that C6M1 was able to completely encapsulate siRNA molecules at molar ratio of 15:1; however, higher molar ratios were required to achieve stable complexes. Naked siRNA was completely degraded in 4 h in the presence of 50% active serum; while, C6M1 protected siRNA against serum nuclease degradation over the period of 24 h. Western blotting experiment showed ~75% decrease in GAPDH protein content of the cells treated with C6M1-siRNA complexes. Considering these results, C6M1 showed high potential as a safe, protective and efficient carrier for siRNA delivery.

Cellular internalization mechanism and kinetics of C6M1-siRNA complexes

The cellular attachment and uptake of C6M1-siRNA complexes in CHO-K1 cells were investigated in this study. The important role of cell surface proteoglycans in the attachment and uptake of the complex was confirmed by heparin and sodium chlorate treatment. The effect of the size of the complex in its internalization mechanism was studied using physical and chemical endocytic inhibitors. It was found that small complexes (mean ~155 nm) internalized the cells via energy-independent non-endocytic mechanism, most likely involving direct translocation; however, larger complexes (mean ~460 nm) mainly utilized endocytosis for cellular uptake. A detailed study using the inhibitors of different pathways identified cholesterol-dependent macropinocytosis as the main pathway of the complex uptake. The poor specificity of some inhibitors in exclusively blocking a specific pathway was revealed using endocytic markers. The internalization kinetics of small complexes showed a quick uptake with a half-time of 25 min; while, that of large complexes followed a typical endocytosis pattern with an uptake half-time of 70 min.

7.2 Recommendations

Based on the studies carried out in this research, the following recommendations for future studies are proposed:

1. The chemical and sequence modification of C6M1 in order to limit the complex size distribution to the size ranges suitable for *in vivo* studies.
2. Co-assembly of C6M1 with fusogenic peptides or sequence modification of C6M1 by introducing histidine residues to enhance the endosomal escape and cytoplasmic release of the complex.
3. Applying confocal microscopy to support the finding in internalization mechanism experiments using the co-localization of the complex and endocytic markers.
4. Evaluating the therapeutic efficiency of C6M1-siRNA complexes *in vivo*.
5. Incorporating cell targeting peptides (CTPs) motifs in the sequence of C6M1 or its modified versions, or decorating the complex with CTPs through amino acid pairing technology developed in our lab, and testing the targeting efficiency of the complex *in vitro* and *in vivo.*

.

Appendix A[1]

BCA Protein Assay Kit

The BCA Protein Assay (Thermo Scientific Pierce) was used to determine total protein concentration before western blot experiment. This assay is a detergent-compatible formulation based on bicinchoninic acid (BCA) for the colorimetric detection and quantitation of total protein. This method combines the well-known reduction of Cu^{+2} to Cu^{+1} by protein in an alkaline medium (the biuret reaction) with the highly sensitive and selective colorimetric detection of the cuprous cation (Cu^{+1}) using a unique reagent containing bicinchoninic acid. The purple-colored reaction product of this assay is formed by the chelation of two molecules of BCA with one cuprous ion. This water-soluble complex exhibits a strong absorbance at 562 nm that is nearly linear with increasing protein concentrations over a broad working range (20-2000 μg/mL). The BCA method is not a true end-point method; that is, the final color continues to develop. However, following incubation, the rate of continued color development is sufficiently slow to allow large numbers of samples to be assayed together.

The macromolecular structure of protein, the number of peptide bonds and the presence of four particular amino acids (cysteine, cystine, tryptophan and tyrosine) are reported to be responsible for color formation with BCA. Studies with di-, tri- and tetrapeptides suggest that the extent of color formation caused by more than the mere sum of individual color-producing functional groups. Accordingly, protein concentrations generally are determined and reported with reference to standards of a common protein such as bovine serum albumin (BSA). A series of dilutions of known concentration are prepared from the protein and assayed alongside the unknown(s) before the concentration of each unknown is determined based on the standard curve.

---

[1] Adapted from http://www.piercenet.com/browse.cfm?fldID=02020101

Appendix B

HPLC and NMR of C6

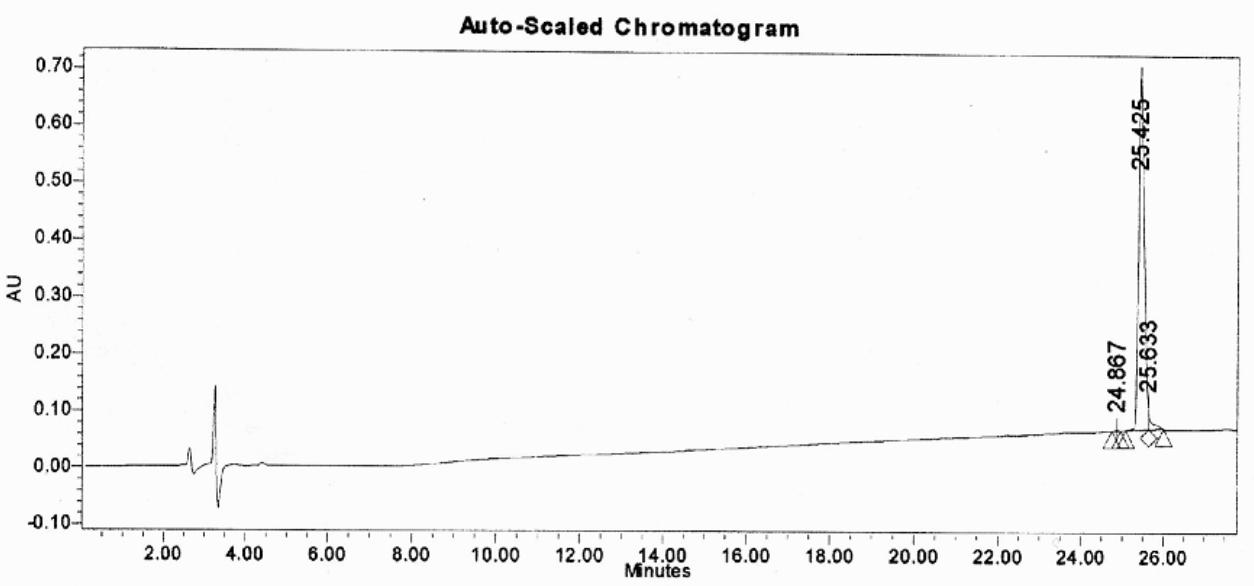

Peak Results

	Name	RT	Area	Height	% Area
1		24.867	12444	1935	0.20
2		25.425	5947823	627362	96.60
3		25.633	196881	35547	3.20

NMR (C6 peptide)

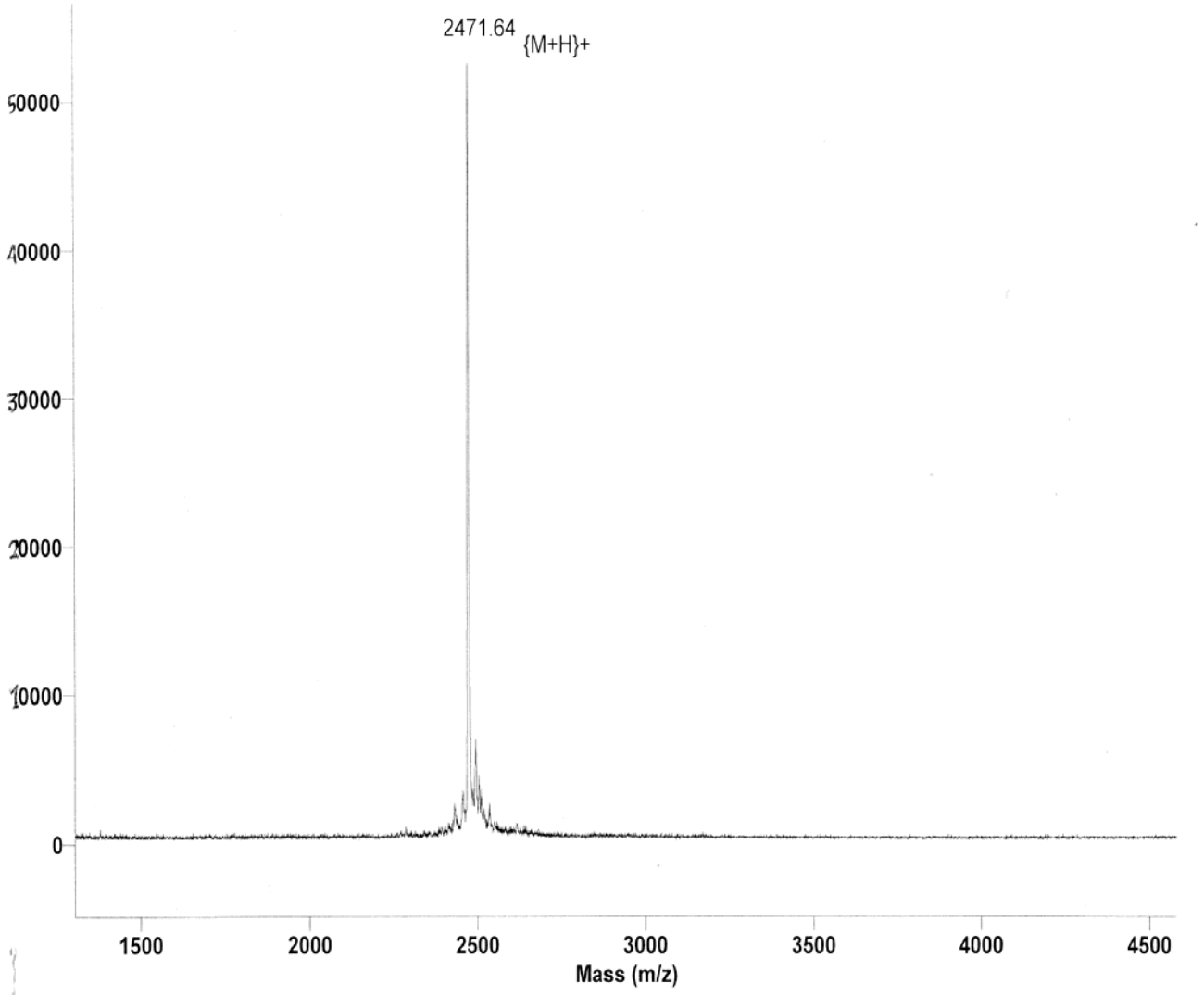

References

[1] S.S. Davis, Drug delivery systems, Interdisipl. Sci. Rev. 25 (2000) 175-183.

[2] A. Fire, S.Q. Xu, M.K. Montgomery, S.A. Kostas, S.E. Driver, C.C. Mello, Potent and specific genetic interference by double-stranded RNA in *Caenorhabditis elegans*, Nature. 391 (1998) 806-811.

[3] P.J. Paddison, P.K. Vogt, RNA Interference, Springer, Berlin, 2008.

[4] D.R.R. Engelke, J.J. Rossi, RNA Interference, Elsevier Academic Press, San Diego, 2005.

[5] D.M. Dykxhoorn, C.D. Novina, P.A. Sharp, Killing the messenger: Short RNAs that silence gene expression, Nat. Rev. Mol. Cell Biol. 4 (2003) 457-67.

[6] J. Benoit, A. Vonarbourg, C. Passirani, P. Saulnier, Parameters influencing the stealthiness of colloidal drug delivery systems, Biomaterials. 27 (2006) 4356-4373.

[7] R.I. Mahato, Biomaterials for Delivery and Targeting of Proteins and Nucleic Acids, CRC Press, Boca Raton, 2005.

[8] M. Manoharan, RNA interference and chemically modified small interfering RNAs, Curr. Opin. Chem. Biol. 8 (2004) 570-579.

[9] S. Verma, S. Jager, O. Thum, M. Famulok, Functional tuning of nucleic acids by chemical modifications: Tailored oligonucleotides as drugs, devices and diagnostics, Chem. Rec. 3 (2003) 51-60.

[10] H.Y. Zhang, Q. Du, C. Wahlestedt, Z.C. Liang, RNA interference with chemically modified siRNA, Curr. Top. Med. Chem. 6 (2006) 893-900.

[11] S. Oliveira, G. Storm, R.M. Schiffelers, Targeted delivery of siRNA, J. Biomed. Biotechnol. 4 (2006) 1-9.

[12] P. Singh, M.J. Gonzalez, M. Manchester, Viruses and their uses in nanotechnology, Drug Dev. Res. 67 (2006) 23-41.

[13] D. Luo, W. Saltzman, Synthetic DNA delivery systems, Nat. Biotechnol. 18 (2000) 33-37.

[14] J. Kang, R. Toita, Y. Katayama, Bio and nanotechnological strategies for tumor-targeted gene therapy, Biotechnol. Adv. 28 (2010) 757-763.

[15] J. Guo, K.A. Fisher, R. Darcy, J.F. Cryan, C. O'Driscoll, Therapeutic targeting in the

silent era: advances in non-viral siRNA delivery, Molecular bioSystems, 6 (2010) 1143-1161.

[16] P. Baque, V. Pierrefite-Carle, A. Gavelli, N. Brossette, D. Benchimol, A. Bourgeon, P. Staccini, M. Saint-Paul, B. Rossi, Naked DNA injection for liver metastases treatment in rats, Hepatology. 35 (2002) 1144-52.

[17] F. Liu, Y. Song, D. Liu, Hydrodynamics-based transfection in animals by systemic administration of plasmid DNA, Gene Ther. 6 (1999) 1258-1266.

[18] G. Zhang, V. Budker, J. Wolff, High Levels of Foreign Gene Expression in Hepatocytes after Tail Vein Injections of Naked Plasmid DNA, Hum. Gene Ther. 10 (1999) 1735-1737.

[19] X. Gao, K. Kim, D. Liu, Nonviral gene delivery: What we know and what is next, AAPS Journal. 9 (2007) E92-E104.

[20] C. Lachmann, G. Kotzamanis, L. D'Aiuto, H. Cooke, C. Huxley, E. Wagner, *In vitro* and *in vivo* delivery of intact BAC DNA - comparison of different methods, J. Gene Med. 6 (2004) 195-209.

[21] M.S. Dosari, J.E. Knapp, D. Liu, Hydrodynamic Delivery, Adv. Genet. 54 (2005) 65-82.

[22] S. Eastman, K. Baskin, B. Hodges, Q. Chu, A. Gates, R. Dreusicke, S. Anderson, R. Scheule, Development of catheter-based procedures for transducing the isolated rabbit liver with plasmid DNA, Hum. Gene Ther. 13 (2002) 2065-2077.

[23] S. Alino, M. Herrero, I. Noguera, F. Dasi, M. Sanchez, Pig liver gene therapy by noninvasive interventionist catheterism, Gene Ther. 14 (2007) 334-343.

[24] H. Yoshino, K. Hashizume, E. Kobayashi, Naked plasmid DNA transfer to the porcine liver using rapid injection with large volume, Gene Ther. 13 (2006) 1696-1702.

[25] J. De Vry, P. Martínez-Martínez, M. Losen, Y. Temel, T. Steckler, H.W.M. Steinbusch, M.H. De Baets, J. Prickaerts, *In vivo* electroporation of the central nervous system: a non-viral approach for targeted gene delivery, Prog. Neurobiol. 92 (2010) 227-244.

[26] E. Wagner, R. Kircheis, G.F. Walker, Targeted nucleic acid delivery into tumors: new avenues for cancer therapy, Biomed. Pharmacother. 58 (2004) 152-161.

[27] M. Lucas, L. Heller, D. Coppola, R. Heller, IL-12 plasmid delivery by *in vivo* electroporation for the successful treatment of established subcutaneous B16.F10

melanoma, Mol. Ther.. 5 (2002) 668-675.

[28] T. Goto, T. Nishi, T. Tamura, Highly efficient electro-gene therapy of solid tumor by using an expression plasmid for the herpes simplex virus thymidine kinase gene, Proc. Natl. Acad. Sci. U. S. A. 97 (2000) 354-359.

[29] Y. Akaneya, B. Jiang, T. Tsumoto, RNAi-induced gene silencing by local electroporation in targeting brain region, J. Neurophysiol. 93 (2005) 594-602.

[30] T. Nozaki, R. Ogawa, L. Feril, G. Kagiya, H. Fuse, T. Kondo, Enhancement of ultrasound-mediated gene transfection by membrane modification, J. Gene Med. 5 (2003) 1046-1055.

[31] R. Ogawa, G. Kagiya, L. Feril, N. Nakaya, T. Nozaki, H. Fuse, T. Kondo, Ultrasound mediated intravesical transfection enhanced by treatment with lidocaine or heat, J. Urol. 172 (2004) 1469-1473.

[32] K. Anwer, G. Kao, B. Proctor, I. Anscombe, V. Florack, R. Earls, E. Wilson, T. McCreery, E. Unger, A. Rolland, S. Sullivan, Ultrasound enhancement of cationic lipid-mediated gene transfer to primary tumors following systemic administration, Gene Ther. 7 (2000) 1833-1839.

[33] P.E. Huber, J. Jenne, J. Debus, M.F. Wannenmacher, A comparison of shock wave and sinusoidal-focused ultrasound-induced localized transfection of HeLa cells, Ultrasound Med. Biol. 25 (1999) 1451-1457.

[34] S. Seemann, P. Hauff, M. Schultze-Mosgau, C. Lehmann, R. Reszka, Pharmaceutical evaluation of gas-filled microparticles as gene delivery system, Pharm. Res. 19 (2002) 250-257.

[35] T. Kitagawa, T. Iwazawa, P. Robbins, M. Lotze, H. Tahara, Advantages and limitations of particle-mediated transfection (gene gun) in cancer immuno-gene therapy using IL-10, IL-12 or B7-1 in murine tumor models, J. Gene Med. 5 (2003) 958-965.

[36] J. Wang, T. Murakami, Y. Hakamata, T. Ajiki, Y. Jinbu, Y. Akasaka, M. Ohtsuki, H. Nakagawa, E. Kobayashi, Gene gun-mediated oral mucosal transfer of interleukin 12 cDNA coupled with an irradiated melanoma vaccine in a hamster model: Successful treatment of oral melanoma and distant skin lesion, Cancer Gene Ther. 8 (2001) 805-12.

[37] A. Høgset, L. Prasmickaite, B.O. Engesaeter, M. Hellum, P.K. Selbo, V.M. Olsen, G.M. Maelandsmo, K. Berg, Light directed gene transfer by photochemical internalisation, Curr. Gene Ther. 3 (2003) 89-112.

[38] J. Kloeckner, L. Prasmickaite, A. Hogset, K. Berg, E. Wagner, Photochemically enhanced gene delivery of EGF receptor-targeted DNA polyplexes, J. Drug Target. 12 (2004) 205-213.

[39] G.H. Guibinga, S. Song, J. Loring, T. Friedmann, Characterization of the gene delivery properties of baculoviral-based virosomal vectors, J. Virol. Methods. 148 (2008) 277-82.

[40] N.K. Green, C.W. Herbert, S.J. Hale, A.B. Hale, V. Mautner, R. Harkins, T. Hermiston, K. Ulbrich, K.D. Fisher, L.W. Seymour, Extended plasma circulation time and decreased toxicity of polymer-coated adenovirus, Gene Ther. 11 (2004) 1256-1263.

[41] L. Wasungu, D. Hoekstra, Cationic lipids, lipoplexes and intracellular delivery of genes, J. Controlled Release. 116 (2006) 255-264.

[42] N.M. Rao, V. Gopal, Cell biological and biophysical aspects of lipid-mediated gene delivery, Biosci. Rep. 26 (2006) 301-324.

[43] P. Xu, S. Li, Q. Li, J. Ren, E.A. Van Kirk, W.J. Murdoch, M. Radosz, Y. Shen, Biodegradable cationic polyester as an efficient carrier for gene delivery to neonatal cardiomyocytes, Biotechnol. Bioeng. 95 (2006) 893-903.

[44] D.W. Pack, A.S. Hoffman, S. Pun, P.S. Stayton, Design and development of polymers for gene delivery, Nat. Rev Drug Dis. 4 (2005) 581-593.

[45] S. Veldhoen, S.D. Laufer, T. Restle, Recent developments in peptide-based nucleic acid delivery, Int. J. Mol. Sci. 9 (2008) 1276-1320.

[46] P. Jarvert, K. Langel, S. El-Andaloussi, U. Langel, Applications of cell-penetrating peptides in regulation of gene expression, Biochem. Soc. Trans. 35 (2007) 770-774.

[47] P. Ghosh, G. Han, M. De, C.K. Kim, V.M. Rotello, Gold nanoparticles in delivery applications, Adv. Drug Deliv. Rev. 60 (2008) 1307-15.

[48] S. Victor, Sunita, T. Kumar. BCP ceramic microspheres as drug delivery carriers: synthesis, characterisation and doxycycline release, J. Mater. Sci. 19 (2008) 283-290.

[49] M.A. Ilies, A.T. Balaban, Recent developments in cationic lipid-mediated gene delivery and gene therapy, Expert Opin. Ther. Pat. 11 (2001) 1729-1752.

[50] S.M. Moghimi, B. Bonnemain, Subcutaneous and intravenous delivery of diagnostic agents to the lymphatic system: applications in lymphoscintigraphy and indirect lymphography, Adv. Drug Deliv. Rev. 37 (1999) 295-312.

[51] A. Sharma, U.S. Sharma, Liposomes in drug delivery: progress and limitations, Int. J. Phar. 154 (1997) 123-140.

[52] B. Ozpolat, A. Sood, G. Lopez-Berestein, Nanomedicine based approaches for the delivery of siRNA in cancer, J Intern. Med. 267 (2010) 44-53.

[53] A. Schroeder, C. Levins, C. Cortez, R. Langer, D. Anderson, Lipid-based nanotherapeutics for siRNA delivery, J. Intern. Med. 267 (2010) 9-21.

[54] K. Gao, L. Huang, Nonviral methods for siRNA delivery, Mol. Pharm. 6 (2009) 651-658.

[55] B. Urban-Klein, S. Werth, S. Abuharbeid, F. Czubayko, A. Aigner, RNAi-mediated gene-targeting through systemic application of polyethylenimine (PEI)-complexed siRNA *in vivo*, Gene Ther. 12 (2005) 461-466.

[56] H. Katas, H.O. Alpar, Development and characterisation of chitosan nanoparticles for siRNA delivery, J. Control. Release. 115 (2006) 216-225.

[57] X. Sun, N. Zhang, Cationic polymer optimization for efficient gene delivery, Mini-Rev. Med. Chem. 10 (2010) 108-125.

[58] G.T. Zugates, D. Anderson, I. Lawhorn, R. Langer, 786. Synthesis of cationic biodegradable polymers for targeted gene delivery to hepatocytes, Mol. Ther. 11 (2005) 305-305.

[59] W. Chen, H. Chen, J. Hu, W. Yang, C. Wang, Synthesis and characterization of polyion complex micelles between poly(ethylene glycol)-grafted poly(aspartic acid) and cetyltrimethyl ammonium bromide, Colloid. Surface. 278 (2006) 60-66.

[60] H.S. Min, H.J. Lee, S.C. Lee, K.H. Kang, J. Lee, K. Park, K.M. Huh, Aqueous solubilization of paclitaxel using hydrotropic polymer micelle, Key Eng Mat. 342-343 (2007) 421-424.

[61] M.L. Adams, A. Lavasanifar, G.S. Kwon, Erratum: Amphiphilic block copolymers for drug delivery, J. Pharm. Sci. 92 (2003) 1343-55.

[62] D. Bhadra, S. Bhadra, N.K. Jain, PEGylated peptide dendrimeric carriers for the delivery of antimalarial drug chloroquine phosphate, Parm. Res. 23 (2006) 623-33.

[63] D. Bhadra, S. Bhadra, N.K. Jain, Pegylated lysine based copolymeric dendritic micelles for solubilization and delivery of artemether, J. pharmacy & pharmaceutical sci. 8 (2005) 467-482.

[64] K.L. Heredia, T.H. Nguyen, C.W. Chang, V. Bulmus, T.P. Davis, H.D. Maynard, Reversible siRNA-polymer conjugates by RAFT polymerization, Chem. Commun. (2008) 3245-3247.

[65] M. Meyer, C. Dohmen, A. Philipp, D. Kiener, G. Maiwald, C. Scheu, M. Ogris, E. Wagner, Synthesis and biological evaluation of a bioresponsive and endosomolytic siRNA-polymer conjugate, Molecular pharmaceutics. 6 (2009) 752-762.

[66] Ü. Langel, Handbook of cell-penetrating peptides, 2nd ed., Taylor & Francis, Boca Raton, 2007.

[67] P. Saeaelik, A. Elmquist, M. Hansen, K. Padari, K. Saar, K. Viht, U. Langel, M. Pooga, Protein cargo delivery properties of cell-penetrating peptides: A comparative study, Bioconj. Chem. 15 (2004) 1246-1253.

[68] M. Zorko, Ü. Langel, Cell-penetrating peptides: Mechanism and kinetics of cargo delivery, Adv. Drug Deliv. Rev. 57 (2005) 529-545.

[69] H. Mok, T.G. Park, Self-crosslinked and reducible fusogenic peptides for intracellular delivery of siRNA, biopolymers. 89 (2008) 881-8.

[70] E. Vives, Present and future of cell-penetrating peptide mediated delivery systems: "Is the Trojan horse too wild to go only to Troy?", J. Controlled Release. 109 (2005) 77-85.

[71] T. Niidome, K. Takaji, M. Urakawa, N. Ohmori, A. Wada, T. Hirayama, H. Aoyagi, Chain length of cationic alpha-helical peptide sufficient for gene delivery into cells, Bioconjug. Chem. 10 (1999) 773-780.

[72] S. Deshayes, T. Plenat, G. Aldrian-Herrada, G. Divita, C.D. Grimmellec, F. Heitz, Primary amphipathic cell-penetrating peptides: structural requirements and interactions with model membranes, Biochemistry. 43 (2004) 7698-7706.

[73] G. Tuunnemann, G. Ter-Avetisyan, R.M. Martin, M. Stoockl, A. Herrmann, C. Cardoso, Live-cell analysis of cell penetration ability and toxicity of oligo-arginines, J. Pep. Sci. 14 (2008) 469-476.

[74] R. Cartier, R. Reszka, Utilization of synthetic peptides containing nuclear localization signals for nonviral gene transfer systems, Gene Ther. 9 (2002) 157-67.

[75] S.D. Conner, S.L. Schmid, Regulated portals of entry into the cell, Nature. 422 (2003) 37(7)-44.

[76] M.E. Herbig, K. Weller, U. Krauss, A.G. Beck-Sickinger, H.P. Merkle, O. Zerbe, Membrane surface-associated helices promote lipid interactions and cellular uptake of human calcitonin-derived cell penetrating peptides, Biophys. J. 89 (2005) 4056-4066.

[77] D. Derossi, S. Calvet, A. Trembleau, A. Brunissen, G. Chassaing, A. Prochiantz, Cell internalization of the third helix of the antennapedia homeodomain is receptor-independent, J. Biol. Chem. 271 (1996) 18188-93.

[78] G. Drin, M. Mazel, P. Clair, D. Mathieu, M. Kaczorek, J. Temsamani, Physico-chemical requirements for cellular uptake of pAntp peptide - Role of lipid-binding affinity, Euro. J. Biochem. 268 (2001) 1304-1314.

[79] D. Derossi, A.H. Joliot, G. Chassaing, A. Prochiantz, The 3rd helix of the Antennapedia homeodomain translocates through biological-membranes, J. Biol. Chem. 269 (1994) 10444-10450.

[80] P. Lundberg, M. Magzoub, M. Lindberg, M. Hallbrink, J. Jarvet, L.E.G. Eriksson, U. Langel, A. Graslund, Cell membrane translocation of the N-terminal (1–28) part of the prion protein, Biochem. Biophys. Res. Commun. 299 (2002) 85-90.

[81] S. Li, S.P. Wu, M. Whitmore, E.J. Loeffert, L. Wang, S.C. Watkins, B.R. Pitt, L. Huang, Effect of immune response on gene transfer to the lung via systemic administration of cationic lipidic vectors, Am. J. Physiol-Lung C. 276 (1999) L796-L804.

[82] M. Pooga, M. Hallbrink, M. Zorko, U. Langel, Cell penetration by transportan, FASEB. J. 12 (1998) 67-77.

[83] A. Elmquist, M. Lindgren, T. Bartfai, Ü. Langel, VE-cadherin-derived cell-penetrating peptide, *p* vec, with carrier functions, Exp. Cell Res. 269 (2001) 237-244.

[84] M. Keller, T. Tagawa, M. Preuss, A.D. Miller, Biophysical characterization of the dna binding and condensing properties of adenoviral core peptide μ (mu), Biochemistry 41 (2002) 652-9.

[85] M. Murata, S. Kagiwada, S. Takahashi, S.I. Ohnishi, Membrane-fusion induced by mutual interaction of the 2 charge-reversed amphiphilic peptides at neutral pH, J. Biol. Chem. 266 (1991) 14353-14358.

[86] P. Midoux, R. Mayer, M. Monsigny, Membrane permeabilization by alpha-helical peptides - a flow-cytometry study, Biochem. Biophys. Acta Biomem. 1239 (1995) 249-256.

[87] I. Freulon, M. Monsigny, P. Midoux, R. Mayer, Spacer length dependence on the efficiency of dimeric anionic peptides in gene transfer by glycosylated polylysine/plasmid complexes, Biosci. Rep. 20 (2000) 383-398.

[88] P. Midoux, A. Kichler, V. Boutin, J.C. Maurizot, M. Monsigny, Membrane permeabilization and efficient gene transfer by a peptide containing several histidines, Bioconjug. Chem. 9 (1998) 260-267.

[89] J.D. Lear, W.F. Degrado, Membrane-binding and conformational properties of peptides representing the nh2 terminus of influenza Ha-2, J. Biol. Chem. 262 (1987) 6500-6505.

[90] P. Midoux, A. Kichler, V. Boutin, J.C. Maurizot, M. Monsigny, Membrane permeabilization and efficient gene transfer by a peptide containing several histidines, Bioconjug. Chem. 9 (1998) 260-7.

[91] J.D. Lear, W.F. Degrado, Membrane-binding and conformational properties of peptides representing the nh2 terminus of influenza Ha-2, J. Biol. Chem. 262 (1987) 6500-05.

[92] J.A. Hughes, A.I. Aronsohn, A.V. Avrutskaya, R.L. Juliano, Evaluation of adjuvants that enhance the effectiveness of antisense oligodeoxynucleotides, Pharm. Res. 13 (1996) 404-410.

[93] S. Oess, E. Hildt, Novel cell permeable motif derived from the PreS2-domain of hepatitis-B virus surface antigens, Gene Ther. 7 (2000) 750-758.

[94] U. Krauss, M. Muller, M. Stahl, A.G. Beck-Sickinger, *In vitro* gene delivery by a novel human calcitonin (hCT)-derived carrier peptide, Bioorg. Med. Chem. Lett. 14 (2004) 51-54.

[95] C. PLANK, B. OBERHAUSER, K. MECHTLER, C. KOCH, E. WAGNER, The influence of endosome-disruptive peptides on gene-transfer using synthetic virus-like gene-transfer systems, J. Biol. Chem. 269 (1994) 12918-12924.

[96] Y.Z. LIN, S.Y. YAO, R.A. VEACH, T.R. TORGERSON, J. HAWIGER, Inhibition of nuclear translocation of transcription factor nf-kappa-b by a synthetic peptide-containing a cell membrane-permeable motif and nuclear-localization sequence, J. Biol. Chem. 270 (1995) 14255-14258.

[97] S. Dokka, D. Toledo-Velasquez, X.L. Shi, L.Y. Wang, Y. Rojanasakul, Cellular delivery of oligonucleotides by synthetic import peptide carrier, Pharm. Res. 14 (1997) 1759-1764.

[98] H. Noguchi, H. Kaneto, G.C. Weir, S. Bonner-Weir, PDX-1 protein containing its own Antennapedia-like protein transduction domain can transduce pancreatic duct and islet cells. (Islet Studies), Diabetes. 52 (2003) 1732(6)-1738.

[99] G. Dom, C. Shaw-Jackson, C. Matis, O. Bouffioux, J.J. Picard, A. Prochiantz, M.P. Mingeot-Leclercq, R. Brasseur, R. Rezsohazy, Cellular uptake of Antennapedia Penetratin peptides is a two-step process in which phase transfer precedes a tryptophan-dependent translocation, Nucleic Acids Res. 31 (2003) 556-561.

[100] C. Rousselle, P. Clair, J.M. Lefauconnier, M. Kaczorek, J.M. Scherrmann, J. Temsamani, New advances in the transport of doxorubicin through the blood-brain barrier by a peptide vector-mediated strategy, Mol. Pharmacol. 57 (2000) 679-686.

[101] J. Oehlke, A. Scheller, B. Wiesner, E. Krause, M. Beyermann, E. Klauschenz, M. Melzig, M. Bienert, Cellular uptake of an α-helical amphipathic model peptide with the potential to deliver polar compounds into the cell interior non-endocytically, BBA-Biomembranes. 1414 (1998) 127-139.

[102] E.L. Snyder, S.F. Dowdy, Cell penetrating peptides in drug delivery, Pharm. Res. 21 (2004) 389-393.

[103] S. Fawell, J. Seery, Y. Daikh, Tat-mediated delivery of heterologous proteins into cells, Proc. Natl. Acad. Sci. 91 (1994) 664-668.

[104] S. Sundaram, S. Viriyayuthakorn, C.M. Roth, Oligonucleotide structure influences the interactions between cationic polymers and oligonucleotides, Biomacromolecules. 6 (2005) 2961-2968.

[105] S.M. Fuchs, R.T. Raines, Internalization of cationic peptides: the road less (or more?) traveled, Cell Mol. Life Sci. 63 (2006) 1819-22.

[106] R.C. Adami, K.G. Rice, Metabolic stability of glutaraldehyde cross-linked peptide DNA condensates, J. Pharm. Sci. 88 (1999) 739-746.

[107] D.L. McKenzie, K.Y. Kwok, K.G. Rice, A potent new class of reductively activated peptide gene delivery agents, J. Biol. Chem. 275 (2000) 9970-7.

[108] S. Pujals, E. Giralt, Proline-rich, amphipathic cell-penetrating peptides, Adv. Drug Deliv. Rev. 60 (2008) 473-484.

[109] N. Ohmori, T. Niidome, T. Kiyota, S. Lee, G. Sugihara, A. Wada, T. Hirayama, H. Aoyagi, Importance of hydrophobic region in amphiphilic structures of α-helical peptides

for their gene transfer-ability into cells, Biochem. Biophys. Res. Commun. 245 (1998) 259-65.

[110] T. Plénat, S. Boichot, P.E. Milhiet, C.L. Grimellec, S. Deshayes, F. Heitz, R.B. Cole, Interaction of primary amphipathic cell-penetrating peptides with phospholipid-supported monolayers, Langmuir. 20 (2004) 9255-9261.

[111] S. Deshayes, M.C. Morris, G. Divita, F. Heitz, Cell-penetrating peptides: tools for intracellular delivery of therapeutics, Cell Mol. Life Sci. 62 (2005) 1839-1849.

[112] F. Simeoni, M.C. Morris, F. Heitz, G. Divita, Peptide-based strategy for siRNA delivery into mammalian cells, Method. Mol. Biol. 309 (2005) 251-260.

[113] M. Jafari, B. Zargar, M. Soltani, N. Karunaratne, B. Ingalls, P. Chen, (2012) Intelligent drug delivery systems for cancer therapy, In: A. Tiwari and H. Kobayashi, (Eds), Biomedical materials and diagnostic devices, John Wiley & Sons, Inc., Hoboken, NJ, USA, 2012.

M.C. Morris, J. Depollier, J. Mery, F. Heitz, G. Divita, A peptide carrier for the delivery of biologically active proteins into mammalian cells, Nat. Biotech. 19 (2001) 1173-76.

[114] K.V. Morris, S.W.-. Chan, S.E. Jacobsen, Small interfering rna-induced transcriptional gene silencing in human cells, Science. 305 (2004) 1289-1292.

[115] S. Labialle, G. Dayan, L. Gayet, D. Rigal, J. Gambrelle, L.G. Baggetto, New invMED1 element cis-activates human multidrug-related MDR1 and MVP genes, involving the LRP130 protein, Nucleic Acids Res. 32 (2004) 3864-76.

[116] M.C. Morris, P. Vidal, L. Chaloin, F. Heitz, G. Divita, A new peptide vector for efficient delivery of oligonucleotides into mammalian cells, Nucleic Acids Res. 25 (1997) 2730-36.

[117] F. Simeoni, M.C. Morris, F. Heitz, G. Divita, Insight into the mechanism of the peptide ‐ based gene delivery system MPG: implications for delivery of siRNA into mammalian cells, Nucleic Acids Res. 31 (2003) 2717-2724.

[118] L. Crombez, G. Aldrian-Herrada, K. Konate, Q.N. Nguyen, G.K. McMaster, R. Brasseur, F. Heitz, G. Divita, A new potent secondary amphipathic cell-penetrating peptide for siRNA delivery into mammalian cells, Mol. Ther. 17 (2009) 95-103.

[119] M.C. Morris, L. Chaloin, J. Méry, F. Heitz, G. Divita, A novel potent strategy for gene delivery using a single peptide vector as a carrier, Nucleic acids Res. 27 (1999) 3510-3517.

[120] M.C. Morris, J. Depollier, J. Mery, F. Heitz, G. Divita, A peptide carrier for the delivery of biologically active proteins into mammalian cells, Nat. Biotech. 19 (2001) 1173-76

[121] W. Li, F. Nicol, F.C. Szoka Jr, GALA: a designed synthetic pH-responsive amphipathic peptide with applications in drug and gene delivery, Adv. Drug Deliv. Rev. 56 (2004) 967-985.

[122] S. Gottschalk, J.T. Sparrow, J. Hauer, M.P. Mims, F.E. Leland, S.L.C. Woo, L.C. Smith, A novel DNA-peptide complex for efficient gene transfer and expression in mammalian cells, Gene Ther. 3 (1996) 448-457.

[123] J. Oehlke, A. Scheller, B. Wiesner, E. Krause, M. Beyermann, E. Klauschenz, M. Melzig, M. Bienert, Cellular uptake of an α-helical amphipathic model peptide with the potential to deliver polar compounds into the cell interior non-endocytically, BBA-Biomembranes. 1414 (1998) 127-139.

[124] L. Chaloin, P. Vidal, P. Lory, J. Méry, N. Lautredou, G. Divita, F. Heitz, Design of carrier peptide-oligonucleotide conjugates with rapid membrane translocation and nuclear localization properties, Biochem. Biophys. Res. Commun. 243 (1998) 601-8.

[125] M.C. Morris, J. Depollier, J. Mery, F. Heitz, G. Divita, A peptide carrier for the delivery of biologically active proteins into mammalian cells, Nat. Biotechnol. 19 (2001) 1173-1176.

[126] L. Chaloin, E. Dé, P. Charnet, G. Molle, F. Heitz, Ionic channels formed by a primary amphipathic peptide containing a signal peptide and a nuclear localization sequence, BBA-Biomembranes. 1375 (1998) 52-60.

[127] E. De, L. Chaloin, A. Heitz, J. Mery, G. Molle, F. Heitz, Conformation and ion channel properties of a five-helix bundle protein, (2001).

[128] R.A. Parente, S. Nir, F.C. Szoka, Mechanism of leakage of phospholipid vesicle contents induced by the peptide GALA, Biochemistry. 29 (1990) 8720-8728.

[129] E. Ruoslahti, M.D. Pierschbacher, Arg-Gly-Asp: A versatile cell recognition signal, Cell. 44 (1986) 517-8.

[130] G. HAo, X. Sun, Cyclization of RGD peptide sequences via the macrocyclic chelator DOTA for integrin imaging, Dalton Trans. 41 (2012) 14051-4.

[131] M.A. Dechantsreiter, E. Planker, B. Mathä, E. Lohof, G. Hölzemann, A. Jonczyk, S.L. Goodman, H. Kessler, *N* -Methylated cyclic rgd peptides as highly active and selective $\alpha_v\beta_3$ integrin antagonists, J. Med. Chem. 42 (1999) 3033-40.

[132] B.R. Meade, S.F. Dowdy, Exogenous siRNA delivery using peptide transduction domains/cell penetrating peptides, Adv. Drug Deliv. Rev. 59 (2007) 134-140.

[133] L. Crombez, A. Charnet, M.C. Morris, G. Aldrian-Herrada, F. Heitz, G. Divita, A non-covalent peptide-based strategy for siRNA delivery, Biochem. Soc. Trans. 35 (2007) 44-46.

[134] H.M. Kang, R. DeLong, M.H. Fisher, R.L. Juliano, Tat-conjugated PAMAM dendrimers as delivery agents for antisense and siRNA oligonucleotides, Pharm. Res. 22 (2005) 2099-2106.

[135] C. Zhang, N. Tang, X. Liu, W. Liang, W. Xu, V.P. Torchilin, siRNA-containing liposomes modified with polyarginine effectively silence the targeted gene, J. Controlled Release. 112 (2006) 229-39.

[136] T.J. Davidson, S. Harel, V.A. Arboleda, G.F. Prunell, M.L. Shelanski, L.A. Greene, C.M. Troy, Highly efficient small interfering RNA delivery to primary mammalian neurons induces MicroRNA-like effects before mRNA degradation, J. Neurosci. 24 (2004) 10040-6.

[137] A. Muratovska, M.R. Eccles, Conjugate for efficient delivery of short interfering RNA (siRNA) into mammalian cells, FEBS letters. 558 (2004) 63-68.

[138] Q.N. Nguyen, R.V. Chavli, J.T. Marques, P.G. Conrad II, D. Wang, W. He, B.E. Belisle, A. Zhang, L.M. Pastor, F.R. Witney, M. Morris, F. Heitz, G. Divita, B.R.G. Williams, G.K. McMaster, Light controllable siRNAs regulate gene suppression and phenotypes in cells, BBA - Biomembranes. 1758 (2006) 394-403.

[139] S. Veldhoen, S.D. Laufer, A. Trampe, T. Restle, Cellular delivery of small interfering RNA by a non-covalently attached cell-penetrating peptide: quantitative analysis of uptake and biological effect, Nucleic Acids Res. 34 (2006) 6561-7.

[140] P. Lundberg, S. El-Andaloussi, T. Sutlu, H. Johansson, U. Langel, Delivery of short interfering RNA using endosomolytic cell-penetrating peptides, FASEB J. 21 (2007) 2664-2671.

[141] T. Endoh, M. Sisido, T. Ohtsuki, Cellular siRNA delivery mediated by a cell-permeant RNA-Binding protein and photoinduced RNA interference, Bioconjug. Chem. 19 (2008) 1017-24.

[142] M. Lee, S.W. Kim, Polyethylene glycol-conjugated copolymers for plasmid DNA delivery, Pharm. Res. 22 (2005) 1-10.

[143] S.W. Huang, R.X. Zhuo, Recent progress in polymer-based gene delivery vectors, Chinese Sci. Bull. 48 (2003) 1304-1309.

[144] J.H. Jeong, T.G. Park, Poly(l-lysine)-g-poly(d,l-lactic-co-glycolic acid) micelles for low cytotoxic biodegradable gene delivery carriers, J. Controlled Release. 82 (2002) 159-166.

[145] S. Deshayes, M. Decaffmeyer, R. Brasseur, A. Thomas, Structural polymorphism of two CPP: An important parameter of activity, BBA-Biomembranes. 1778 (2008) 1197-1205.

[146] M. Jafari, P. Chen, Peptide mediated sirna delivery, Curr. Top. Med. Chem. 9 (2009) 1088-97.

[147] A.T. Jones, Macropinocytosis: searching for an endocytic identity and role in the uptake of cell penetrating peptides, J. Cell. Mol. Med. 11 (2007) 670-684.

[148] J.P. Richard, K. Melikov, H. Brooks, P. Prevot, B. Lebleu, L.V. Chernomordik, Cellular uptake of unconjugated TAT peptide involves clathrin-dependent endocytosis and heparan sulfate receptors, J. Biol. Chem. 280 (2005) 15300-15306.

[149] H. Hirose, T. Takeuchi, H. Osakada, S. Pujals, S. Katayama, I. Nakase, S. Kobayashi, T. Haraguchi, S. Futaki, Transient focal membrane deformation induced by arginine-rich peptides leads to their direct penetration into cells, Mol. Ther. 20 (2012) 984-993.

[150] K. Konate, L. Crombez, S. Deshayes, M. Decaffmeyer, A. Thomas, R. Brasseur, G. Aldrian, F. Heitz, G. Divita, Insight into the cellular uptake mechanism of a secondary amphipathic cell-penetrating peptide for siRNA delivery, Biochemistry. 49 (2010) 3393-3402.

[151] S. Fung, H. Yong, P. Sadatmousavi, Y. Sheng, T. Mamo, R. Nazaian, P. Chen, Amino acid pairing for de novo design of self-assembling peptides and their drug delivery potential, Adv.Func. Mater. 21 (2011) 2456-2464.

[152] P. Sadatmousavi, M. Soltani, R. Nazarian, M. Jafari, P. Chen, Self-assembling peptides: potential role in tumor targeting, Curr. Pharm. Biotechnol. 12 (2011) 1089-1100.

[153] M. Wang, M. Law, J. Duhamel, P. Chen, Interaction of a self-assembling peptide with oligonucleotides: complexation and aggregation, Biophys. J. 93 (2007) 2477-2490.

[154] M. Law, M. Jafari, P. Chen, Physicochemical characterization of siRNA-peptide complexes, Biotechnol. Prog. 24 (2008) 957-963.

[155] I. Nakase, A. Tadokoro, N. Kawabata, T. Takeuchi, H. Katoh, K. Hiramoto, M. Negishi,

M. Nomizu, Y. Sugiura, S. Futaki, Interaction of arginine-rich peptides with membrane-associated proteoglycans is crucial for induction of actin organization and macropinocytosis, Biochemistry. 46 (2007) 492-501.

[156] S. Futaki, T. Suzuki, W. Ohashi, T. Yagami, S. Tanaka, K. Ueda, Y. Sugiura, Arginine-rich peptides. An abundant source of membrane-permeable peptides having potential as carriers for intracellular protein delivery, J. Biol. Chem. 276 (2001) 5836-5840.

[157] P.Y. Chou, G.D. Fasman, P.Y. Chou, G.D. Fasman, Structural and functional role of leucine residues in proteins, J. Mol. Biol. 74 263-281.

[158] H. Maeda, J. Wu, T. Sawa, Y. Matsumura, K. Hori, Tumor vascular permeability and the EPR effect in macromolecular therapeutics: a review, J. Controlled Release. 65 (2000) 271-284.

[159] J. Fang, H. Nakamura, H. Maeda, The EPR effect: Unique features of tumor blood vessels for drug delivery, factors involved, and limitations and augmentation of the effect, Adv. Drug Deliv. Rev. 63 (2011) 136-151.

[160] V. Torchilin, Tumor delivery of macromolecular drugs based on the EPR effect, Adv. Drug Deliv. Rev. 63 (2011) 131-135.

[161] J. Rejman, V. Oberle, I.S. Zuhorn, D. Hoekstra, Size-dependent internalization of particles via the pathways of clathrin- and caveolae-mediated endocytosis, Biochem. J. 377 (2004) 159-169.

[162] S. Jun, Y. Hong, H. Imamura, B.-. Ha, J. Bechhoefer, P. Chen, Self-assembly of the ionic peptide EAK16: the effect of charge distributions on self-assembly, Biophys. J. 87 (2004) 1249-1259.

[163] R. Stolarski, Thermodynamics of specific protein-RNA interactions, Acta Biochim. Pol. 50 (2003) 297-318.

[164] H. Klump, Calorimetric studies of the interaction between DNA and poly-L-lysine, Biophys. Chem. 5 (1976) 363-367.

[165] T. Zhou, B. Rosen, Tryptophan fluorescence reports nucleotide- induced conformational changes in a domain of the ArsA ATPase, FASEB J. 11 (1997) A1147-A1147.

[166] S. Veldhoen, S.D. Laufer, A. Trampe, T. Restle, Cellular delivery of small interfering RNA by a non-covalently attached cell-penetrating peptide: quantitative analysis of uptake and biological effect, Nucleic Acids Res. 34 (2006) 6561-6573.

[167] C. Tros de Ilarduya, Y. Sun, N. Düzgüneş, Gene delivery by lipoplexes and polyplexes, European journal of pharmaceutical sciences : official journal of the European Federation for. Pharm. Sci. 40 (2010) 159-170.

[168] S. Deshayes, M. Morris, F. Heitz, G. Divita, Delivery of proteins and nucleic acids using a non-covalent peptide-based strategy, Adv. Drug Del. Rev. 60 (2008) 537-547.

[169] L. Kurzawa, M. Pellerano, M.C. Morris, PEP and CADY-mediated delivery of fluorescent peptides and proteins into living cells, Biochim. Biophys. Acta. 1798 (2010) 2274-2285.

[170] D.M. Lawson, P.J. Artymiuk, S.J. Yewdall, J.M. Smith, J.C. Livingstone, A. Treffry, A. Luzzago, S. Levi, P. Arosio, G. Cesareni, Solving the structure of human H ferritin by genetically engineering intermolecular crystal contacts, Nature. 349 (1991) 541-544.

[171] A. Fotin, Y. Cheng, N. Grigorieff, T. Walz, S.C. Harrison, T. Kirchhausen, Structure of an auxilin-bound clathrin coat and its implications for the mechanism of uncoating, Nature. 432 (2004) 649-653.

[172] A.J. Olson, G. Bricogne, S.C. Harrison, Structure of tomato busy stunt virus IV. The virus particle at 2.9 A resolution, J. Mol. Biol. 171 (1983) 61-93.

[173] J. McLaurin, D. Yang, C.M. Yip, P.E. Fraser, Review: modulating factors in amyloid-beta fibril formation, J. Struct. Biol. 130 (2000) 259-270.

[174] A. Mann, G. Thakur, V. Shukla, A.K. Singh, R. Khanduri, R. Naik, Y. Jiang, N. Kalra, B.S. Dwarakanath, U. Langel, M. Ganguli, Differences in DNA condensation and release by lysine and arginine homopeptides govern their DNA delivery efficiencies, Mol. Pharm. 8 (2011) 1729-1741.

[175] P.A. Wender, D.J. Mitchell, K. Pattabiraman, E.T. Pelkey, L. Steinman, J.B. Rothbard, The design, synthesis, and evaluation of molecules that enable or enhance cellular uptake: peptoid molecular transporters, Proc. Natl. Acad. Sci. 97 (2000) 13003-13008.

[176] M. Jafari, W. Xu, S. Naahidi, B. Chen, P. Chen, A new amphipathic, amino-acid-pairing (aap) peptide as sirna delivery carrier: physicochemical characterization and *in vitro* uptake, J Phys Chem B. 116 (2012) 13183-13191.

[177] S.Y. Fung, C. Keyes, J. Duhamel, p. Chen, Concentration effect on the aggregation of a self-assembling oligopeptide, Biophys. J. 85 (2003) 537-548.

[178] C. Louis‐jeune, M.A. Andrade‐navarro, C. Perez‐iratxeta, Prediction of protein secondary structure from circular dichroism using theoretically derived spectra, Proteins:

Str. Func. Bioinfo. 80 (2012) 374-381.

[179] S.E. Gratton, P.A. Ropp, P.D. Pohlhaus, J.C. Luft, V.J. Madden, M.E. Napier, J.M. DeSimone, The effect of particle design on cellular internalization pathways, Proc. Natl. Acad. Sci. 105 (2008) 11613-11618.

[180] H.A. Rydberg, M. Matson, H.L. Amand, E.K. Esbjorner, B. Norden, Effects of tryptophan content and backbone spacing on the uptake efficiency of cell-penetrating peptides, Biochemistry. 51 (2012) 5531-9.

[181] J. Eastoe, J.S. Dalton, Dynamic surface tension and adsorption mechanisms of surfactants at the air-water interface, Adv. Colloid Interface Sci. 85 (2000) 103-144.

[182] D. Matulis, C.G. Baumann, V.A. Bloomfield, R.E. Lovrien, 1-Anilino-8-naphthalene sulfonate as a protein conformational tightening agent, Biopolymers. 49 (1999) 451-458.

[183] S.Y. Fung, H. Yang, P. Chen, Sequence effect of self-assembling peptides on the complexation and *in vitro* delivery of the hydrophobic anticancer drug ellipticine, PLoS One. 3 (2008) e1956.

[184] O. Danylyuk, V. Fedin, Solid-State Supramolecular assemblies of tryptophan and tryptamine with cucurbit[6]uril, Crystal Growth Des. 12 (2012) 550-555.

[185] M.E. Houston, L.H. Kondejewski, D.N. Karunaratne, M. Gough, S. Fidai, R.S. Hodges, R.E. Hancock, Influence of preformed alpha- helix and alpha- helix induction on the activity of cationic antimicrobial peptides, The journal of peptide research. 52 (1998) 81-88.

[186] M.A. Sani, T.C. Whitwell, F. Separovic, Lipid composition regulates the conformation and insertion of the antimicrobial peptide maculatin 1.1, Biochim. Biophys. Acta. 1818 (2012) 205-211.

[187] C. Bechara, M. Pallerla, Y. Zaltsman, F. Burlina, I.D. Alves, O. Lequin, S. Sagan, Tryptophan within basic peptide sequences triggers glycosaminoglycan-dependent endocytosis, FASEB J. doi: 10.1096/fj.12-216176 (2012).

[188] E. Koren, V.P. Torchilin, Cell-penetrating peptides: breaking through to the other side, Trends Mol. Med. 18 (2012) 385-393.

[189] Rajpal, A. Mann, R. Khanduri, R.J. Naik, M. Ganguli, Structural rearrangements and chemical modifications in known cell penetrating peptide strongly enhance DNA delivery efficiency, J. Control. Release. 157 (2012) 260-271.

[190] Z. Shi, C.A. Olson, A.J. Bell Jr, N.R. Kallenbach, Stabilization of alpha-helix structure by polar side-chain interactions: complex salt bridges, cation-pi interactions, and C-H em leader O H-bonds, Biopolymers. 60 (2001) 366-380.

[191] C. Aleman, Effect of the environment and role of the pi-pi stacking interactions in the stabilization of the 3(10)-helix conformation in dehydroalanine oligopeptides, Int. J. Pept. Protein Res. 46 (1995) 408-418.

[192] M. Kallberg, H. Wang, S. Wang, J. Peng, Z. Wang, H. Lu, J. Xu, Template-based protein structure modeling using the RaptorX web server, Nat. Protoc. 7 (2012) 1511-1522.

[193] C. He, Y. Hu, L. Yin, C. Tang, C. Yin, Effects of particle size and surface charge on cellular uptake and biodistribution of polymeric nanoparticles, Biomaterials. 31 (2010) 3657-3666.

[194] E.H. Harutyunyan, I.P. Kuranova, B.K. Vainshtein, W.E. Hohne, V.S. Lamzin, Z. Dauter, A.V. Teplyakov, K.S. Wilson, X-ray structure of yeast inorganic pyrophosphatase complexed with manganese and phosphate, Eur. J. Biochem. 239 (1996) 220-228.

[195] J. Hao, X. Sha, Y. Tang, Y. Jiang, Z. Zhang, W. Zhang, Y. Li, X. Fang, Enhanced transfection of polyplexes based on pluronic-polypropylenimine dendrimer for gene transfer, Arch. Pharm. Res. 32 (2009) 1045-1054.

[196] R. Elshereef, H. Budman, C. Moresoli, R.L. Legge, Fluorescence spectroscopy as a tool for monitoring solubility and aggregation behavior of beta-lactoglobulin after heat treatment, Biotechnol. Bioeng. 95 (2006) 863-874.

[197] S.A. Bode, M. Thevenin, C. Bechara, S. Sagan, S. Bregant, S. Lavielle, G. Chassaing, F. Burlina, Self-assembling mini cell-penetrating peptides enter by both direct translocation and glycosaminoglycan-dependent endocytosis, Chem. Commun. 48 (2012) 7179-7181.

[198] C.Y. Jiao, D. Delaroche, F. Burlina, I.D. Alves, G. Chassaing, S. Sagan, Translocation and endocytosis for cell-penetrating peptide internalization, J. Biol. Chem. 284 (2009) 33957-33965.

[199] I.M. Kaplan, J.S. Wadia, S.F. Dowdy, Cationic TAT peptide transduction domain enters cells by macropinocytosis, J. Control. Release. 102 (2005) 247-253.

[200] F. Madani, S. Lindberg, U. Langel, S. Futaki, A. Graslund, Mechanisms of cellular uptake of cell-penetrating peptides, J. Biophys. 2011 (2011) 414729.

[201] G.J. Cannon, J.A. Swanson, The macrophage capacity for phagocytosis, J. Cell. Sci. 101

(1992) 907-913.

[202] G. Sahay, D.Y. Alakhova, A.V. Kabanov, Endocytosis of nanomedicines, J. Control. Release. 145 (2010) 182-195.

[203] C.L. Francis, T.A. Ryan, B.D. Jones, S.J. Smith, S. Falkow, Ruffles induced by Salmonella and other stimuli direct macropinocytosis of bacteria, Nature. 364 (1993) 639-642.

[204] L.A. Gobeil, R. Lodge, M.J. Tremblay, Macropinocytosis-like HIV-1 internalization in macrophages is CCR5-dependent and leads to efficient but delayed degradation in endosomal compartments, J. Virol. doi:10.1128/JVI.01802-12 (2012).

[205] I. Nakase, A. Tadokoro, N. Kawabata, T. Takeuchi, H. Katoh, K. Hiramoto, M. Negishi, M. Nomizu, Y. Sugiura, S. Futaki, Interaction of arginine-rich peptides with membrane-associated proteoglycans is crucial for induction of actin organization and macropinocytosis, Biochemistry. 46 (2007) 492-501.

[206] G.J. Doherty, H.T. Mcmahon, Mechanisms of endocytosis, Annu. Rev. Biochem. 78 (2009) 857.

[207] D. Vercauteren, M. Piest, L.J. van der Aa, M. Al Soraj, A.T. Jones, J.F. Engbersen, S.C. De Smedt, K. Braeckmans, Flotillin-dependent endocytosis and a phagocytosis-like mechanism for cellular internalization of disulfide-based poly(amido amine)/DNA polyplexes, Biomaterials. 32 (2011) 3072-3084.

[208] A. Rydstrom, S. Deshayes, K. Konate, L. Crombez, K. Padari, H. Boukhaddaoui, G. Aldrian, M. Pooga, G. Divita, Direct translocation as major cellular uptake for CADY self-assembling peptide-based nanoparticles, PLoS One. 6 (2011) e25924.

[209] T. Letoha, A. Keller-Pinter, E. Kusz, C. Kolozsi, Z. Bozso, G. Toth, C. Vizler, Z. Olah, L. Szilak, Cell-penetrating peptide exploited syndecans, Biochim. Biophys. Acta. 1798 (2010) 2258-2265.

[210] A.I. Ivanov, Exocytosis and endocytosis, Humana Press, Totowa, N.J., 2008.

[211] J.A. Swanson, C. Watts, Macropinocytosis, Trends Cell Biol. 5 (1995) 424-428.

[212] M. Hao, S. Mukherjee, Y. Sun, F.R. Maxfield, Effects of cholesterol depletion and increased lipid unsaturation on the properties of endocytic membranes, J. Biol. Chem. 279 (2004) 14171-14178.

[213] P. Sampath, T.D. Pollard, Effects of cytochalasin, phalloidin, and pH on the elongation of actin filaments, Biochemistry. 30 (1991) 1973-1980.

[214] J.P. Baudoin, C. Alvarez, P. Gaspar, C. Metin, Nocodazole-induced changes in microtubule dynamics impair the morphology and directionality of migrating medial ganglionic eminence cells, Dev. Neurosci. 30 (2008) 132-143.

[215] A. Motley, N.A. Bright, M.N. Seaman, M.S. Robinson, Clathrin-mediated endocytosis in AP-2-depleted cells, J. Cell Biol. 162 (2003) 909-918.

[216] R.D. Singh, V. Puri, J.T. Valiyaveettil, D.L. Marks, R. Bittman, R.E. Pagano, Selective caveolin-1-dependent endocytosis of glycosphingolipids, Mol. Biol. Cell. 14 (2003) 3254-3265.

[217] Y. Kitajima, T. Sekiya, Y. Nozawa, Freeze-fracture ultrastructural alterations induced by filipin, pimaricin, nystatin and amphotericin B in the plasmia membranes of Epidermophyton, Saccharomyces and red complex-induced membrane lesions, Biochim. Biophys. Acta. 455 (1976) 452-465.

[218] A. Kakigi, T. Okada, T. Takeda, D. Taguchi, R. Nishioka, M. Nishimura, Actin filaments and microtubules regulate endocytosis in marginal cells of the stria vascularis, Acta Otolaryngol. 128 (2008) 856-860.

[219] A.C. Allison, P. Davies, Interactions of membranes, microfilaments, and microtubules in endocytosis and exocytosis, Adv. Cytopharmacol. 2 (1974) 237-248.

[220] S. Gerbal-Chaloin, C. Gondeau, G. Aldrian-Herrada, F. Heitz, C. Gauthier-Rouvière, G. Divita, First step of the cell-penetrating peptide mechanism involves Rac1 GTPase-dependent actin-network remodelling, Biology of the cell. 99 (2007) 223-238.

[221] I. Mager, K. Langel, T. Lehto, E. Eiriksdottir, U. Langel, The role of endocytosis on the uptake kinetics of luciferin-conjugated cell-penetrating peptides, Biochim. Biophys. Acta. 1818 (2012) 502-511.